# Abstract

Direct Numerical Simulation of channel flow was utilized to study the evolution of various vortex configurations presented as flow initial conditions. Simulations of longitudinally, laterally and cross-flow oriented vortices suggested that the predominant form of turbulent structure was the half hairpin vortex. This vortical structure was dominant in the simulations seen in this as well as other investigations. In all cases hairpin vortices quickly degenerated to half hairpin or inclined vortical structures. It is hypothesized that these structures function as the predominant momentum transfer mechanism within the boundary layer, entraining fluid into the vortex cores like miniature tornados and transporting this fluid to the top of the boundary layer while simultaneously dragging fluid viscously around the inclined core of the vortex causing mixing of low-speed and high-speed flows.

# Acknowledgments

I would like to thank Professor William Durgin for his continued assistance and patience in the conduct of this work. I am equally grateful for the technical assistance of Professor Gretar Tryggvason who has taught me much of what I know of Computation Fluid Dynamics and has provided many of the computational tools for this work. Special thanks to Sia Najafi who provided unending IT support and Dr. Janet Cowan for many helpful suggestions in the preparation of this paper.

I am also grateful for the exceptional patience of my family, both parents and children as well as my friends who have waited a long time for this work to be finished.

All computations were preformed on Linux operating systems. This document was published using Open Office running on Linux.

# Table of Contents

## *List of Figures*

# Nomenclature

| | | |
|---|---|---|
| $\alpha$ | wave number (real) | |
| $A_\tau$ | mixing coefficient (Boussinesq) | |
| $B$ | body force, gravity, charge, acceleration | |
| $c$ | complex wave speed | |
| $C_f$ | friction coefficient, wall friction | |
| $\delta$ | boundary layer thickness | |
| $\delta_{ij}$ | Kronecker delta function | |
| $\varepsilon$ | turbulent dissipation function | $\varepsilon = u_0^3 / L$ |
| $\varepsilon_\tau$ | virtual kinematic viscosity | |
| $T_{ij}$ | stress tensor | |
| $p$ | pressure | |
| $\mu$ | absolute viscosity | |
| $\nu$ | kinematic viscosity, | $\nu = \mu / \rho$ |
| $v$ | velocity | |
| $v_a(r)$ | velocity at as function of radius (Biot-Savart law) | |
| $S_{ij}$ | stress tensor | |
| $t$ | time | |

| | | |
|---|---|---|
| $\nabla$ | Del or gradient operator | $\nabla = \boldsymbol{i}\frac{\partial}{\partial x} + \boldsymbol{j}\frac{\partial}{\partial y} + \boldsymbol{k}\frac{\partial}{\partial z}$ |
| $\Gamma$ | circulation | |
| $\lambda_2$ | second eigenvalue of $A_{ij} = \sum_{k=1}^{3}\left(\Omega_{ik}\Omega_{kj} + S_{ik}S_{kj}\right)$, which provides a scalar field viewable as an iso-surface of vortical structures. | |
| $\tau_w$ | wall shear stress | $\tau_w = \mu\frac{(d\bar{U})}{dy}(0)$ |
| $\tau_l$ | shear stress, laminar flow | |
| $\tau_t$ | shear stress, turbulent flow | |
| $\overline{u'v'}$ | Reynolds stress | |
| $R_e$ | Reynolds number | $R_e = \frac{UL\rho}{\mu}$ |
| $l$ | mixing length | |
| $\phi$ | amplitude function, potential function | |
| $\psi$ | stream function | |
| $\eta$ | Kolmogorov length scale | $\eta \equiv \nu^{(3/4)}/\varepsilon^{(1/4)}$ |
| $t_d$ | Kolmogorov time scale | $t_d = \left(\frac{\nu}{\varepsilon}\right)^{(1/2)}$ |
| $v$ | Kolmogorov velocity scale | $v \equiv (\nu/\varepsilon)^{(1/4)}$ |
| $x, y, z$ | orthogonal position variables | |
| $x^+, y^+, z^+$ | non-dimensional wall length units | |

| | |
|---|---|
| $u, v, w$ | velocity vector components |
| $U, u_0$ | velocity in free stream |
| $U_\tau$ | friction velocity |

# 1.Introduction

## *1.1 Mechanism of Turbulent Bursts*

Turbulent bursts are a fundamental component of the generation of turbulence at the wall. Turbulence at a boundary wall results from boundary layer instabilities. The exact mechanisms are not clear at this time.

Turbulence at the wall affects the behavior of the boundary layer and many of the physical effects of flow. The boundary layer determines wall shear stress, skin friction and ultimately drag on the body or vehicle. Also affected is mixing of the fluid and heat transfer between the wall and fluid. These effects are a function of turbulent shear stress.

With so many physical effects from turbulence determined by activity in the boundary layer, the phenomenon of turbulence initiation through bursts has been the subject of extensive study. Within this study there have been two schools of thought regarding the formation of turbulent bursts.

Turbulent bursts resulting from horseshoe shaped vortices is one mechanism that has received much study. This mechanism will be further discussed in the background section. The formation of a burst by this mechanism starts with lateral vortices resulting from laminar boundary layer shear. Such a segment,

lifted by a disturbance, is carried downstream faster than the adjacent section of vortex causing stretching and folding of the vortex until there is a counter rotating parallel vortex pair. At this point the upward flow between the vortices of the pair pushes slow moving fluid rapidly upward. This upward moving fluid is replaced by high speed fluid that sweeps in close to the wall resulting in a high shear stress at the surface.

There is another school of thought that suggests turbulent bursts are formed as a result of parallel vortices without requiring the folding and stretching that produces the canonical hairpin shape. Dahm (2000)[1] suggested that turbulent bursts are caused by counter-rotating parallel vortices adjacent the wall that suddenly leave the wall due to vortex dynamics described by the Biot-Savart effect.

## *1.2 Goal of this work*

The goal of this work is to clarify the mechanism for creation of turbulent bursts by conducting numerical simulations of channel flow with initial conditions that include embedded vortices and other flows that could not easily be produced using experimental apparatus. These embedded vortices and flows were chosen to simulate the effects of devices such as bumps, flippers or jets. The purpose was to clarify which of the components present in turbulent bursts, either those

created by hairpin vortices or by parallel vortices, were necessary for the initiation of the turbulent burst.

Much of this research involved the numerical modeling of vortices, oriented parallel (longitudinally) and perpendicular (transversely) to the direction of the channel flow. Transversely placed vortices were located parallel to the wall in some simulations and in other simulations perpendicular to the wall spanning the channel from wall to wall. These vortical structures were introduced numerically into the flow as initial conditions that were superimposed onto the channel flow. Channel boundary conditions were introduced to model devices such as fluid injection and trip bars or blades extending into the flow.

The objective was to develop the capability to reliably produce turbulent bursts in order to provide turbulent burst specimens to facilitate developing and testing burst control methodologies. Additionally these simulations could help identify the predominant structures in the turbulent boundary layer and provide clues to the mechanism of these structures.

## *1.3 Active control of turbulence*

The goal of active control of turbulent bursts and the resulting reduction in drag is

a fundamental objective of research in turbulence and Micro Electro-Mechanical Systems (MEMS) devices for flow control. MEMS devices for burst control may be constructed as flippers, suction, jet injectors or vortex generators on or near the burst. A better understanding of the mechanism of the burst may suggest other mechanisms and methods of burst control.

An active control system for turbulence consists of three major components: 1. Sensors that will determine the condition of the boundary layer, 2. Some form of algorithm or artificial intelligence that will observe the information provided by the sensors and determine the required actions of the flow control devices, 3. The flow control devices being used.

A better understanding of the mechanism of turbulent burst will aid in determining what conditions within the boundary layer must be known for effective boundary layer control and thus the requirements for sensors. Understanding the relationship between the condition of the boundary layer and the required actions on the fluid to control bursting will assist in determination of an appropriate algorithm for control. And, understanding the required actions on the fluid to control bursting will help determine the devices required for turbulence control.

Prior investigators have utilized mechanisms for the control of turbulent bursts

that are both physical and numerical. For example, Bewley[2] constructed simulations using Direct Numerical Simulation governed by neural network control and Dahm demonstrated physical systems using electrokinetically driven jets governed by deterministic controls.

# 2.Background

This section presents material necessary for the understanding of turbulence and mechanisms for the formation of turbulence. Starting with elements of fluid mechanics boundary layer theory and a description of boundary layer stability, the report investigates the effects of Reynolds number, boundary layer wall length units the turbulent sublayer, transition to turbulence, classical work in boundary layer and modern investigations of boundary layer mechanisms and control.

## *2.1 Fluid Mechanics*

The relationship between fluid stress and the rate of strain is expressed in the constitutive equations also known as Newton's Viscosity Law. The constitutive equations in tensor notation are:

$$T_{ij} = -p\,\delta_{ij} - \frac{2}{3}\mu\,\partial_k \upsilon_k \delta_{ij} + 2\mu\,S_{ij} \quad , \qquad \text{(Eq 1)}$$

where $T_{ij}$ is the stress tensor, $p$ is pressure, $\mu$ absolute viscosity, $v$ velocity and $S_{ij}$ the stress tensor $\delta_{ij}$ the Kronecker delta function.

The continuity equation expresses the fact that for a unit volume there is balance between the mass entering and leaving and the density of the fluid. The continuity equation in vector notation is:

$$\frac{\partial \rho}{\partial t} + \nabla \cdot (\rho V) = 0 \quad . \qquad \text{(Eq 2)}$$

where $\rho$ is the density, t is time, $V$ is the velocity vector and $\nabla$ is the Del operator, $\nabla = i\frac{\partial}{dx} + j\frac{\partial}{dy} + k\frac{\partial}{dz}$ .

The momentum equation is Newton's second law for a continuum. It cannot be applied directly because a fluid does not support the principle of a point mass. However the momentum equation couples the actions of body forces such as gravity with surface forces such as pressure to fluid flow. The momentum equation in vector form is:

$$\rho\left(\frac{\partial v}{\partial t} + v \cdot \nabla v\right) + \nabla p - \rho B = 0 \qquad \text{(Eq 3)}$$

Where $B$ is the body force per unit mass.

The Navier Stokes Equations couple the momentum equation with the constitutive equations to reflect the effects of viscosity. The Navier Stokes equation in vector form is:

$$\rho\left(\frac{\partial v}{\partial t} + v \cdot \nabla v\right) = -\nabla p + \nabla \cdot T - \rho B \qquad \text{(Eq 4)}$$

where $\nabla \cdot T$ is representative of shear forces due to viscosity. For incompressible flow the Navier Stokes equation reduces to:

$$\rho\left(\frac{\partial v}{\partial t}+v\cdot\nabla v\right)=-\nabla p+\mu\nabla^2 v+\rho B \qquad \text{(Eq 5)}$$

The simulations in this work were conducted assuming incompressible flow using the incompressible Navier-Stokes equations.

Another very important quantity is the Reynolds number $R_e=\frac{(UD\rho)}{\mu}$ which is the ratio of inertial forces to viscous forces. Where U is the average velocity, D is the characteristic length (in this case the pipe diameter), $\rho$ the density and $\mu$ the kinematic viscosity.

## *2.2 Boundary Layer Mechanics (Blasius Velocity Profile)*

Fluid flow along a surface has an associated boundary layer in which the effects of viscosity are predominant. Prandtl showed that boundary layers are thin so that the outer flow is largely unaffected.

Boundary layer theory takes advantage of the continuum properties of a fluid so that the velocity at the wall is always equal to zero. This is a reasonable assumption for fluids that can be modeled as a continuum, but becomes invalid for flows of gases at very low pressure where gases must be modeled as particles. Flow regions far from the boundary will feel little effect from the

boundary and move at a velocity approaching the average velocity of the flow that would exist for inviscid flow. The thin region that is affected by the presence of the boundary is called the boundary layer. Boundary layers are categorized as laminar or turbulent according to the nature of the flow characteristics.

The laminar boundary layer is characterized by flow that moves smoothly in layers or lamina. Beginning at the boundary where the velocity is zero and moving outward into the flow each layer moves progressively faster until the layer far from the boundary is moving at the average or outer flow velocity.

In the laminar flow boundary layer the velocity profile is of constant slope near the boundary. Further from the boundary the velocity profile transitions to uniform flow of zero slope. The shear and resulting stress applied to the wall are proportional to the slope of the boundary layer velocity profile near the wall.

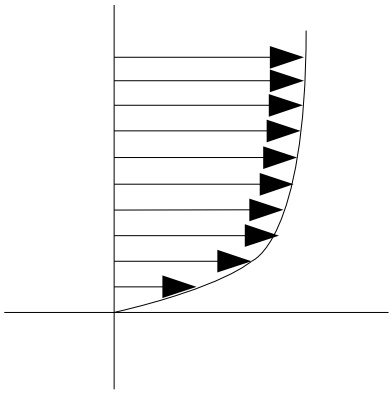

*Figure1: Blasius boundary layer*

An analytical solution to the boundary layer velocity profile over a flat plate with a zero pressure gradient was found by Blasius in 1908. Blasius used the boundary conditions for flow over a plate in conjunction with the equations for continuity:

$$\partial u/\partial x+\partial v/\partial y=0 \qquad \text{(Eq 6)}$$

and momentum:

$$u\frac{(\partial u)}{(\partial x)}+v\frac{(\partial u)}{(\partial y)}=v\frac{(\partial^2 u)}{(\partial y^2)} \qquad \text{(Eq 7)}$$

to solve for the the boundary layer velocity profile. This non-linear partial differential equation was solved using similarity techniques, which yielded functions for the velocity profile for $u/u_0=0.99$ [3] are:

the wall shear stress;

$$\tau_w=\frac{(0.332\rho U^2)}{\sqrt{R_{ex}}} \qquad \text{(Eq 8)}$$

and the friction coefficient;

$$C_f = \frac{(0.664)}{(\sqrt{R_{ex}})} \qquad \text{(Eq 9)}$$

boundary layer thickness;

$$\delta \propto \sqrt{\frac{\nu x}{U}} \approx \frac{5.0}{\sqrt{U/\nu x}} = \frac{5.0\text{x}}{\sqrt{R_{ex}}} \qquad \text{(Eq 10)}$$

where the x is the starting point at which flow has come in contact with the wall or surface. These expressions are valid for $R_e \leq 3\text{x}10^6$ . Above this value flow begins transition into turbulence.

Typically physical experiments conducted to study turbulent boundary layer flow often induced turbulence with some trip device such as a wire or strip of sandpaper. This induced instability of the boundary layer and is necessary for flows of low Reynolds number. However, above a critical value of Reynolds number, a disturbance in not required to induce unstable flow.

## *2.3 Turbulent Boundary Layer*

For flow over a surface, turbulent flow may be divided into three distinct regions. The region closest to the wall is the inner layer which is dominated by viscosity. The intermediate layer which is dominated by momentum exchanges due to velocity fluctuations and the outer layer where the influence of the boundary

becomes negligible. The inner layer can be further divided into the viscous layer and the buffer layer. The viscous layer is a very thin layer attached to the wall where velocities are very low and dominated by viscous effects. It can be shown that the velocity profile in this region is essentially linear. The buffer layer connects the viscous sublayer to the intermediate layer. It is believed that the buffer layer is the region where turbulence is created.[4]

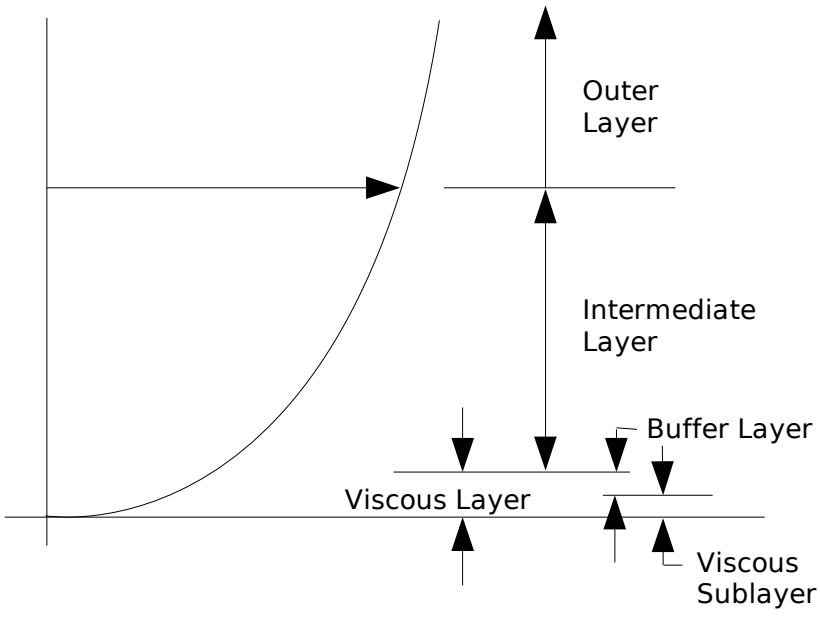


*Figure 2: Boundary layer regions*

## *2.4 Classical Work*

### 2.4.1 Reynolds Experiment

Initial investigations into transition to turbulent flow were demonstrated in a classic experiment by Osborne Reynolds[5] in the 19th century. Reynolds' very simple experimental apparatus consisted of a very smooth glass pipe with a bell mouth entrance immersed within a tank and a valve at the pipe outlet. The pipe was fed from the tank and a means to inject dye into the inlet of pipe was provided. Using this apparatus, Reynolds measured the distance from the entrance of the pipe to the point where the dye stream became unstable. From numerous experiments, Reynolds determined an empirical expression for a dimensionless number that bears his name and correlates flow to transition to turbulence. Reynolds found that at values of $R_e$ above 12000, flow would transition to turbulence and below 2000, flow would always become laminar.

Other investigators managed to achieve a $R_e$ of 40,000 by letting the water in the tank stand for several days and isolating the apparatus from vibration. This

upper number is of no engineering value, but suggests that the initial conditions of the fluid have a significant effect on transition and stability.

When considering flow over a surface or plate, the characteristic length is the distance from the leading edge of the plate. Therefore in flow over a plate $R_e$ starts at zero and increases linearly with distance. The channel flow simulated in this experiment starts with $R_e = 0$ and increases throughout the simulation.

At higher Reynolds numbers all boundary layers will eventually become turbulent. The point of transition depends upon factors such as pressure gradient, wall curvature and wall roughness. Common examples of favorable pressure gradient affecting boundary layer and turbulent flow is channel or pipe flow with lower downstream pressure. Favorable pressure gradient tends to delay the onset of boundary layer instability and turbulence.

Flow over an airfoil is an example of an adverse pressure gradient. After passing the point of lowest pressure above the airfoil, the pressure begins to increase to meet the ambient conditions at the trailing edge. During this increase in pressure or adverse pressure gradient, boundary layer instability generally occurs causing flow reversal and turbulence.

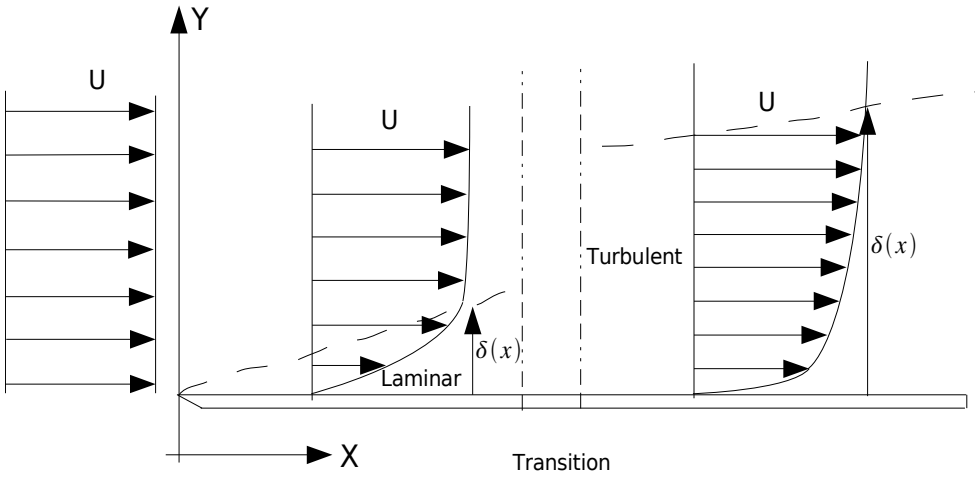


*Figure 3: Transition to turbulent flow over flat plate*

## 2.4.2 Prandtl's Mixing Length Theory[6]

In 1925, Prandtl hypothesized a model of turbulent flow. Prandtl made an assumption that fluid passing along a wall in a turbulent boundary layer could be conceptually coalesced into lumps. A lump displaced from a lower layer $(y_1 - l)$ will have a velocity $u(y_1 - l)$ when displaced $l$ and the resulting change in velocity will be:

$$\Delta u_1 = \bar{u}(y_1) - \bar{u}(y_1 - l) \approx l\left(\frac{d\bar{u}}{dy}\right) \qquad \text{(Eq 11)}$$

and a lump displaced downward from $(y_1 + l)$ will have a velocity

$$\Delta u_2 = \bar{u}(y_1 + l) - \bar{u}(y_1) \approx l\left(\frac{d\bar{u}}{dy}\right) \qquad \text{(Eq 12)}$$

where $l$ is Prandtl's mixing length.

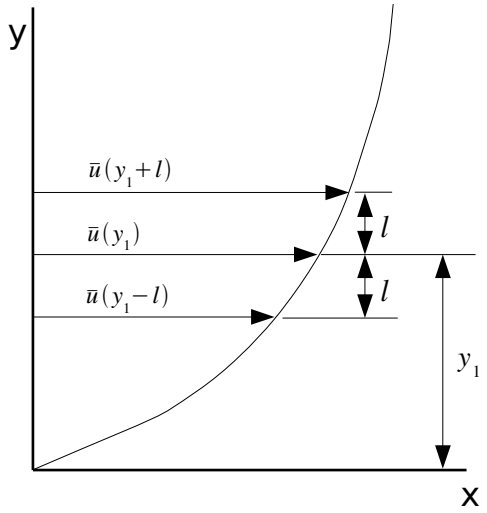


*Figure 4: Diagram of Prandtl's mixing length theory*

The mixing length concept also contributes to developing an important relationship.

From mixing length theory it is possible to determine an expression for an effective or virtual viscosity that results from turbulence. Starting with Stokes's law for laminar flow the shear stress which is:

$$\tau_l = \mu \frac{\partial u}{\partial y} \qquad \text{(Eq 13)}$$

Where $\rho$ is the density $\mu$ the absolute viscosity and $\nu$ is the kinematic viscosity $\nu = \mu / \rho$ .

The concept of a mixing coefficient $A_\tau$ was introduced by Boussinesq[7]. This

leads to an expression for the turbulent shear stress:

$$\tau_t = -\rho \overline{u' v'} = A_\tau \frac{d\bar{u}}{dy} \qquad \text{(Eq 14)}$$

where $\overline{u' v'}$ is the Reynolds stress. Since the mixing coefficient $A_t$ corresponds to the viscosity $\mu$ it is often called the apparent, virtual or eddy viscosity. If the apparent kinematic viscosity $\varepsilon = A_\tau / \rho$ is used in the same manner as the kinematic viscosity $\nu = \mu / \rho$ then:

$$\tau_l = \rho \nu \frac{du}{dy} \qquad \text{(Eq 15 )}$$

for laminar flow may be written in a similar form representing turbulent flow:

$$\tau_t = \rho \varepsilon_\tau \frac{d\bar{u}}{dy} \quad . \qquad \text{(Eq 16)}$$

Equations 12 and 13 may be written:

$$\left|\bar{u}\right| = ½ (\left|\Delta u_1\right| + \left|\Delta u_2\right|) = l \left| \left( \frac{d\bar{u}}{dy} \right) \right| \qquad \text{(Eq 17)}$$

from equation 18 and reasoning regarding the movement of fluid lumps it may be shown that;

$$\overline{u' v'} = -l^2 \left( \frac{d\bar{u}}{dy} \right)^2 \qquad \text{(Eq 18)}$$

The expression for turbulent shear stress may be written:

$$\tau_t = \rho l^2 \left( \frac{d\bar{u}}{dy} \right)^2 \qquad \text{(Eq 19)}$$

however the sign of $\tau_t$ will change and the more correct form is:

$$\tau_t = \rho l^2 \left| \frac{d\bar{u}}{dy} \right| \frac{d\bar{u}}{dy} \qquad \text{(Eq 20)}$$

which is Prandtl's mixing-length hypothesis.

The mixing length concept has proved very useful for the description of turbulent flows where the mixing length must vanish near a smooth wall and for flow over rough surfaces where the mixing length has been shown to be the scale of the surface roughness. Perhaps most important is that the mixing length concept has lead to the concept of virtual kinematic viscosity:

$$\varepsilon_\tau = l^2 \left| \frac{d\bar{u}}{dy} \right| \qquad \text{(Eq 21)}$$

which has been verified by experimental evidence.

### 2.4.3 Boundary Layer Instabilities (Orr-Sommerfeld)

The boundary layer described by Blasius becomes unstable above a critical Reynolds number. This instability was first expressed in the Orr-Sommerfeld equation. Derived first by Orr (1907), then Sommerfeld (1908). It forms the basis of hydrodynamic stability theory.

The Orr-Sommerfeld equation was developed by introducing the perturbation stream function expressed mathematically as a wave function with complex amplitude. These expressions for the stream function were then substituted into the Navier Stokes equations to form the Orr-Sommerfeld equation:

$$(U-c)\left(\frac{d^2\phi}{dy^2}-\alpha^2\phi\right)-\phi\frac{d^2U}{dy^2}=\frac{1}{i\alpha R_e}\left(\frac{d^2}{dy^2}-\alpha^2\right)^2\phi \quad \text{(Eq 22)}$$

This formulation allows the flow to be expressed where $U$ is the free stream velocity, $\phi$ is the amplitude function dependent on y, $\alpha$ is the wave number (real) in the x direction, c is the complex wave speed, amplification factor and circular frequency.

The resulting waves suggested to Tollmien and Schlichting a solution to the Orr-Sommerfeld equation from which they predicted the formation of instability waves above a critical value of Reynolds number. These waves would later be called Tollmien-Schlichting waves.

In the diagram below (figure 5) two curves are shown in Reynolds number- wave-number space. Curve a represents behavior of an adverse pressure gradient $dp/dx>0$ while curve b represents Blasius flow where the pressure gradient is $dp/dx=0$ . The Blasius boundary layer has a critical Reynolds number of

$R_e = U\delta^*/\nu$ =520 and is stable until this value is reached. At $R_e = 520$ the boundary later is unstable to a wave of wavenumber $\alpha\delta^* = 0.3$ . This corresponds to a wavelength of $L \approx 6\delta$ . As the boundary layer thickens the $R_e$ increases and the range of unstable wavelengths becomes larger.

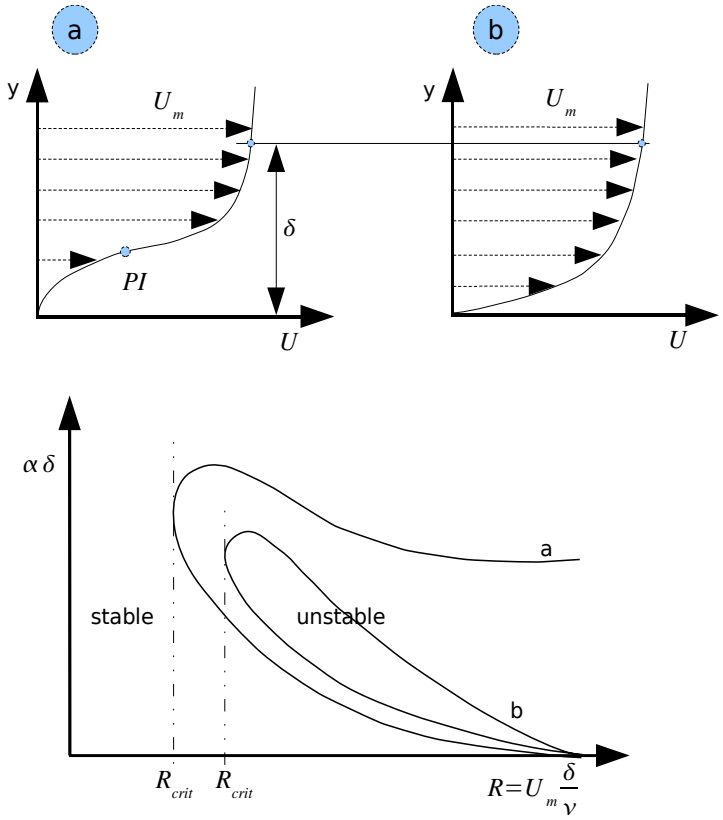


*Figure 5: Boundary layer stability, a) boundary layer with inflection, b) boundary layer without inflection*

When $R_e \to \infty$ the Orr-Sommerfeld equation reduces to a simplified form:

$$\frac{d^2\phi}{dy^2} - \left[\alpha^2 + \frac{1}{U-c}\frac{d^2U}{dy^2}\right]\phi = 0 \qquad \text{(Eq 23)}$$

Known as Rayleigh's equation, where $U$ is the free stream velocity, $\phi$ is the amplitude function dependent on y, $\alpha$ is the wave number (real) in the x direction, c is the complex wave speed, amplification factor and circular frequency.

### 2.4.4 Kolmogorov Length Scale

Kolmogorov hypothesized that turbulent dissipation occurs in a manner that approaches an equilibrium for all flows. While turbulence may be introduced into a flow on various scales by mechanical action, energy dissipation would take place at one equilibrium scale for all flows. From this Kolmogorov argued that there existed a length scale:

$$\eta \equiv \frac{\nu^{(3/4)}}{\varepsilon^{(1/4)}}$$ a time scale, $$t_d = \left(\frac{\nu}{\varepsilon}\right)^{(1/2)}$$ and a velocity scale,

$$v \equiv (\nu\varepsilon)^{(1/4)}$$

where $\varepsilon \approx \frac{u_0^3}{L}$ was the dissipation function, $L$ and $u_0$ were length and velocity scales that characterize large eddies and turbulent dissipation.

The Reynolds number computed from $\eta$ and $\nu$, $\eta v/\nu = 1$ suggests that turbulent structures become smaller in size until they reach a Reynolds number of 1. This has also been described as an "energy cascade" where structures

cascade downward in size and energy.

The Kolmogorov scale has implications for Direct Numerical Simulation. For finite difference computations of partial derivatives to properly resolve the fluid, it is logical to assume that the grid scale should be approximately equal to the Kolmogorov length scale. Experience has shown that a grid spacing of four to six times the length scale is sufficient to provide accurate results.[8]

### 2.4.5 Vortex Dynamics

An import characteristic of the behavior of vortex pairs is that they will propel themselves. This is best recognized by the example of a canoe paddle that induces a pair of vortices after each stroke. The vortices in the water continue to be propelled by their mutual induction. This is a result of the Biot-Savart law that defines the velocity field in proximity to a vortex:

$$v_a(r) = \frac{\Gamma}{2\pi |r - r_a|} \qquad r \neq r_a \quad . \qquad \text{(Eq 24)}$$

In the case of a pair of vortices, each vortex affects the field of the other, resulting in their moving together, and for two vortices of equal strength, moving perpendicular to the line between them. This characteristic is important for the turbulent burst phenomenon.

## *2.5 Modern Work*

### 2.5.1 Boundary layer wall units

From similarity modeling, it has been customary to designate dimensionless units to characterize flow near walls.

The turbulent wall shear stress is defined:

$$\tau_w = \mu \frac{(d\bar{U})}{dy}(0) \qquad \text{(Eq 25)}$$

the wall shear stress can be combined with the fluid density to create a "friction velocity":

$$U_\tau \equiv \left(\frac{\tau_w}{\rho}\right)^{(1/2)} \qquad \text{(Eq 26)}$$

and, hence a corresponding length scale $\nu/U_\tau$ which when used to scale the $y$ coordinate gives the inner variable:

$$y^+ = \frac{(U_\tau y)}{\nu} \qquad \text{(Eq 27)}$$

This expression provides a means for scaling flow in near wall or boundary layer conditions. Notable is that the expression for $y^+$ is very similar to the Reynolds number. The ratio of channel half-width, $h/2$, to $\nu/U_\tau$ is the Reynolds number:

$$R_\tau = \frac{(U_\tau h)}{(2\nu)} \quad . \qquad \text{(Eq 28)}$$

This value may be thought of as the number of wall length scales from the wall to

the channel centerline.

A non dimensional form of wall shear stress and Reynolds stress may be written,

$$\frac{(d\bar{U}^{+})}{dy^{+}} - \overline{uv}^{+} = 1 - \frac{y^{+}}{R_{\tau}} \qquad \text{(Eq 29)}$$

where $\bar{U}^{+} = \bar{U}/U_{\tau}$ and $\overline{uv}^{+} = \overline{uv}/U_{\tau}^{2}$ . When plotted across a channel where $R_{\tau} = 590$ shows that the total stress varies linearly from the wall to the channel centerline. The total stress is the sum of mean viscous stress and Reynolds stress. These are plotted in figure 6 below, showing that the viscous stress is predominant at $y^{+} = 0$ where turbulent stress is negligible but by $y^{+} = 42$ the effects of turbulent stress have become predominant and remain so until reaching the channel centerline. From this it is clear that the majority of turbulence generating activity takes place between $0 \le y^{+} \le 42$ .

Turbulent flow has a significant effect on the boundary layer velocity profile. The slope of the turbulent boundary layer is significantly greater then the laminar boundary layer (figure 7) resulting in significantly greater shear stress, surface friction and drag.

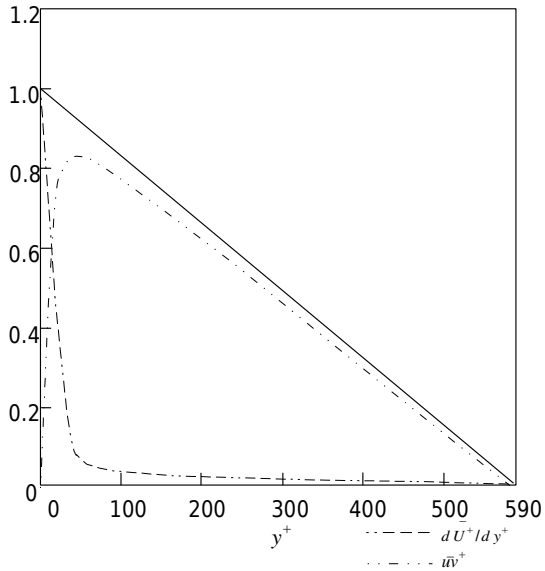


*Figure 6: Decomposition of total stress in turbulent boundary layer, viscous stress, turbulent stress*

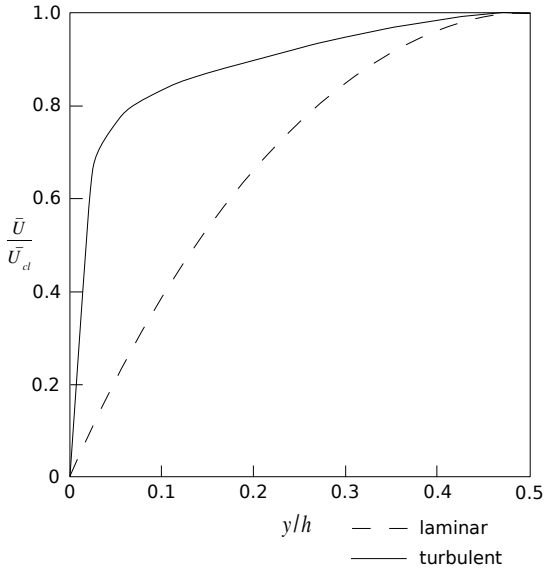


*Figure 7: Boundary layer profiles, turbulent, laminar*

## 2.5.2 Modern Investigators

### *Turbulent Burst Phenomenon*

The phenomenon of turbulent bursts was first discovered in the 1950s[9]. Since

then it has been the subject of considerable study. Initially, physical experiments revealed the nature of the development of the turbulent burst from Schlichting[10] rollers through the process of lifting, folding and stretching of what started as a lateral vortex filament.

There are two schools of thought about the mechanism for formation of the turbulent burst. The first school suggests that the turbulent burst is the result of lifting a section of a vortex oriented parallel to the wall and perpendicular to the flow. This lateral vortex is a result of boundary layer instability. Once lifted, the section of vortex now further from the wall moves faster than the remainder of the vortex. However, the vortex is still a single structure and as the lifted section moves ahead the vortex is stretched into a U shape. This produces the canonical hairpin vortex shape consisting of inclined stretched parallel vortices joined at the head. Bursting occurs when the parallel vortices suddenly move away from the wall bringing slow speed fluid with them and allowing high speed fluid to be swept in underneath. It is the high speed fluid brought in close proximity to the wall that provides the increase in shear stress and resulting drag.

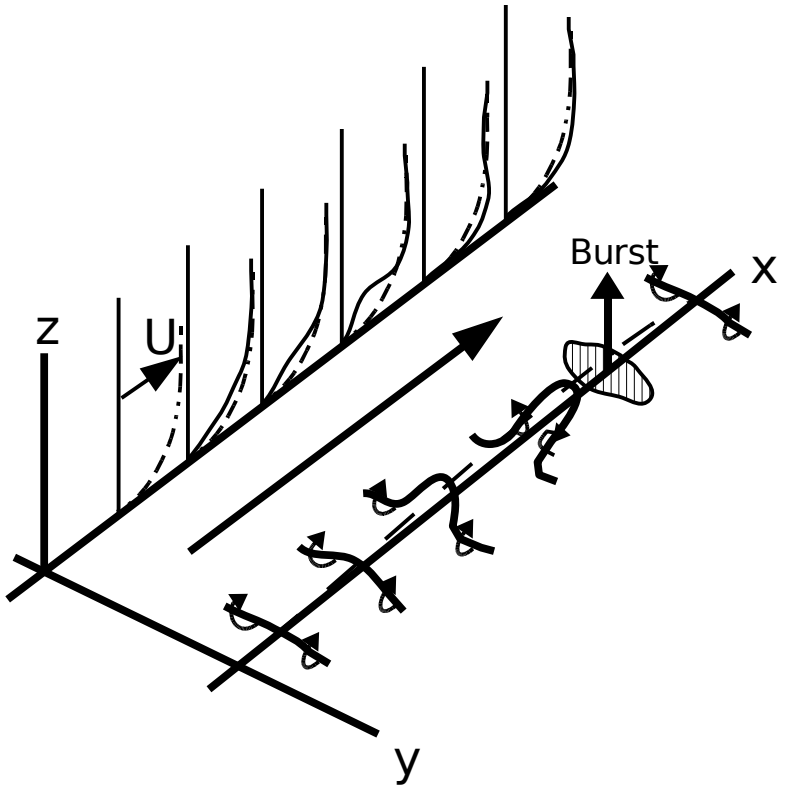


*Figure 8: Concept of turbulent burst cycle with hairpin vortex formation*

The other theory suggests that vortical structures are always present along the wall as a result of folding and stretching of vortices created by boundary layer instability. The turbulent burst is the result of a vortex pair lying parallel to the wall rotating upward between the vortices (figure 9). In a manner similar to the first theory, the upward lifting action results in moving slow speed fluid away from the wall, which is then replaced by high speed fluid in a bursting action.

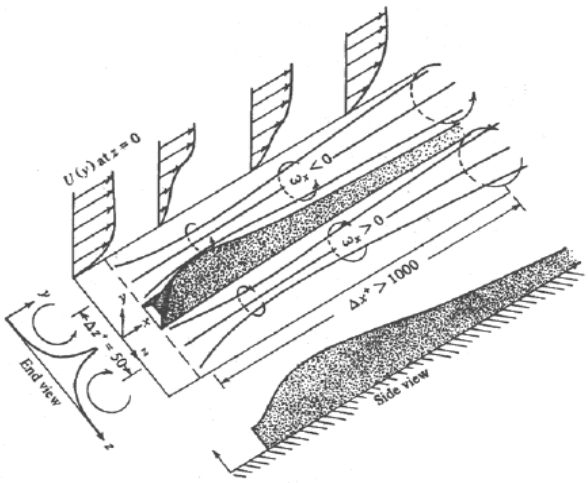


*Figure 9: Counter-rotating streamwise vortices, (Blackwelder and Kaplan, 1976)*

The two theories differ in the way the parallel vortices are arranged. The first theory describes a hairpin structure that is inclined to the flow and bursts occur because of vortex dynamic actions. The second theory suggests that the vortices are merely parallel, not inclined to the flow, do not require stretching or a hairpin shape however bursting still occurs due to vortex dynamics.

### *Sublayer Vortical Structure*

The turbulent boundary layer in equilibrium has a universal and scalable structure.[11] This makes possible the study of general conditions rather than specific turbulent boundary layer conditions. Of most concern is the boundary layer velocity profile or velocity with increasing distance from the wall $y^+$ . At the wall $y \equiv 0$ and $u = 0.$ Very close to the wall, the primary contribution to momentum is molecular diffusion where the kinematic viscosity $\nu$ is the momentum diffusivity. Further from the wall, molecular diffusion remains

relatively constant and effects of momentum transfer due to fluctuation velocity of the flow increase. Since flow velocity at the wall is zero, there cannot be velocity fluctuation. Moving further from the wall, the effect of fluctuation velocity eventually dominates the transfer of momentum.

From this argument, it is customary to define the inner layer as the region of the boundary that is immediately adjacent the wall and dominated by viscous effects and an outer layer that is dominated by turbulent effects. The connecting layer or overlap layer is often referred to as the log layer. This name comes from the "law of the wake" (Coles, 1956) who postulated that the outer part of the inner inner layer and inner part of the outer layer, or overlap region, must form a velocity profile independent of pressure gradient. Asymptotic matching requires that the region have a logarithmic profile.

The inner layer, excluding the log layer extends from $0 \le y^+ \le 30$ , while the viscous inner layer is $0 \le y^+ \le 10$ . The physical thickness depends upon the the physical properties of the fluid such as density, viscosity and pressure gradient.

Because viscous effects are dominant close to the wall $(0 \le y^+ \le 10),$ the velocity profile is linear and results in a uniform vorticity layer adjacent the wall.

Velocity must increase linearly with distance from the wall and thus in the region close to the wall $(0 \le y^+ \le 10)$ the relationship $u^+ = y^+$ will hold. This limits velocities in $y$ and provides stability to the boundary layer. Further from the wall, the no-slip requirement cannot maintain stability; instabilities develop in the form of sinusoidal disturbances in the cross-stream or span-wise direction. Further instability results in elevation of sections of cross-stream vortices, which become exposed to higher speed flow. The elevated sections of vortex move faster and are elongated and oriented in the streamwise direction folding and stretching the vortices. The resulting vortical structures reside at the outer edge of the sublayer have a spacing of about $z^+ = 100,$ a length of $x^+ = 1000,$ varying from 400-1500. The vortical structures are at about $y^+ = 10$ and therefore advect at $u^+ = 10$ [12].

At the outer edge of the viscous sublayer these vortical structures provide the momentum transport from the outer to inner layer and hence the wall. This mechanism provides the greatest influence on the shear stress at the wall. The action of the Biot-Savart law causes the vortices to group into pairs of alternate rotation. The streamwise pairs remain steady until the induced motion of the vortex pair causes the pair to be lifted abruptly from the near-wall region and into the outer layer. This process is called “bursting”. The bursting process

transports low momentum fluid from the near wall region into the outer layer at a much higher rate than would be accomplished by diffusion alone with the result of much higher shear stress and drag.

### *Observations of Coherent Structures*

Hassain, Schoppa and Kim (1997)[13] examined coherent structures (CS) using a then newly developed technique of $\lambda_2$ visualization of vortical structures. The $\lambda_2$ technique clearly identified vortical structures by computing values of vortical structure intensity for the flow field. This results in a scalar field for $\lambda_2$ that can be plotted as an iso-surface. This technique is also used in this work for visualization and production of movies. The $\lambda_2$ technique will be further discussed in *Methodology.* Hassain et al examined the results of numerical simulation in a channel flow examining the region $y^+ < 60$ . Their observations show coherent vortical structures that are inclined with the flow, approximately 9 degrees from horizontal and yawed to the flow +/-4 degrees.

Hassain et. al. evaluated these structures statistically to determine the spatial relation of near wall coherent vortical structures, ensemble averaging the significant structural properties and compared them with experimentally observed events of the bursting process. Their results showed excellent correlation with

experimentally observed events such as Reynolds stress distribution, low speed streaks and pressure variation.

The results also showed that the vast majority of vortical structures were oriented roughly in the streamwise direction and were generally much shorter than the $y^+$ = 1000 length indicated by the evidence of low speed streaks and more on the order of length $y^+$ = 200. Further hairpin vortices were rarely observed in keeping with the observations of the work of this paper.

Vortical structures arranged in head to tail groups produce low-speed streaks (figure 8) much longer than the structures themselves. This explains the previous observation of low speed steaks of $y^+ = 1000$ .

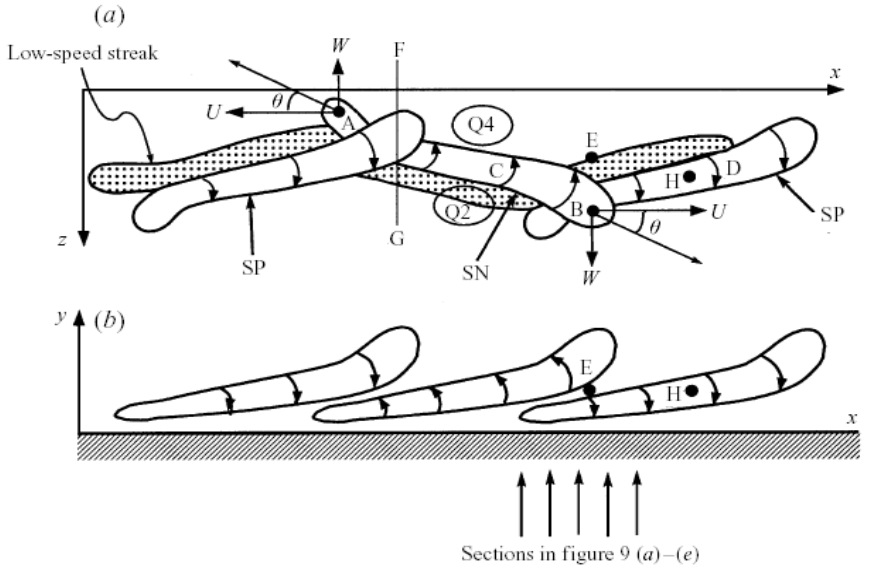


*Figure 10: Low speed streaks from groups of vortical structures, Hassain, Schoppa and Kim (1997)*

Sectional views of the vortical structures taken in the x-y plane (figure 10) above show vortical structures that were often stacked and counter rotating.

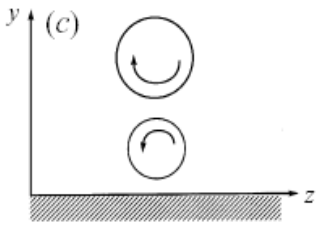


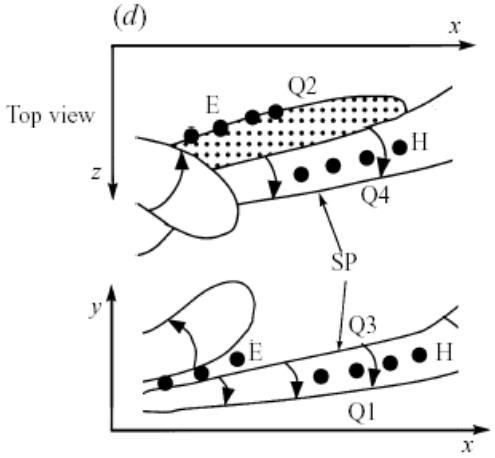


*Figure 11: Stacked counter rotating vortical structures, plan view shown at right Hassain, Schoppa and Kim (1997)*

Stacked counter rotating vortical structures provide a mechanism for exchange of fluid momentum between inner and outer boundary layer. The flow field about the vortex core sweeping the wall transports slow speed fluid up to the vortex above, and is then swept by the upper vortex to the outer region of the boundary layer. Simultaneously high speed fluid is swept down to the lower vortex and then down to the wall.

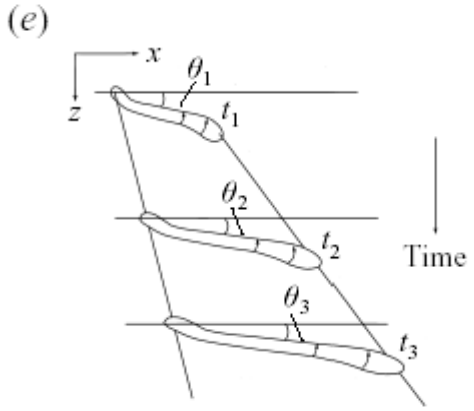


*Figure 12: Growth of vortical structures with time, Hassain, Schoppa and Kim (1997)*

The canonical hairpin vortex was seldom seen in these simulations. This suggests that the predominant turbulent feature is the single sided vortical structure. This is in contrast to the study of the hairpin vortex and the turbulent burst phenomenon.

## *2.6 Control Using Actuators*

Interruption of bursting mechanism has been one of the targets for control of the burst process. It is believed that using a device to disturb the pairs of vortices, either by increasing or decreasing their separation distance thereby preventing the effect of the Biot-Savart principle can arrest the burst development process. This disturbance has been introduced in the form of an array of electrokinetically controlled microactuators (Dahm & Diez-Garias, 2000). These microactuators either pushed or pulled a small amount of fluid into or out of the channel. The resulting effect was to separate the longitudinal vortex pairs that would otherwise be induced by the Biot-Savart principle to form a burst.

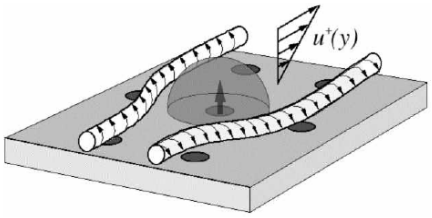


*Figure 13: Electro kinetic actuator (Dahm, 2000)*

These arrays were controlled using a closed-loop control system or deterministic approach where sensors measured wall shear stresses and or pressure and actuators were controlled through a specific algorithm. Another control approach was to use artificial intelligence in the form of a neural network that

observed and trained to the same sensor inputs as used for the deterministic system to control the actuators.[14] Both forms of control have been successfully demonstrated in experiments with remarkably similar results. The deterministic control and neural network control both provide reductions in wall shear stress and drag of 20-30%.

## *2.7 Previous Research in Boundary Layer Control*

Investigations have shown that the primary precursors to turbulent burst involve a region of locally adverse pressure gradient[15], a lifting of the boundary layer due to flow over some obstruction such as flapper or hemispherical bump[16], by injection of fluid[17] or an acoustic excitation through a small hole in the floor of the test apparatus[18]. These experiments resulted in either single or multiple turbulent bursts and accompanying vortical structures. In some cases the disturbances spread laterally in the flow to form wider turbulent spots, while in others hairpin vortices also appeared upstream of the primary vortex. In all cases secondary vortical structures were formed in addition to the primary hairpin vortex. The development of these structures was a function of the Reynolds number of the flow and the size and duration of the disturbance introduced into the flow field.

Other research suggests that the initial instability leading to the onset of turbulence and turbulent burst can be driven by disturbances in the freestream

flow at some distance from the wall. If these disturbances occur at the appropriate frequency or wave number, they will penetrate the boundary layer causing instabilities and transition to turbulence.

### 2.7.1 Flow Fields Resulting from Devices

Several experimental studies were conducted that involved injection of fluid into the flow field resulting in what at least could be interpreted as a turbulent burst. The rate and volume of injection separates the injection process into two categories.

#### *Fluid Injection*

Singer and Joslin (1995) conducted an experiment using numerical simulation where fluid was injected slowly at a velocity of approximately 25% of average velocity ( $.25U$ ) for a long duration through a longitudinally oriented slot (figure 14). The primary effect was a decrease in the momentum of the boundary layer and the introduction of a boundary layer velocity profile inflection.[19] The resulting flow structures were observed by plotting pressure as an iso-surface.

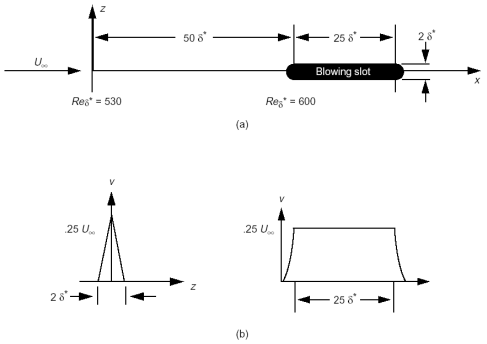


*Figure 14: Geometry of fluid injection slot, (Singer, Joslin, 1995)*

Structures resulting from fluid injection are accurately shown as pressure iso-surfaces. The developed hairpin vortex along with in-line and side-lobe secondary vortices, necklace vortices and a new u-shaped vortex are described in the figures shown below. This development continues to become a young turbulent spot.

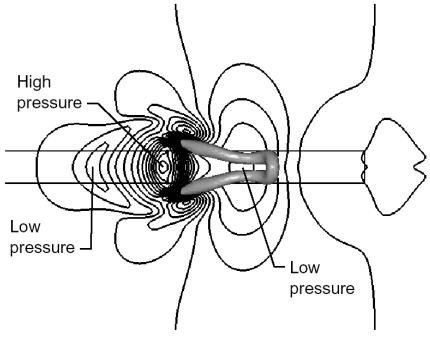


*Figure 15: Plan view, hairpin vortex resulting from fluid injection, t=42.0 iso-pressure plot (Singer, Joslin, 1995)*

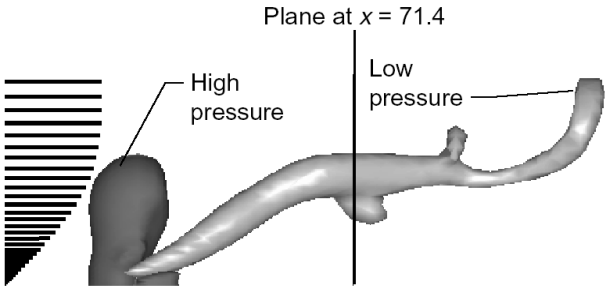


*Figure 16: Elevation view, hairpin vortex resulting from fluid injection, t=50.25, iso-pressure plot (Singer, Joslin, 1995)*

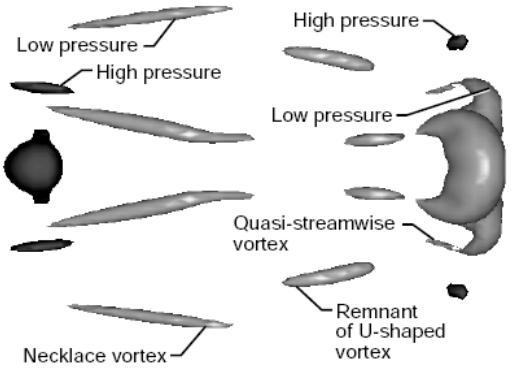


*Figure 17: Plan view of turbulent structure, t=80.70, iso-pressure plot (Singer, Joslin, 1995)*

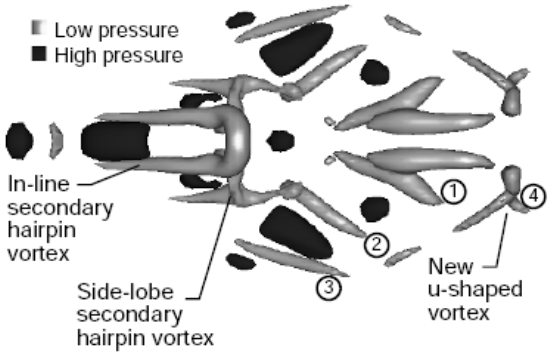


*Figure 18: Plan view of turbulent structure, t=153.10, iso-pressure plot, (Singer, Joslin, 1995)*

In a similar but physical experiment conducted by Haidari and Smith (1994), fluid

was injected through a long, longitudinally oriented 2 mm wide slot at a velocity similar to that of Singer and Joslin. Here flow was visualized using hydrogen bubbles or dye in the fluid. Haidari and Smith intended to duplicate the slow spot or streak that preceded the observed turbulent burst. With this apparatus Haidari and Smith were able to produce excellent examples of hairpin vortices throughout a range of Reynolds numbers from 250 to 490 based on boundary layer thickness. Their measurements of the boundary layer profile downstream of the injection point were fundamentally similar to those of Singer and Joslin; both experiments showed a boundary layer inflection leading to instability and subsequent formation of a canonical hairpin vortex.

In an experiment conducted by Amini and Lespinard (1982), fluid was injected through a horizontal plate parallel to the flow. The jet, driven by an acoustic device, was formed through a hole rather than a slot as in the experiments described above. The jet velocity was approximately $1.25U$. This relatively high speed, short duration jet provided the effect of lifting of the flow in the vicinity of the hole rather than creating a boundary layer velocity inflection. The measured effects were less pronounced than the experiments previously described where slow speed injection produced a boundary layer inflection however provided evidence of turbulent spot generation measured near the injection port and at repeated downstream locations.

### *Hemispherical Obstruction*

Tufo, Fischer, Papka and Szymanski (1999) conducted an experiment using direct numerical simulation (DNS), to investigate the flow field in a channel where a single stationary hemispherical roughness element was placed on the channel floor.[20] The flow about this obstruction displayed a standing horseshoe vortex about the upstream edge of the hemisphere and adjacent the floor of the channel. Hairpin vortices were periodically shed from the top of the hemisphere leaving a series of hairpin vortices advected downstream. The flow field was visualized using the $\lambda_2$ techniques of Jeong and Hussain. Observation of the boundary layer velocity profile showed results similar to the experimental and DNS work described above by Singer and Joslin, Hadair and Smith and Amini and Lespinard.

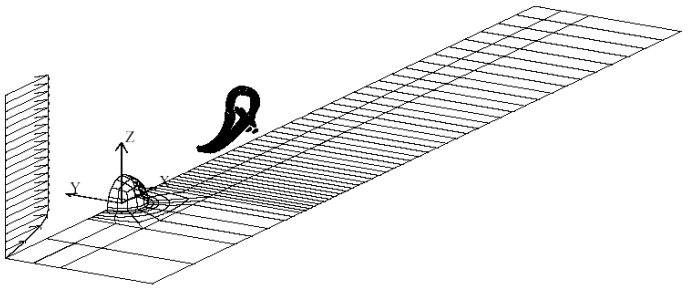


*Figure 19: Computational grid for hemispherical bump, (Tufo, Fischer, Papka and Szymanski, 1999)*

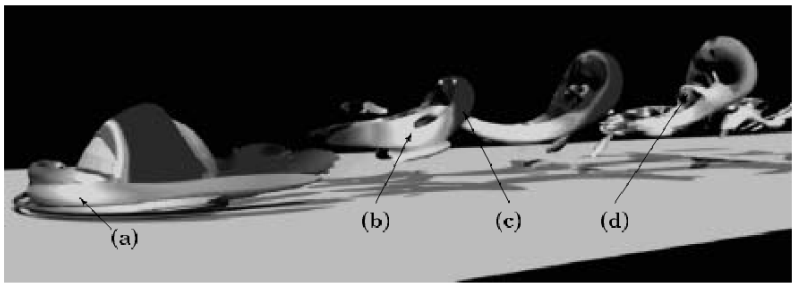


*Figure 20: Flow over hemispherical bump showing repeating hairpin vortices and upstream vortex at wall, (Tufo, Fischer, Papka and Szymanski, 1999)*

### 2.7.2 Transition Excited by Freestream Disturbances

A recent work by Durbin and Wu (2007)[21] takes a different approach to the transition to turbulence in a boundary layer by examining how disturbances in the flow some distance from the wall effect the formation of boundary layer instabilities and transition to turbulence. This work did have precedence. Taylor (1936) had argued that the absence of evidence to support Tollmein-Schlichting waves suggested that instability leading to transition could be driven from disturbances located in the freestream. When the Reynolds experiment was repeated after allowing the tank supplying the pipe to settle for several days, the settling period extended the Reynolds number for transition from 12,000 to 40,000, suggesting that the initial conditions within the fluid away from the boundary layer play a significant role in transition to turbulence.

Earlier work by Klebanoff (1971) observed characteristic low frequency disturbances in the flow that induced variations in the thickness of the boundary layer. These fluctuations in the boundary layer were referred to as "breathing" modes which were characterized by buffeting of the laminar layer.

Durbin et. al. performed numerical simulations of decaying grid turbulence that showed freestream turbulence of low frequency could penetrate the boundary layer causing longitudinal jets.[22] These jets of high-velocity flow are shown as contours in *u* velocity. Within the jets, turbulent spots may appear, which arise without previous instability at the surface as indicated by slow speed streaks. Orr-Sommerfeld theory provides an explanation of the transition of the freestream turbulence into jets within the boundary layer, but not the transition to turbulence.

Numerical simulations of regions prior to the transition to a turbulent spot showed that the disturbances above the boundary layer induced fluctuations in the boundary layer bringing up slow speed fluid causing instabilities leading to transition to turbulence.

This research was motivated in part from the investigation of turbine cascades and passage of wakes from blades and vanes on downstream surfaces as well

as fundamental research of turbulence over flat plates. Previous investigation by Schlichting suggested that the surface roughness of turbine blades and vanes should not exceed 0.002 mm[23]; however the initiation of boundary layer instability and transition to turbulence due to wake passage suggests that a super-finished surface has limited effectiveness in avoiding transition to turbulence in a turbine cascade.

## 2.7.3 Near Wall Vortical Flows

### *Vortex Stretching*

Work of Moffatt, Kida and Ohkitani (1994)[24] indicated that for a vortex to persist in viscous fluid with dissipation requires the vortex be subject to positive strain. Failure to maintain strain, or negative strain, will cause the vortex to die out and the vortex will tend to align itself with the strain direction. Their mathematical analysis was done in the context of subscale vortices present in turbulent boundary layer flow.

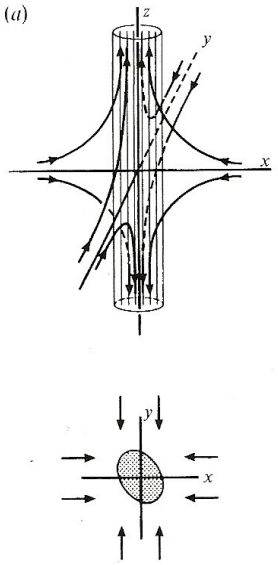


*Figure 21: Vortex stretching, vortex shown in axial strain with fluid entering sides of vortex core, (Moffatt, Kida and Ohkitani, 1994)*

In a series of physical experiments by Petitjeans (2001)[25], a standing vortex was created across the bottom of a transparent water channel. The vortex was initiated by the vorticity present in the boundary layer profile at the bottom of the channel. The vortex was maintained in strain and kept stationary by suction applied through a pair of opposing slots located at the side walls of the channel and adjacent the bottom wall. Dye was added to the flow to readily observe the vortex. Increased suction directly affected the size and vorticity of the vortex, which is consistent with increased rate of entrainment of fluid and increased rate of strain. Notable is that the strain applied to the vortex not only was able to align the vortex, but also to keep the vortex from being swept downstream by the channel flow.

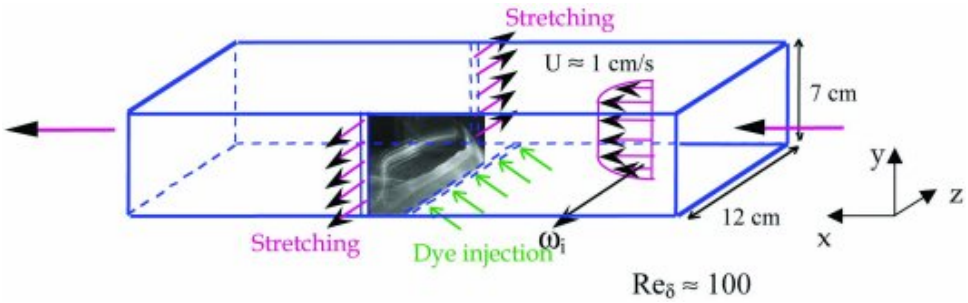


*Figure 22: Diagram of experimental apparatus for vortex stretching, suction ports located opposed adjacent bottom wall, dye injected through bottom wall upstream of vortex. (Petitjeans, 2001)*

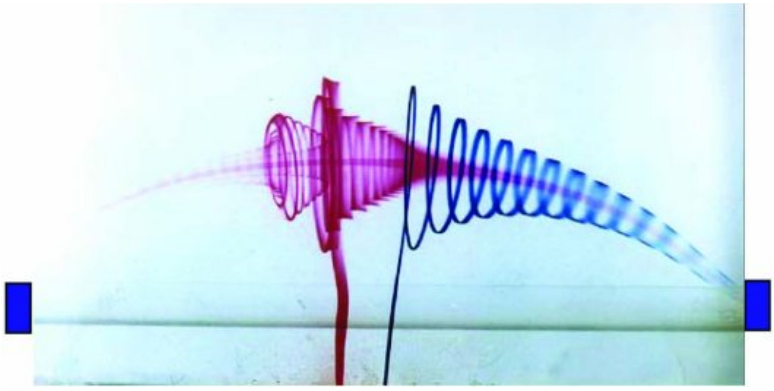

*Figure 23: Stretched vortex captured in channel shown with dye injected (Petitjeans, 2001)*

In a second experiment, two rotating disks 10cm in diameter with suction ports at their center were placed in a tank face-to-face spaced approximately 15cm apart. The disks were rotated to establish a rotating flow then suction was applied to the

ports at the center of the disks. The flow rate through the suction ports was measured before and after the vortex was established. The lower pressure in the vortex center balanced the flow through the suction ports regulating the rate of flow and the rate of strain on the vortex. This suggests that the vortex has a built in pressure feedback mechanism that keeps the vortex stable and will keep the vortex intact for as long as axial strain is maintained.

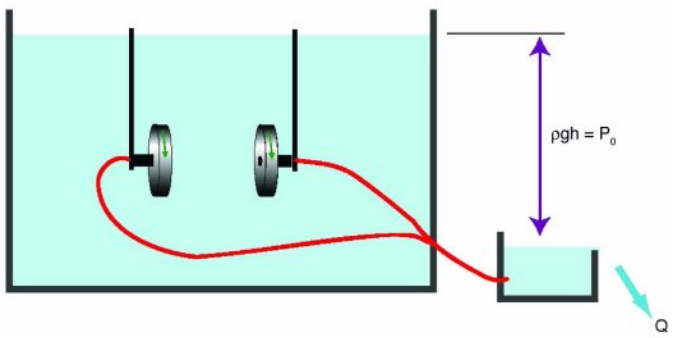


*Figure 24: Apparatus for starting and sustaining a vortex in continuous strain. (Petitjeans, 2001)*

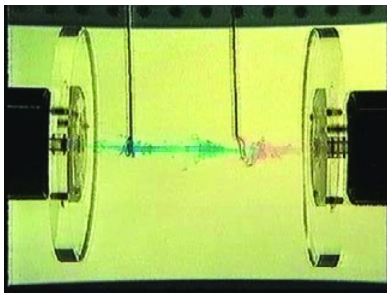

*Figure 25: Vortex between plates sustained in continuous strain marked with dye injection (Petitjeans, 2001)*

Experiments by Petitjeans demonstrated the phenomenon of vortex stretching and fluid entrainment and complimented the mathematical work of Moffatt, Kida and Ohkitani (1994). The work showed that the vortex must be kept in axial strain to persist, will align with the axial strain and will entrain fluid through the walls of the vortex core and deliver that fluid out the ends of the vortex. The vortex will also produce a circular flow field around its core that is of importance to the structure of the boundary layer.

# 3. Methodology

## *3.1 Direct Numerical Simulation (DNS)*

Modeling was conducted using Direct Numerical Simulation with an incompressible finite difference solver on a staggered grid. The algorithm was Gauss-Seidel using Black and Red successive over relaxation (SOR). The domain of the solver was 66 x 66 x 66. The channel was dimensioned $x=2\pi, y=2$ and $z=\pi$ . The upper and lower boundaries, perpendicular to the y axis, were solid, fixed and no slip. The boundaries perpendicular to x and z axes were periodic.

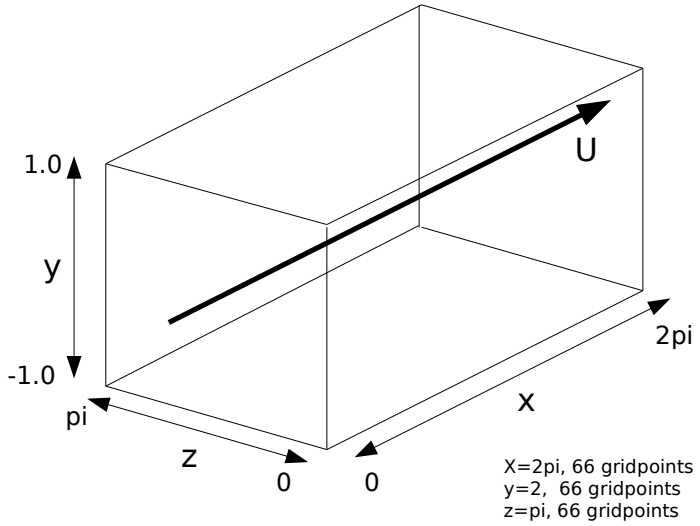


*Figure 26: Rectangular channel computational domain*

Initial flow conditions consisting of uniform channel flow and some combination of embedded vortices that were computed separately then introduced into the channel prior to beginning computation of the flow field time solution. Uniform

flow was achieved by assigning all grid locations the same velocity vector values and pressure scalar values. In this case velocity values in v, and w =0.

Periodic boundaries have the effect of an infinite domain in the direction of the periodicity. A boundary was made periodic by setting the flow field values at the grid locations at one wall (inlet) of the channel equal to the flow field values at the grid locations on the opposite wall (outlet). To create a periodic boundary in x, for example, requires that the values for velocity u, v, w and pressure p at 1, y, z are equal to the values of velocity u, v, w and pressure p at 66, y, z. This was accomplished during execution of a subroutine that updates the boundary conditions. Fixed or moving wall boundary conditions are updated in a similar manner by specifying that the boundary velocities equal zero or for a moving wall some specified value.

The periodic boundary was useful for eliminating channel wall effects where a boundary layer was not desired. Another valuable attribute was the effect of reducing the required computational domain size. Rather than compute a channel of very large length to establish boundary layer properties the periodic boundary allowed the flow characteristics to develop by recirculating the flow. This was an important advantage. The disadvantage was that computational flow features that are long may overlap on themselves. In this work, the flow

features were generally short and did not overlap. In some cases, flow features moved upstream, intersected and passed through downstream moving features, but did not seem to have an effect on the flow solution.

## *3.2 Grid spacing and Kolmogorov length*

The Kolmogorov length is the dimension of the smallest disturbance than can exist within a flow. This suggests that for numerical simulations of turbulent flows that the grid size should be roughly equal to the Kolmogorov length for partial derivatives to be properly resolved. In practice a grid size of four to six times the Kolmogorov length has proved adequate.[26] Further because of wall effects flow adjacent the wall is characterized by turbulent structures of smaller dimensions. This permitted the use of a grid that was closely spaced near the wall with progressively larger spacing away from the wall. In this work the grid in x and z was uniform while the grid in y was sinusoidally spaced.

Calculations of the Kolmogorov length, using units of the channel dimensions, showed that the grid had adequate resolution. The grid spacing in the x direction was:

$$\frac{2\pi}{66} = 0.09519 \qquad \text{(Eq 30)}$$

and in the z direction,

$$\frac{\pi}{66}=0.04759\,. \qquad \text{(Eq 31)}$$

The sinusoidal grid spacing in y varied from 0.04869 at mid-channel to 0.001764 at the wall. The Kolmogorov length scale is a function of the dissipation and the kinematic viscosity:

$$\eta\equiv\nu^{(3/4)}/\varepsilon^{(1/4)}. \qquad \text{(Eq 32)}$$

Dissipation $\varepsilon$ may be estimated using:

$$\varepsilon\approx\left(\frac{\bar{U}}{\rho}\right)\left(\frac{dP}{dx}\right)=\left(\frac{0.55}{1.0}\right)(0.00178)=0.000979 \qquad \text{(Eq 33)}$$

then the Kolmogorov length scale was:

$$\eta\equiv\mu^{(3/4)}/\varepsilon^{(1/4)}=\frac{(0.000333)^{.75}}{(0.000979)^{.25}}=0.01394\,. \qquad \text{(Eq 34)}$$

Comparing the Kolmogorov length with the grid spacing for x,

$$\frac{dx}{\eta}=\frac{(0.095419)}{(0.01394)}=6.8469, \qquad \text{(Eq 35)}$$

and z,

$$\frac{dz}{\eta}=\frac{(0.04759)}{(0.01394)}=3.4139, \qquad \text{(Eq 36)}$$

shows reasonable grid size for numerical simulation. Comparing the grid spacing in the y direction at mid-channel,

$$\frac{dy}{\eta}=\frac{(0.04869)}{(0.01394)}=3.4928, \qquad \text{(Eq 37)}$$

and at the wall,

$$\frac{dy}{\eta} = \frac{(0.001764)}{(0.01394)} = .1265. \qquad \text{(Eq 38)}$$

These grid spacings were well within the requirements for resolving partial derivatives in direct numerical simulation.

## *3.3 Initial conditions*

In each instance the preprocessor generated a uniform flow field in the x direction $(u = const, v = 0, w = 0).$ Added to this flow field were vortices oriented in various directions. Vortices were placed longitudinally within the flow, i.e. in the x direction, laterally or perpendicular to the flow direction and parallel to the bottom wall of the channel and vertically across the channel extending from the bottom wall to the upper wall of the channel.

Where vortices were placed parallel to the solid boundaries, the simulation included single and multiple vortices both co-rotating and counter-rotating. These vortices were placed at various locations from close to the wall to mid-channel.

Where vortices were placed perpendicular to the solid boundaries, the protocol included simulations of counter rotating vortex pairs placed at various spacing equidistant from the end of the channel. Vortex pairs were introduced where

flow between the vortices was both upstream and downstream.

## *3.4 Upstream and downstream vortices*

When vortex pairs extending wall to wall were introduced into the channel as part of the initial conditions two rotation configurations were possible. These were labeled upstream vortex pair and down stream vortex pair. Diagrams describing these vortical arrangements and their rotation are shown below.

The upstream vortex pair shown in the diagram below was characteristic of the pair of vortices that would be created by flow about an obstruction or as the result of a hairpin vortex.

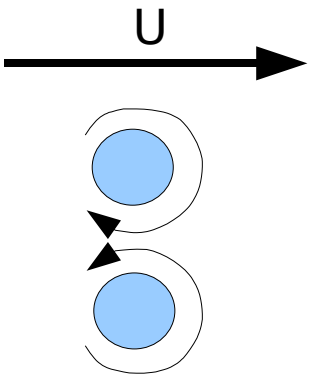


*Figure 27: Upstream vortex*

This type of vortex pair tended to be more persistent when introduced into the channel as an initial condition.

The downstream vortex pair as shown in the diagram below was introduced into

the channel for comparison with the upstream vortex pair. The rotation was opposite of the upstream vortex pair and was opposite rotation produced by flow about an obstacle or hairpin vortex.

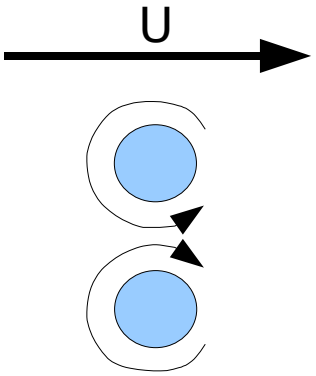


*Figure 28: Downstream vortex*

## *3.5 Channel Flow Parameters*

Simulations were conducted using values flow velocities, pressure gradient, channel dimensions and other parameters which have been previously used in other successful investigations of turbulent flow.

Flow parameters for the channel were:

Initial velocities,

$$u = 0.55, v = 0.0, w = 0.0,$$

pressure gradient,

$$dp/dx = 0.00178,$$

channel height,

$$h=2.0,$$

viscosity,

$$\mu=0.000333,$$

and density,

$$\rho=1.0.$$

Units are based upon channel dimensions of $x=2\pi, y=2.0$ and $z=\pi$ which resulted in all calculated length values to be in the units of the channel dimensions. Using the channel height as the characteristic length the Reynolds number was:

$$R_e=\frac{Uh\rho}{\mu}=\frac{0.55(2.0)1.0}{0.000333}=3300 \qquad \text{(Eq 39)}$$

The initial velocity profile in the channel was uniform and with no boundary layer. Throughout the simulation a boundary layer was established and grew in thickness, however, the flow remained laminar except for the vortical structures that were deliberately introduced as part of the initial conditions.

Most simulations were conducted for a period from $t_1=0$ to $t_2=21.$ For this period the Reynolds number based upon the distance of travel along the wall varied from zero to:

$$R_e = \frac{U(U t_2)\rho}{\mu} = \frac{0.55(0.55)21.0(1.0)}{0.000333} = 19076. \qquad \text{(Eq 40)}$$

This corresponded to a boundary layer thickness ranging from zero at the start of the simulation to:

$$\delta_x = \frac{5.0\text{x}}{\sqrt{R_{ex}}} = \frac{5.0(21.0)0.55}{\sqrt{19076}} = 0.418, \qquad \text{(Eq 41)}$$

at the end of the simulation period. The velocity profile for the channel was plotted for various times and is shown below. The calculated value for boundary layer thickness corresponds to the measured thickness shown below.

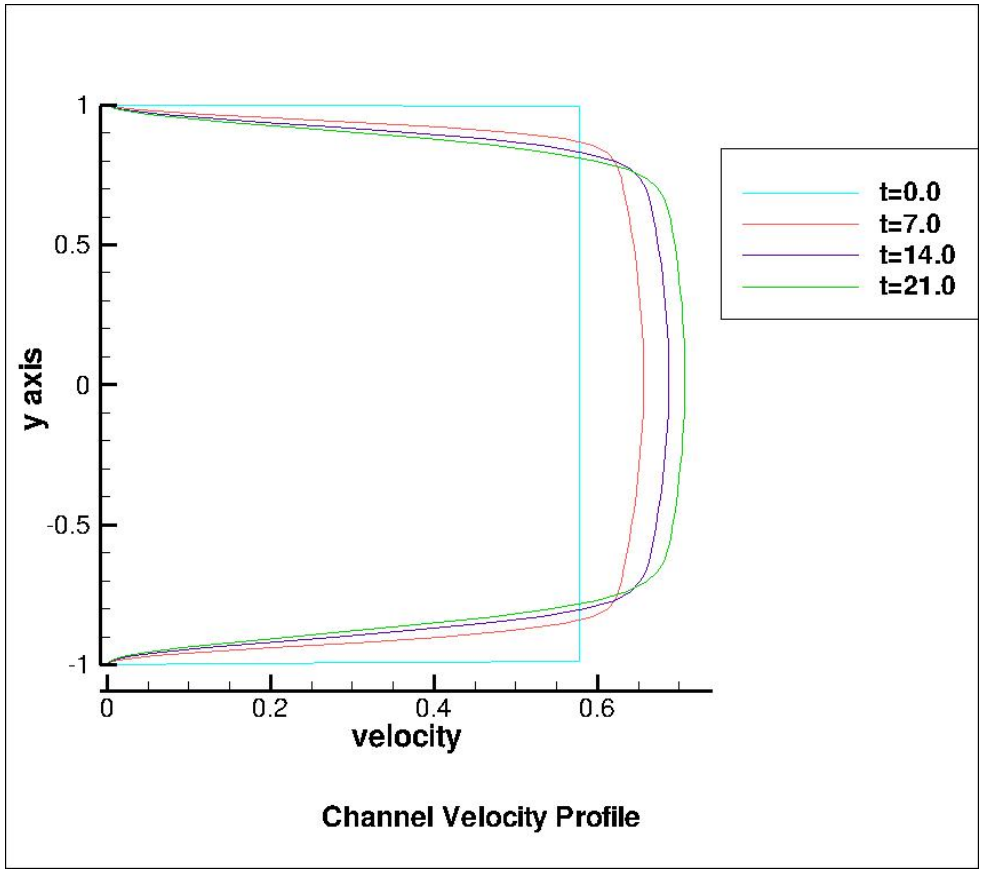


*Figure 29: Channel velocity profile at t=0.0, 7.0, 14.0 and 21.0.*

## *3.6 Vortex Calculation*

During preprocessing the initial flow field was established and written to file as an array of velocity vectors $(u, v, w)$ and pressure $(p)$ values. These values corresponded to grid locations within the channel $(i, j, k)$ . Vortices were then computed and superimposed on the initial flow field file.

Vortices were added by computing the required velocity vectors to represent vortices in the desired locations. The velocity vectors were calculated in two dimensions in the plane, or layer of grid points, perpendicular to the axis of the vortex. The calculations were repeated for each layer of grid points until the entire channel had been completed. First, the location of vortex center, vortex strength and other parameters such as time and direction of rotation were specified. For each grid point within the plane the orthogonal distances between the vortex center and grid point were calculated. These values were used to form a vector orthogonal to the radius vector and extended from the grid point. This vector was the same length as the radius vector. The vector was normalized by dividing by the magnitude of the radius and then scaled to the proper magnitude by computing the tangential velocity as a function of radius using the formula for tangential velocity of the Taylor vortex;

$$v_\theta = \frac{H}{8\pi}\frac{r}{\nu t^2}\exp\left(-\frac{r^2}{4\nu t}\right) \qquad \text{(Eq 42)}$$

where $v_\theta$ is the velocity, $H$ is the total angular momentum in the vortex, $r$ is the radius, $\nu$ the viscosity and $t$ the time.

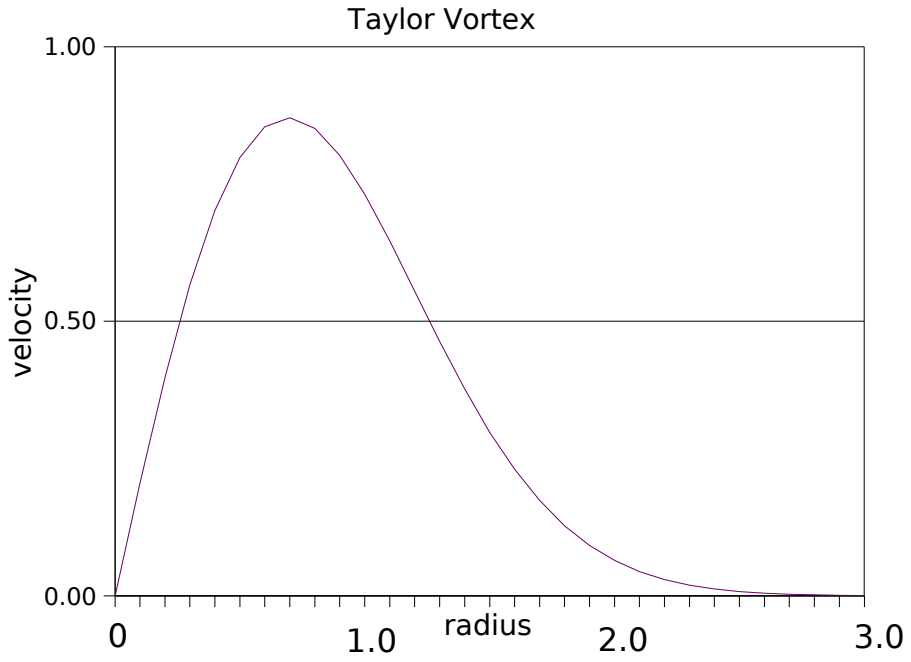


*Figure 30: Taylor vortex velocity distribution*

This process was repeated for each gridpoint throughout the plane and then repeated for each plane throughout the channel. The calculated vector values for the vortex were then added to the flow field vectors.

Values for time and total momentum for the Taylor vortex calculation were selected to limit the maximum initial velocity of the vortex to be within stability requirements for the DNS flow solver. The other criteria was to generate a vortex

with velocities similar to that generated by flow about an obstruction or device placed within the flow.

## *3.7 Obstructions*

In several simulations vortices were created by placing obstructions in the flow field for specified time intervals. These obstructions were simulated by introducing code in the boundary condition subroutine of the flow field solver. At the end of each time step the boundaries were reestablished setting velocities to zero at no slip boundaries and velocities and pressures at repeating boundaries to the value of the opposite wall. This section of the boundary condition subroutine set velocities to zero at locations corresponding to the boundaries of obstructions.

Where longitudinal vortices were introduced into the channel some simulations included a lateral trip bar which is shown in the diagram below.

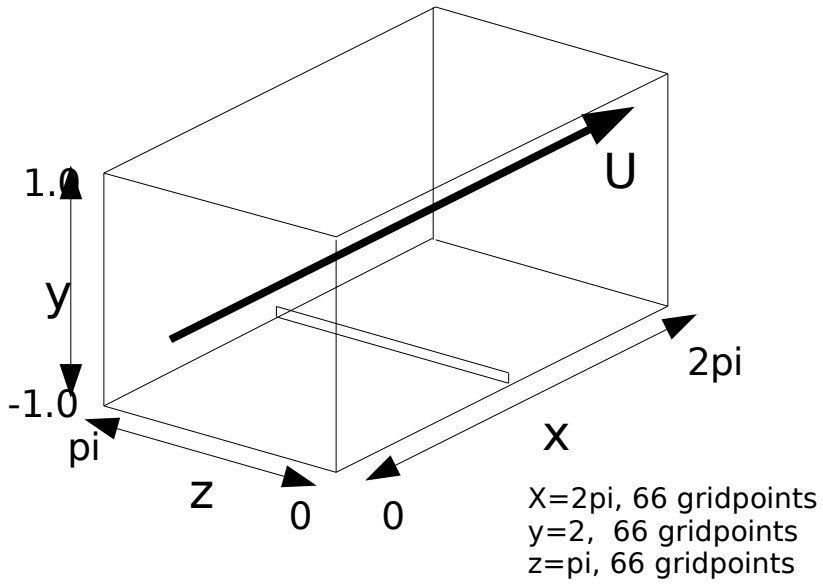


*Figure 31: Trip rail at wall*

Vortices were created in the channel by placing a narrow obstruction extending from wall to wall as shown in the diagram below.

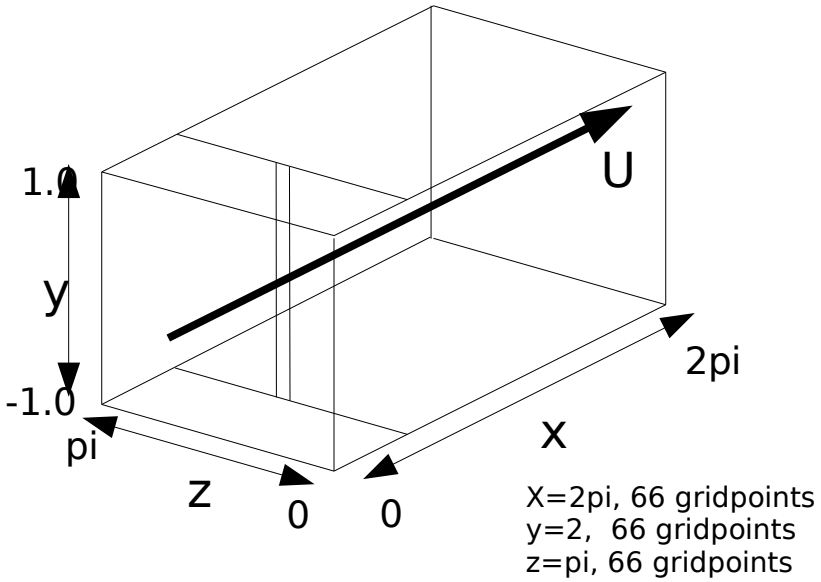


*Figure 32: Narrow obstruction, wall to wall*

Vortices were created in the channel in a pattern that resembled the unstable

lateral vortex. This was accomplished by placing a lateral bar along the bottom wall with a small blade projecting up at the center of the bar. This is shown in the diagram below.

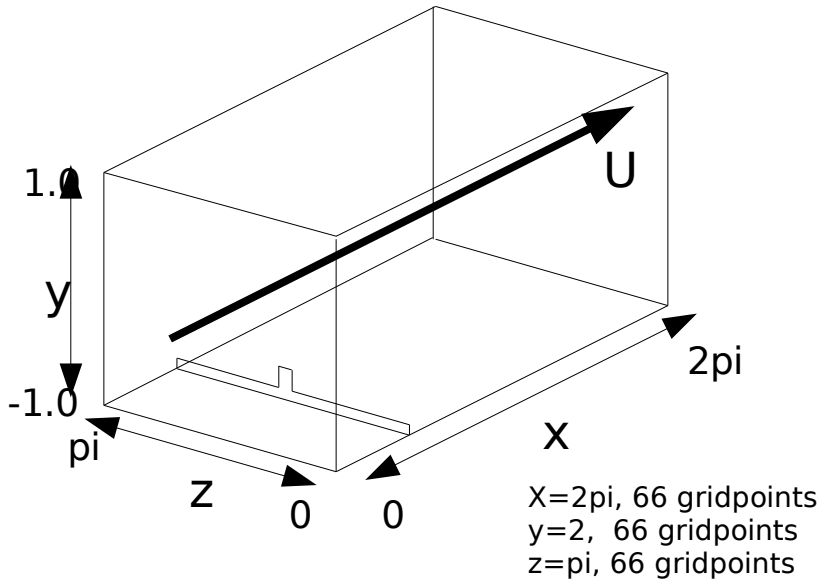


*Figure 33: Rail and blade obstruction*

## *3.8 Fluid Source and Sink*

One method of inducing a hairpin vortex is to inject fluid into the boundary layer. Slowly introducing fluid into the boundary layer has the effect of locally decreasing the boundary layer velocity and momentum. This creates a boundary layer inflection and some degree of lifting of the flow. The boundary layer inflection then leads to an unstable boundary layer profile that results in a lateral vortex in the flow that has been lifted. The lifted portion is stretched by the shearing action of the boundary layer ultimately creating a hairpin shaped vortex. This technique is similar to the work of Singer and Joslin[27].

Fluid injection was simulated by adding code to the boundary condition subroutine of the flow solver. After the flow solver updated the boundary conditions an additional routine set values at the boundary in the desired velocity and shape to form an inlet source. To assure that the pressure solver would converge an outlet was also created with the same flow rate as the inlet.

The velocity for the inlet source was set to approximately 25% of the average flow or $0.25U$ , in a manner similar to Singer and Joslin. The injection slot had proportions of approximately 1 x 5 oriented longitudinally parallel to the flow. The outlet slot was created with the same size and velocity.

## *3.9 Vortex Identification and Visualization*

The identification and visualization of vortices has been difficult because behavior rules for vorticity are valid in the inviscid limit whereas vorticity in the boundary layer is largely dependent upon viscosity effects. In general methods that use pressure minima, vorticity maxima or vortex line integration often lead to incorrect vortex identification.

Jeong & Hussain[28] developed a robust method for identification and visualization based upon the local pressure behavior. Jeong & Hussain recognized that the

effects of unsteady straining can create a pressure minimum without vortical or swirling motion and viscous effects can eliminate a pressure minimum in flow with vorticity. They separated these effects by taking the gradient of the Navier-Stokes equations:

$$a_{(i,j)} = -(\frac{1}{p})\, p_{(,ij)} + \nu u_{(i,jkk)}, \qquad \text{(Eq 43)}$$

where $a_{(i,j)}$ is the acceleration gradient and decomposing into

$$a_{(i,j)} = \left( DS_{ij}/Dt + \Omega_{ik}\Omega_{kj} + S_{ik}S_{kj} \right) + \left( D\Omega_{ij}/Dt + \Omega_{ik}S_{ki} + S_{ik}\Omega_{kj} \right) \qquad \text{(Eq 44)}$$

symmetric and antisymmetric parts

The antisymmetric part is the vorticity transport equation and the symmetric part is:

$$\frac{DS_{ij}}{Dt} - \nu\, S_{(ij,kk)} + \Omega_{ik}\Omega_{kj} + S_{ik}S_{kj} = -\frac{1}{\rho}\, p_{(,ij)} \qquad \text{(Eq 45)}$$

The first two terms, unsteady irrotational straining and viscous effects are discarded leaving $S^2 + \Omega^2$ the only parts that determine local pressure minima due to vortical motion. Jeong & Hussain defined a vortex core as a connected region with two negative eigenvalues. Functionally if the second eigenvalue $(\lambda_2)$ is negative then the location is within the vortex core.

In practice $\lambda_2$ is found by taking the eigenvalues of the 3 x 3 symmetric tensor:

$$A_{ij} = \sum k = 1,3 \left( \Omega_{ik} \Omega_{kj} + S_{ik} S_{kj} \right) \quad \text{(Eq 46)}$$

where,

$$\Omega_{ij} = \frac{1}{2} \left( \partial u_i / \partial x_j + \partial u_j / \partial x_i \right) \quad \text{(Eq 47)}$$

and,

$$S_{ij} = \frac{1}{2} \left( \partial u_i / \partial x_j - \partial u_j / \partial x_i \right) \quad \text{(Eq 48)}$$

are the symmetric and antisymmetric components of the velocity gradient tensor, $\nabla u$ .[29]

Sorting the eigenvalues $\lambda_1 \leq \lambda_2 \leq \lambda_3$ if $\lambda_2$ is negative then there are two negative eigenvalues. The resulting computation yields a scalar value for $\lambda_2$ at each grid point. When visualizing a vortex a value of $\lambda_2$ slightly less than zero is used for iso-surface plotting to indicate the envelop of the vortex.

## *3.10 Movie Production*

Much of this work involved identification of turbulent vortical structures as they developed in time. The post processing routines developed for $\lambda_2$ calculation provided a time series of files containing $\lambda_2$ scalar data for each grid point. Using Tecplot[30], iso-surfaces of $\lambda_2$ were plotted revealing the details of vortices

within the flow field.

Tecplot provided for automation of movie making using a relatively comprehensive macro language. Movies were made to depict the time evolution of vortical structures by combining the series of flow field $\lambda_2$ iso-surface files into a movie using the AVI format. Various views were chosen to best show the important details of the flow field.

The process of conducting a simulation involved numerous steps which are outlined below.

The flow DNS flow solver required specification of a number of parameters describing the fluid, channel size, number of grid points, output file names and times, and total duration of flow field simulation. These parameters were contained in an input batch file read by the flow solver program at the beginning of the simulation.

The solver also read a file containing the starting flow field file or flow field initial condition. The starting flow field file was generated by an additional program that allowed for the insertion of vortices in the flow field. Any number of vortices could be inserted parallel to any of the three orthogonal axes and at any set of

locations specified in a batch file. Vortices could be of constant value over their length or vary sinusoidally as a function of longitudinal position.

Once the flow field calculation was completed the flow field data must be further processed. The post processor program first read the parameters in a batch file which described the file names of the flow field files to be read and corresponding file names of the $\lambda_2$ data to be written. The post processor then read each individual flow field file and computed the $\lambda_2$ value at each grid point within the flow field. The values for $\lambda_2$ were then written to a file with the corresponding grid point locations and in the appropriate format for plotting in Tecplot. The post processor ran automatically, reading each flow field file, computing values of $\lambda_2$ and writing the data to each of the files specified in the batch file.

Once the $\lambda_2$ files were written, a Tecplot macro was used to assemble the individual files into a movie in the .avi format. Once in the .avi format the movie could be viewed using any of numerous windows movie viewers.

# 4. Results

The following results describe the movies made from a time series of iso-surfaces of $\lambda_2$ scalar fields. These scalar fields resulted from Direct Numerical Simulations of a channel with various devices placed in the flow or initial conditions which included vortices placed in the flow before the simulation was begun. These techniques were used to simulate the production of vortical structures and hairpin vortices.

## *4.1 Longitudinal Vortices*

Longitudinal orientation referred to alignment with the x axis of the channel and in the predominant flow direction. Longitudinal vortices were placed in the channel at various spacing and various distances from the wall, out to the centerline of the channel. Vortices were placed in pairs or multiples, co-rotating and counter-rotating.

### 4.1.1 Longitudinal Vortex Pairs

Simulations of pairs of longitudinal vortices showed that the vortex pair induced four other vortices. These additional vortices were located 45 degrees above and below the vortex centerline. These vortices dissipated after traveling several lengths of the channel without showing any signs of instability that could lead to the generation of turbulent bursts. Of note was that the vortices did not travel due to Biot-Savart effects.

Movie: WorkE_iso.avi pair of longitudinal vortices at y=-0.5

## *4.2 Lateral Vortices*

### 4.2.1 Lateral and Parallel to Wall

In the next group of simulations lateral vortices were placed in the channel parallel to the lower wall and transverse or perpendicular to the direction of flow. Because these vortices extend from one recurring boundary to the opposite recurring boundary they are essentially infinitely long vortices. These vortices were placed in the flow as initial conditions and at various distances from the lower wall, out to the centerline of the channel. Vortices were placed individually, in pairs or multiples , co-rotating and counter-rotating.

#### *Eight Co-Rotating Vortices*

In this simulation multiple vortices were immediately induced by the initial eight vortices. The vortices appeared unstable in their vertical location. In some cases bumps appeared on the surfaces of the vortices however all vortices remained intact and did not breakdown or form longitudinal or stretched vortical structures. As the simulation proceeded the smaller vortices dissipated or coalesced into larger vortices that appeared to roll along the lower wall of the channel. By the end of the simulation the vortices had coalesced into two large vortices that were approximately three times the diameter of the original vortices and appeared to roll along the bottom wall of the channel.

Movie: tst020_iso.avi, eight laterally placed co-rotating vortices at y=-0.9

#### *0.0.0.1 Eight Lateral Counter-Rotating Vortices*

As in the previous simulation, multiple vortices were immediately induced by the initial eight vortices. The vortices exhibited significant vertical movement. Numerous bumps were observed on the surface of the vortices; however no vortex instabilities were observed. The vortices largely dissipated by the end of the simulation leaving one small vortex. No instabilities occurred that could lead to stretched vortical structures or hairpin vortices.

Movie: tst036_iso.avi, eight laterally placed counter-rotating vortices at y=-0.9

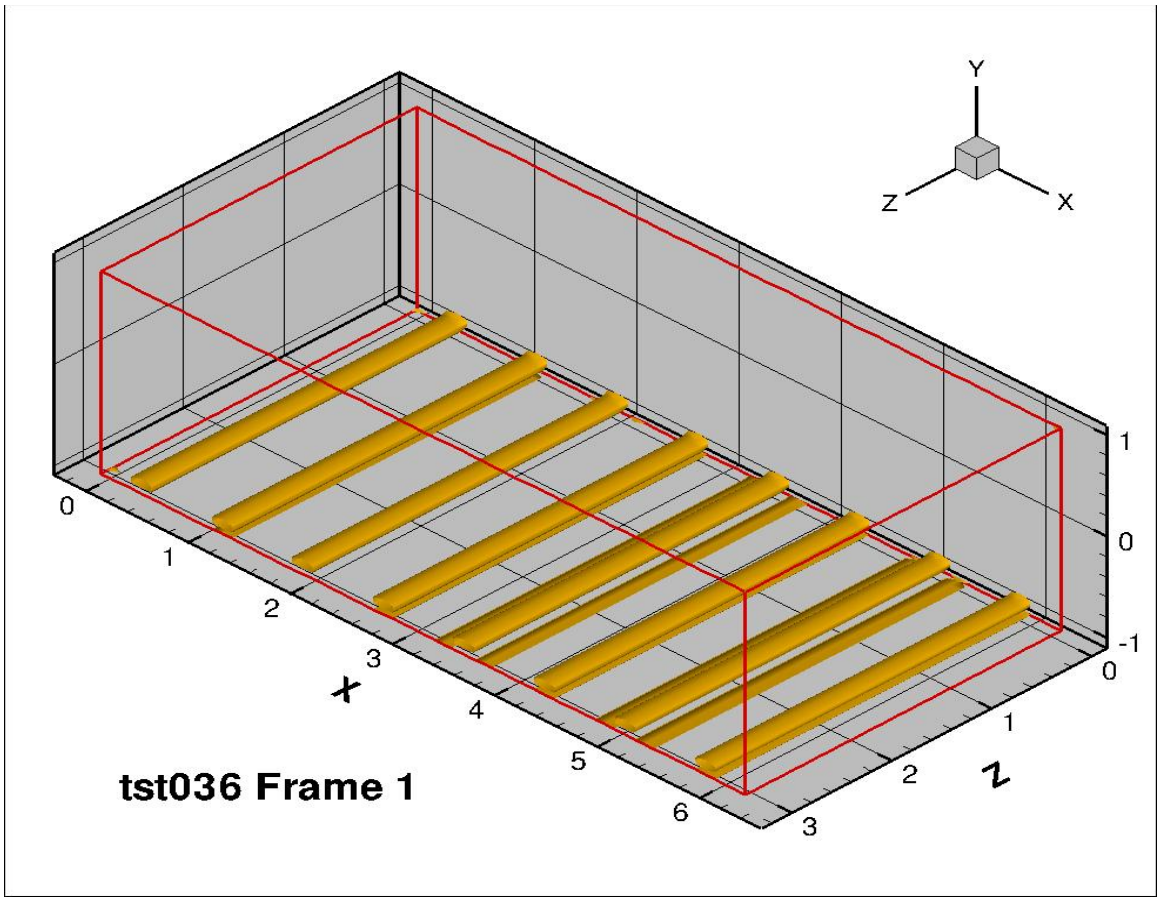

*Figure 34: 8 lateral counter rotating vortices, frame 1*

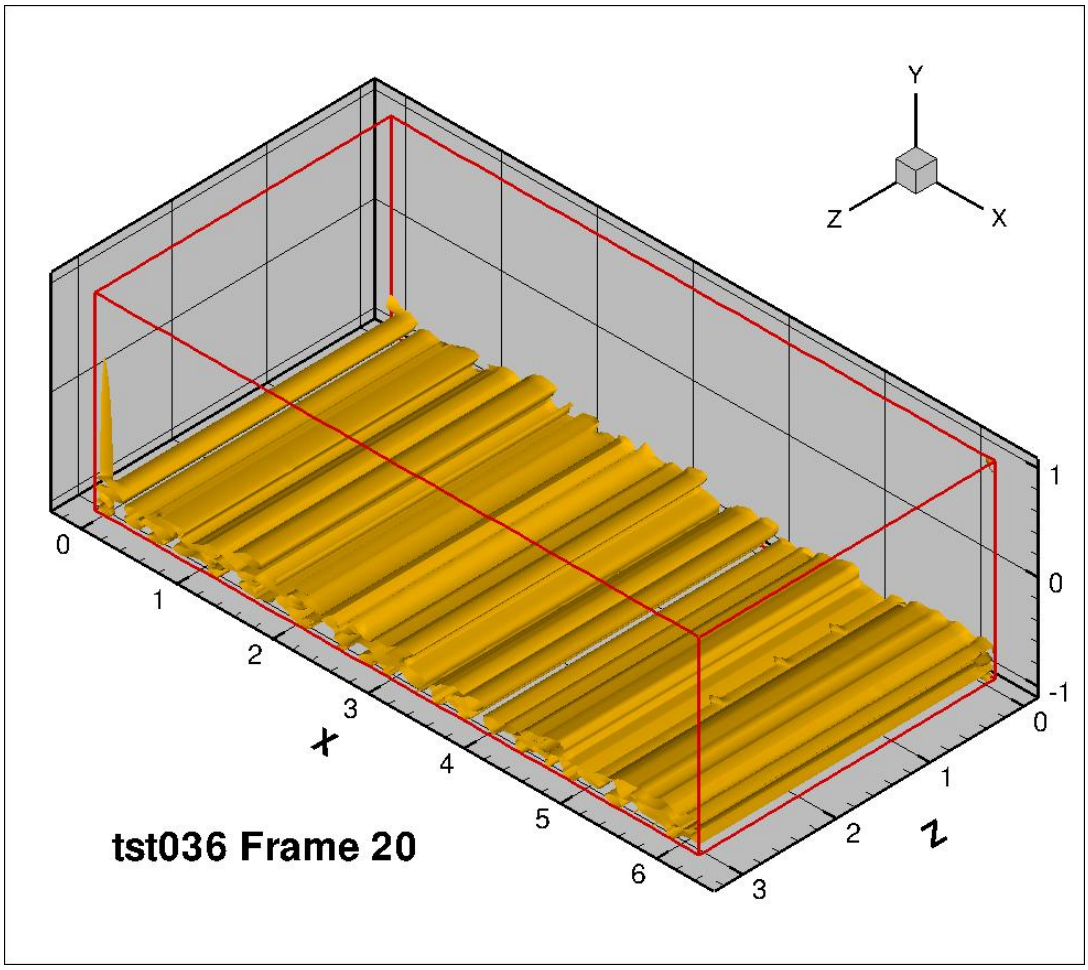

*Figure 35: 8 lateral counter rotating vortices, frame 20*

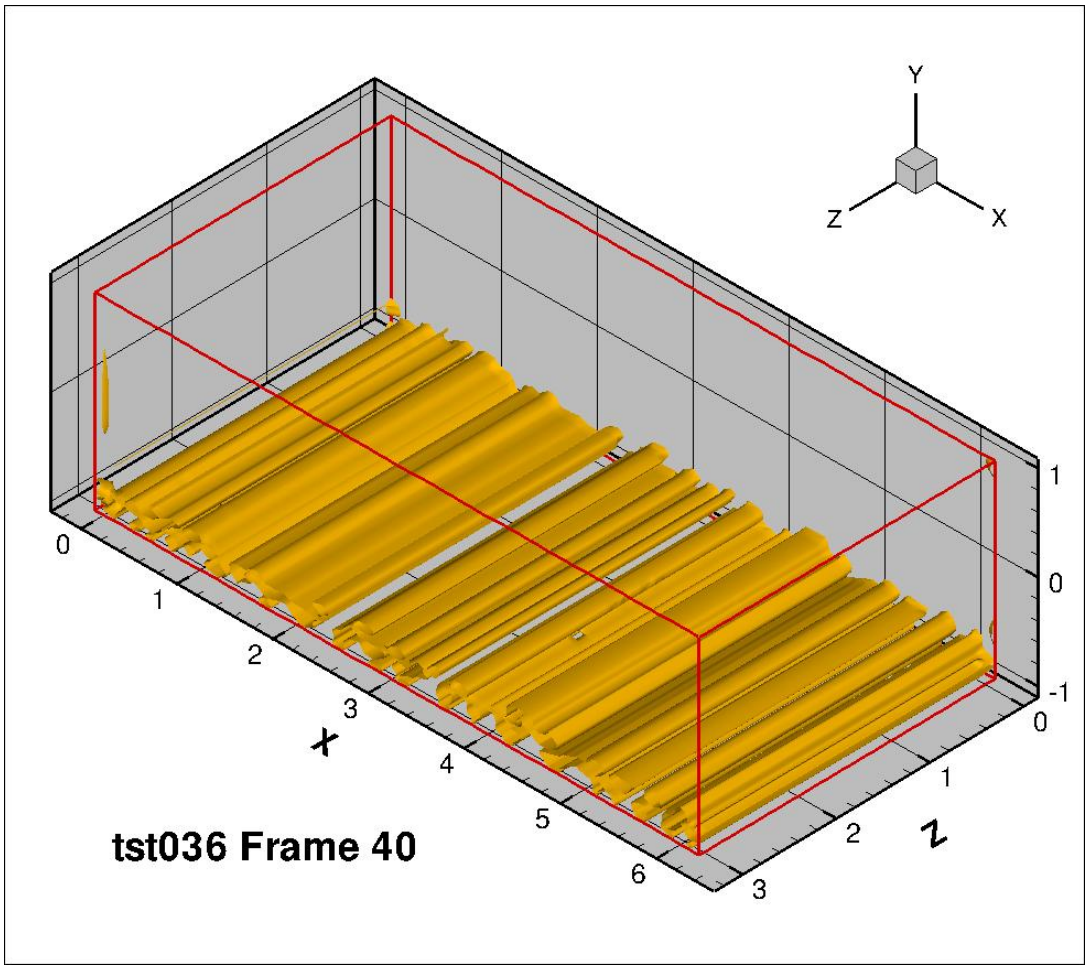

*Figure 36: 8 lateral counter rotating vortices, frame 40*

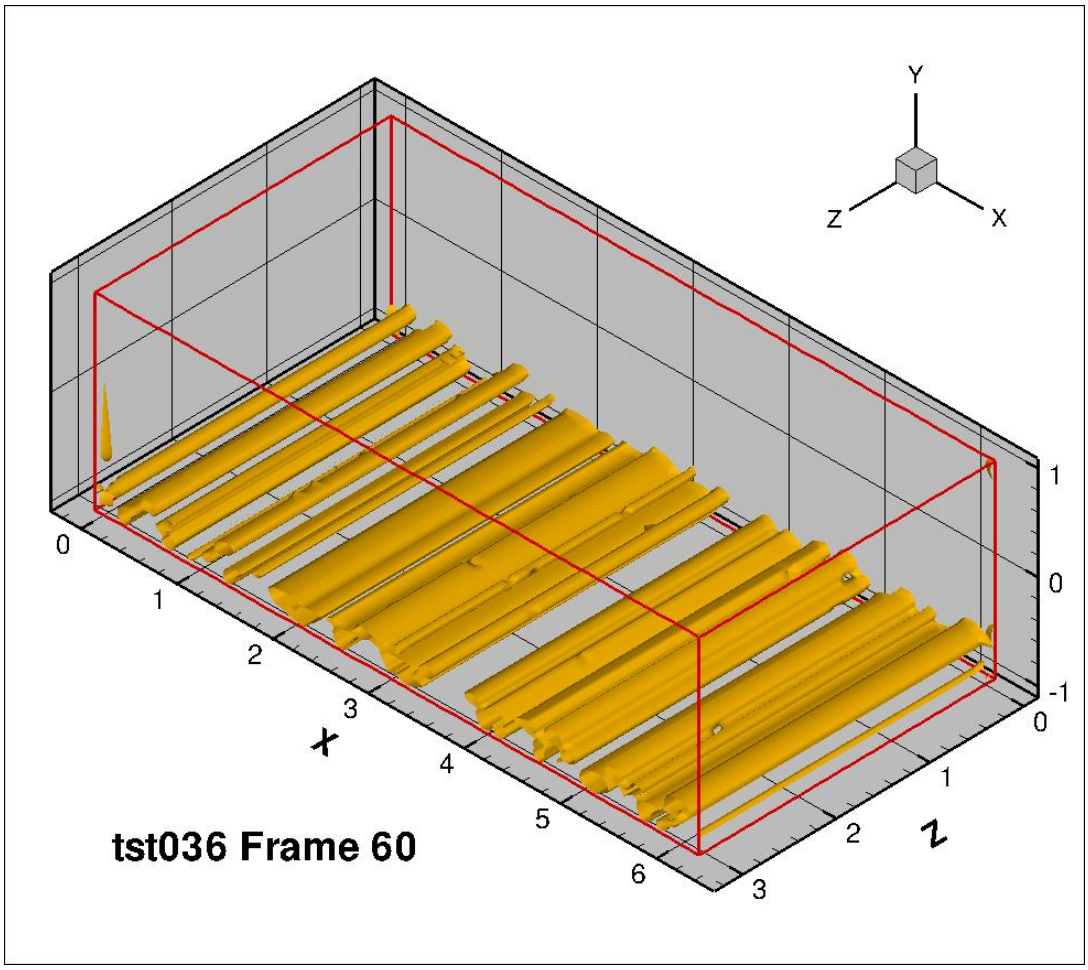

*Figure 37: 8 lateral counter rotating vortices, frame 60*

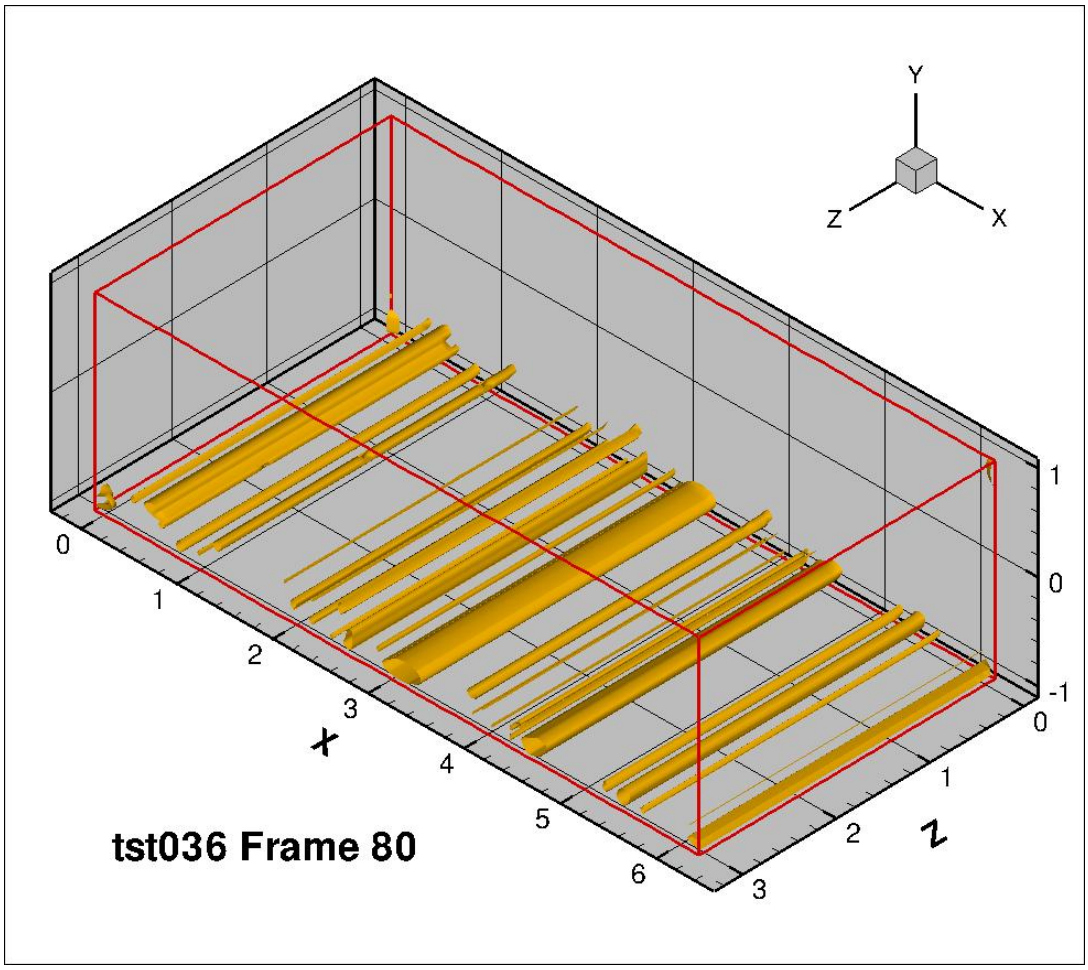

*Figure 38: 8 lateral counter rotating vortices, frame 80*

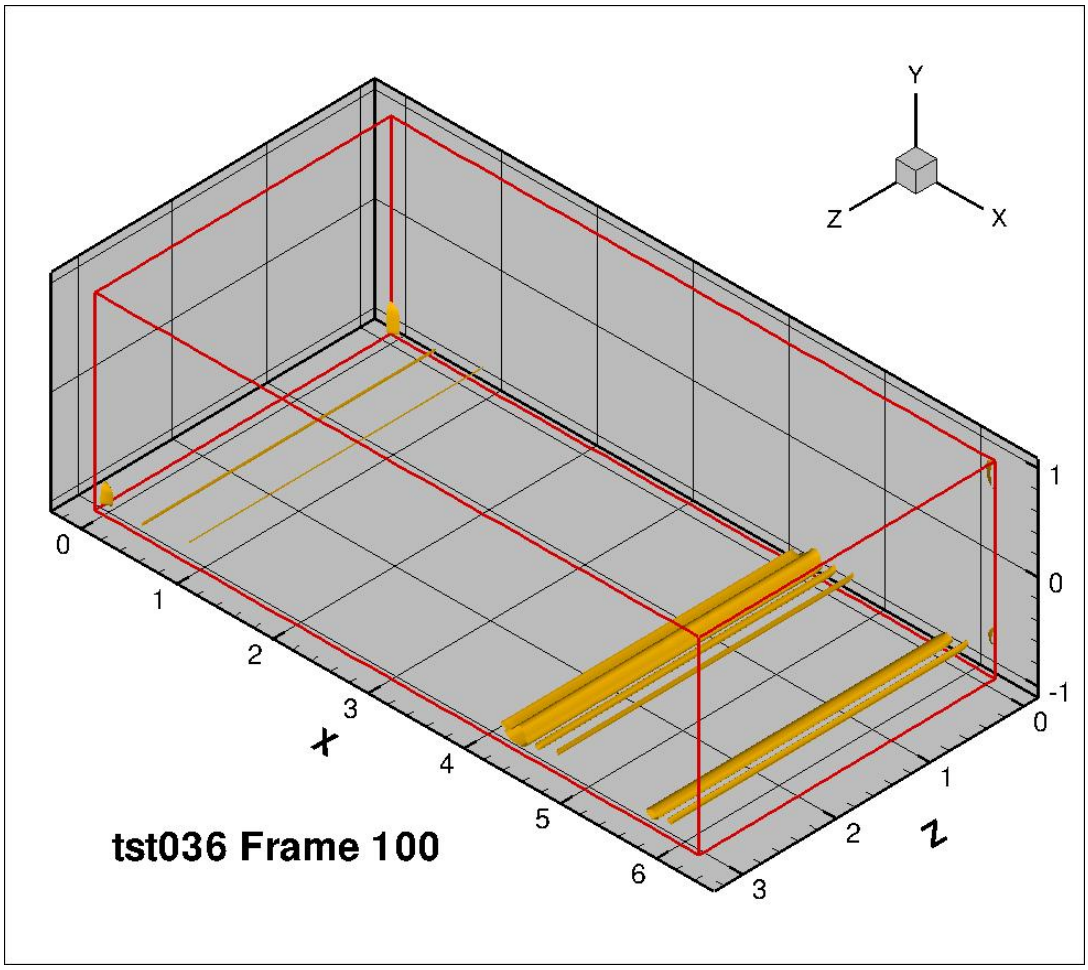

*Figure 39: 8 lateral counter rotating vortices, frame 100*

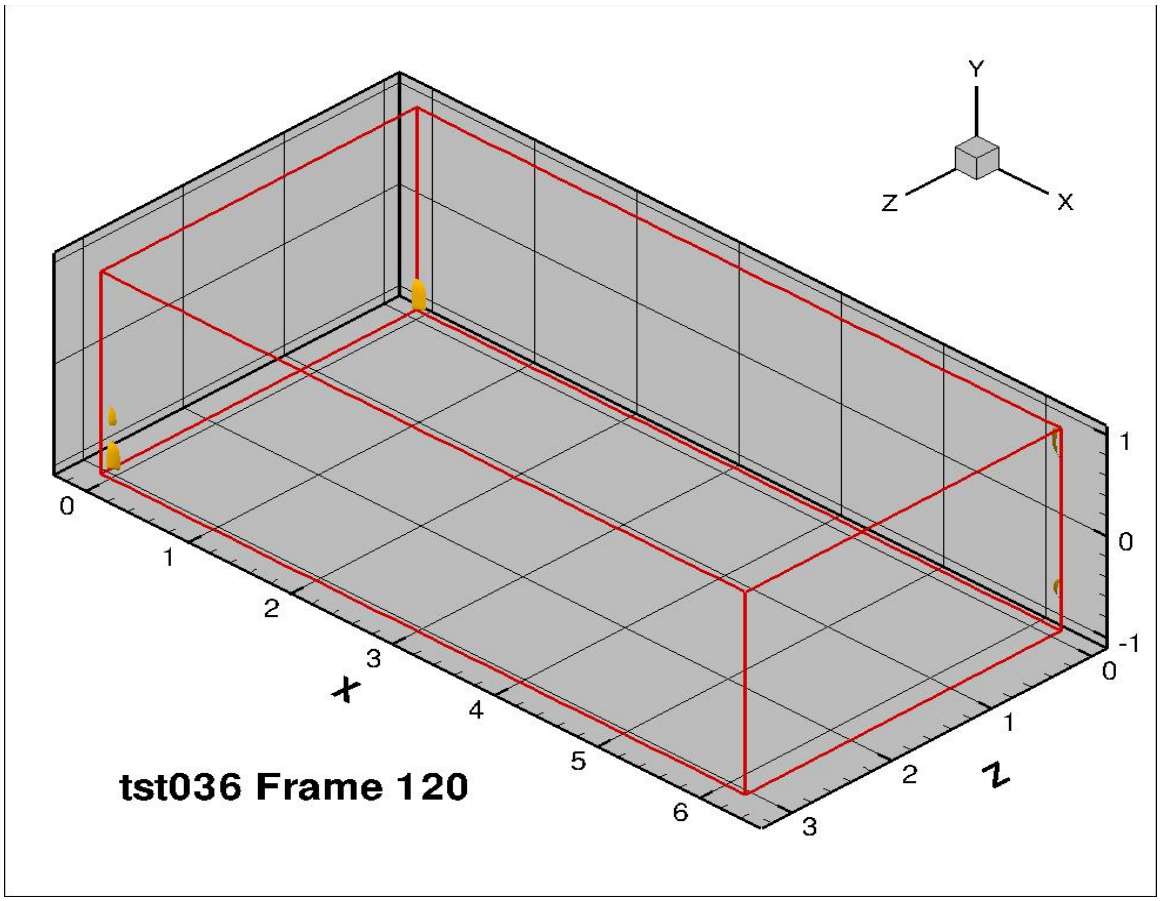

*Figure 40: 8 lateral counter rotating vortices, frame 120*

## 4.2.2 Multiple Longitudinal Vortices

### *Eight Counter-Rotating Vortices*

Multiple longitudinal vortices were simulated. In the following movie eight longitudinal vortices of alternating rotation were placed near the wall @ y=-0.9. These vortices behaved similarly to the vortices of WorkE_iso.avi, inducing other vortices at 45 degrees to each of the initial vortices. These vortices showed no sign of instability and dissipated viscously before the end of the simulation.

Movie: tst050_iso.avi eight longitudinally placed vortices at y=-0.9

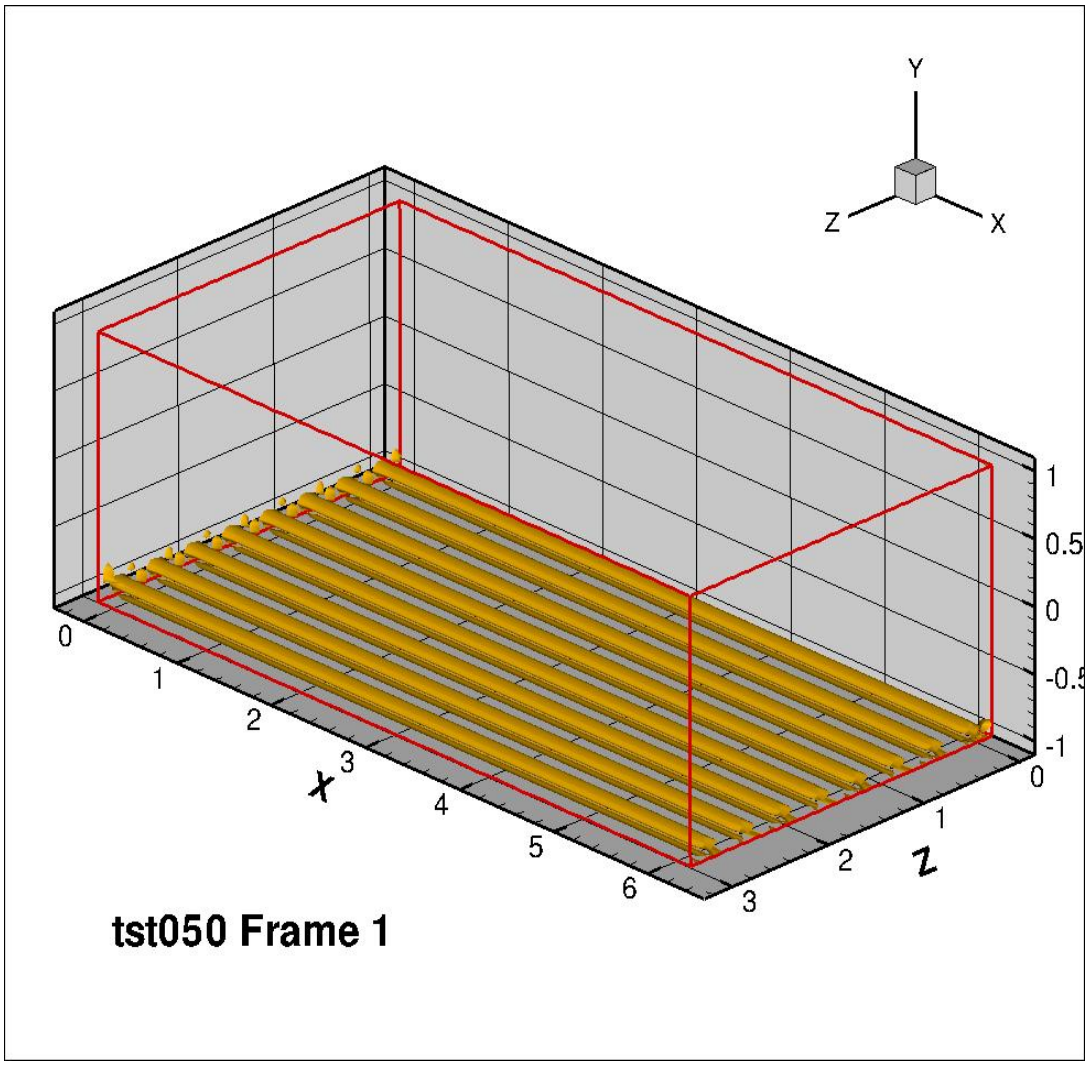


*Figure 41: 8 Longitudinal counter rotating vortices, frame 1*

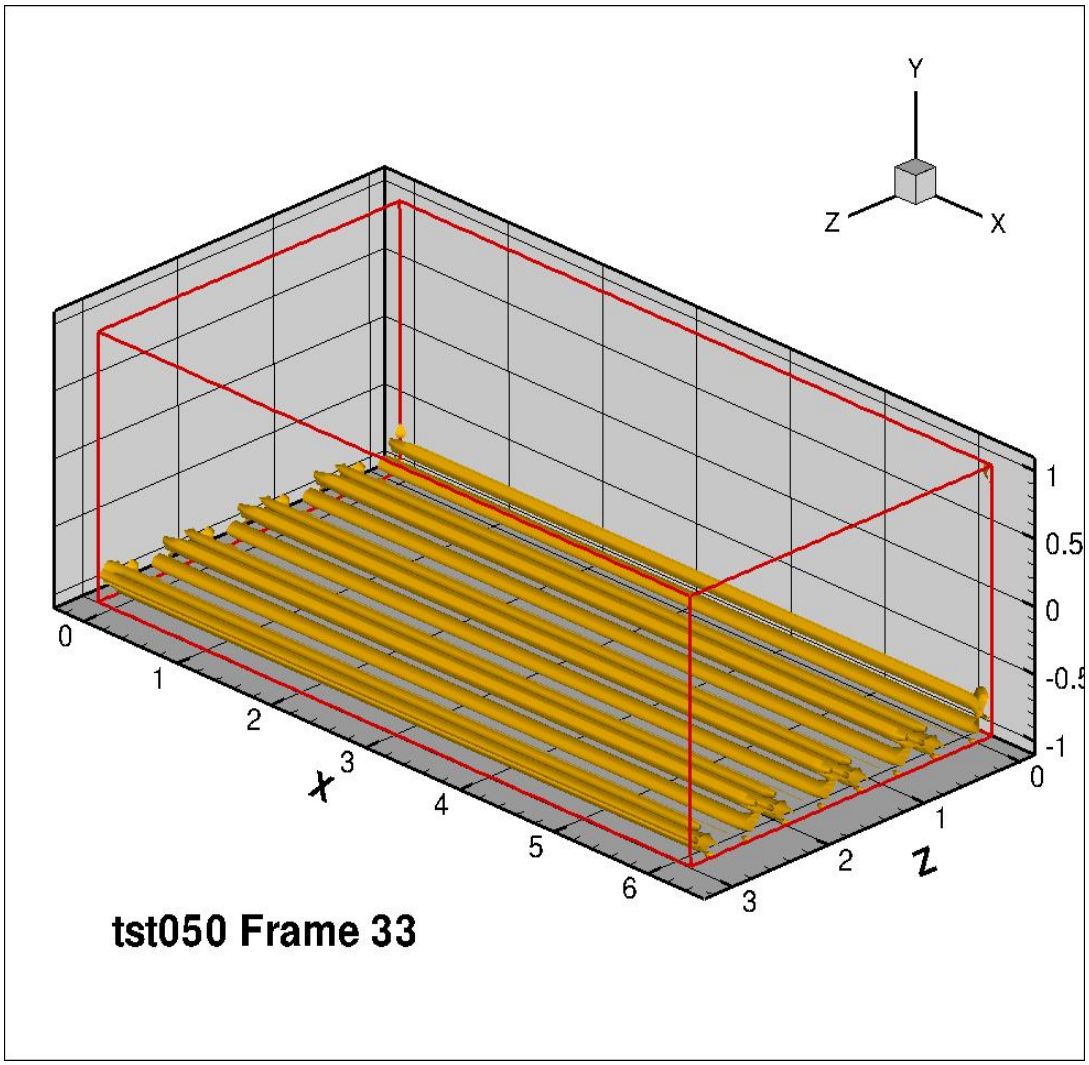


*Figure 42: 8 counter rotating longitudinal vortices, frame 33*

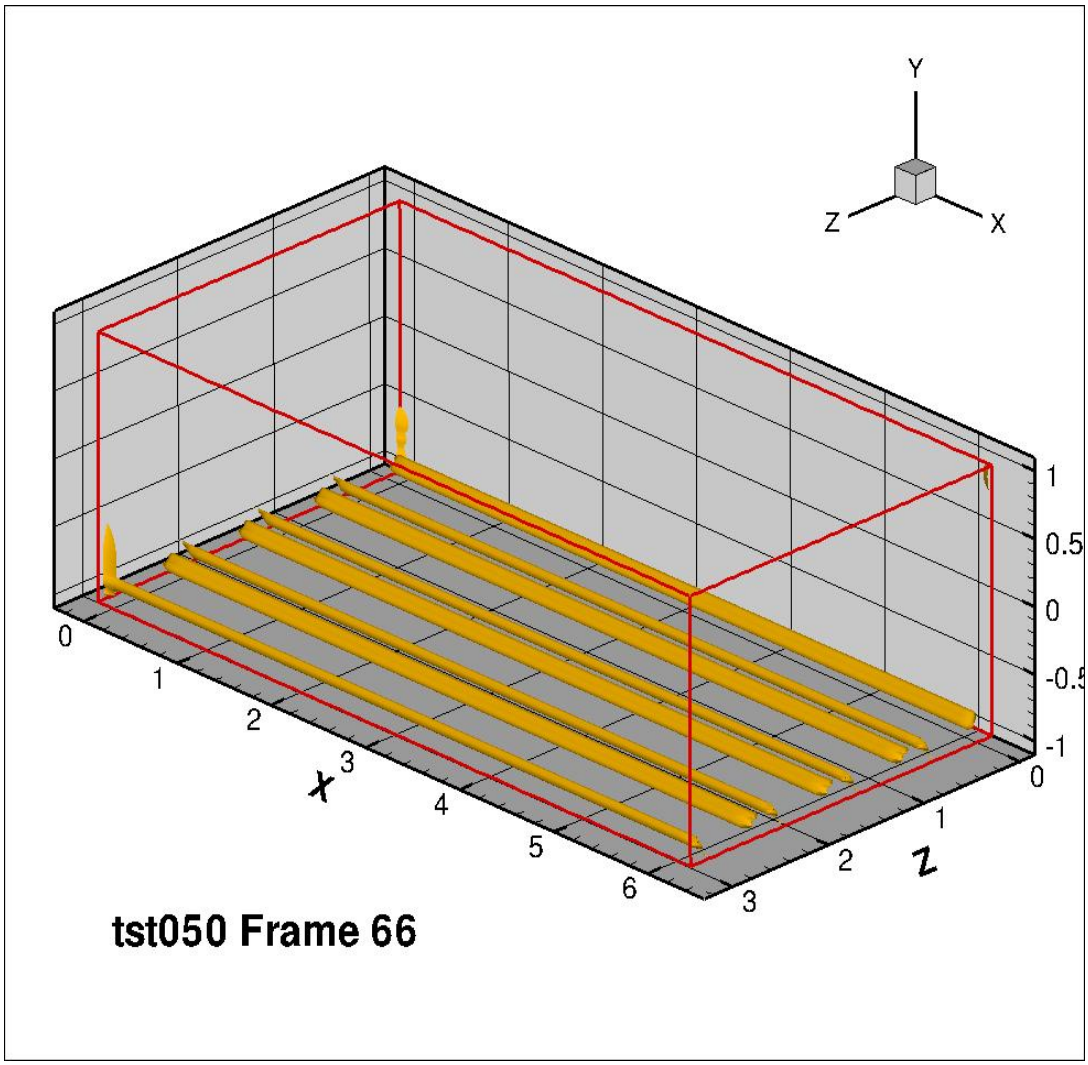


*Figure 43: 8 longitudinal counter rotating vortices, frame 66*

### *Twelve Co-Rotating Vortices with Trip Bar*

Multiple longitudinal vortices were simulated. Twelve longitudinal co-rotating vortices were simulated with trip bar placed at the lower wall and perpendicular to the direction of flow. This simulation immediately displayed significant instability. In the vicinity of the trip bar the vortices became very unstable with lifted vortical structures appearing before and after the trip bar. These disturbed lifted vortical structures moved both upstream and downstream simultaneously. After the

downstream moving lifted vortical structures left the trip bar, they were replaced by small stretched vortical structures that were inclined with the flow. The upstream traveling vortical structures did not clear the trip bar, but remained attached as the instabilities extended upstream. Instabilities traveling upstream passed through the upstream boundary and reentered the channel through the downstream recurring boundary and then moved upstream and passed through the downstream moving instabilities. The vortical structures moving upstream eventually dissipated leaving a series of standing up stream waves parallel to the trip bar. The vortical structures that had first appeared downstream dissipated leaving a series of small standing waves running parallel to the trip bar.

Hairpin vortices were not observed; however, stretched vortices, which were similar to those seen in other investigations were observed just downstream of the trip bar shortly after the beginning of the simulation. These vortices dissipated as they were overtaken by the upstream moving instabilities at the end of the simulation.

Movie: tst055_iso.avi twelve longitudinally placed co-rotating vortices at y=-0.9, with trip bar

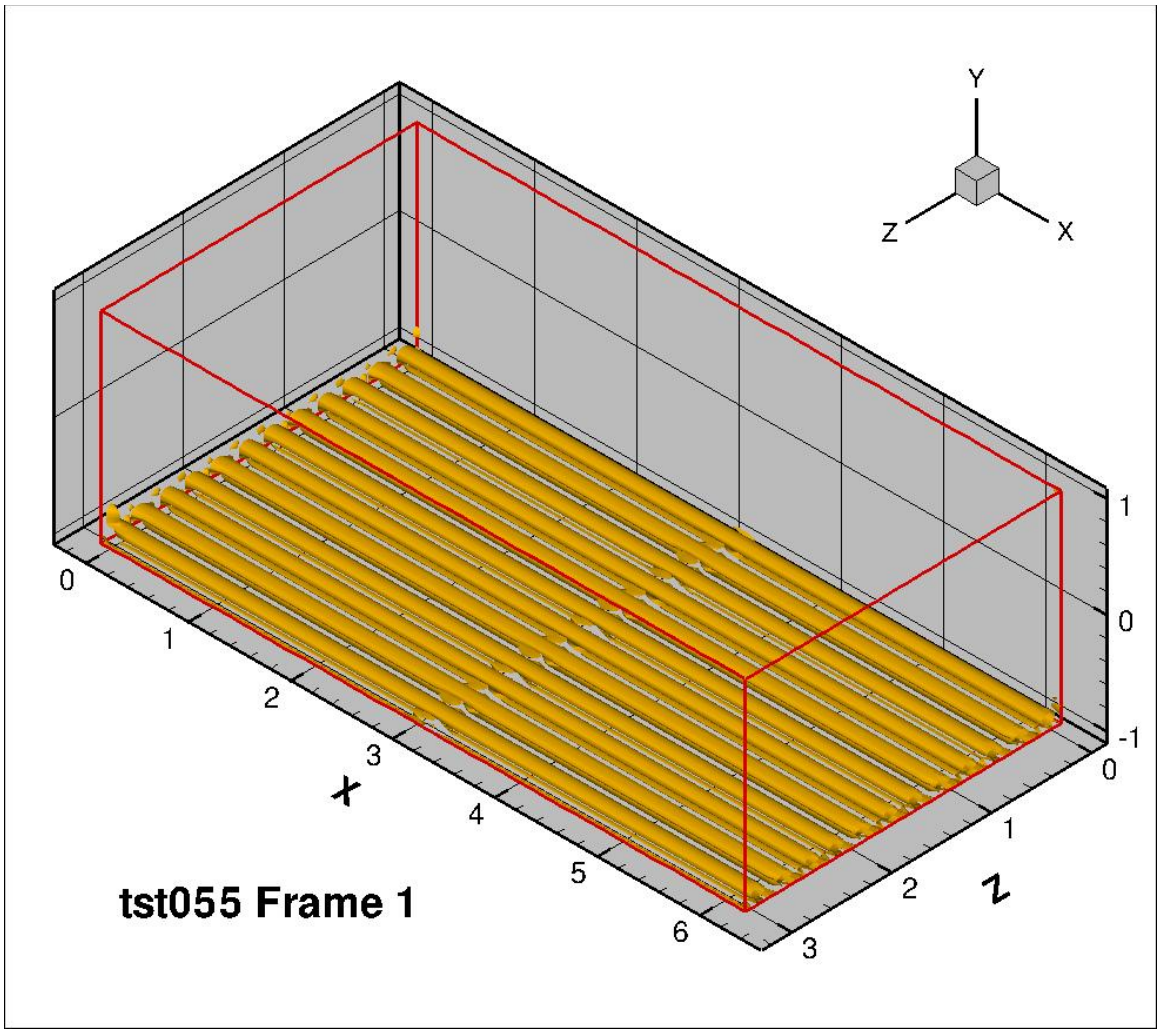

*Figure 44: 12 longitudinal co-rotating vortices with trip bar, frame 1*

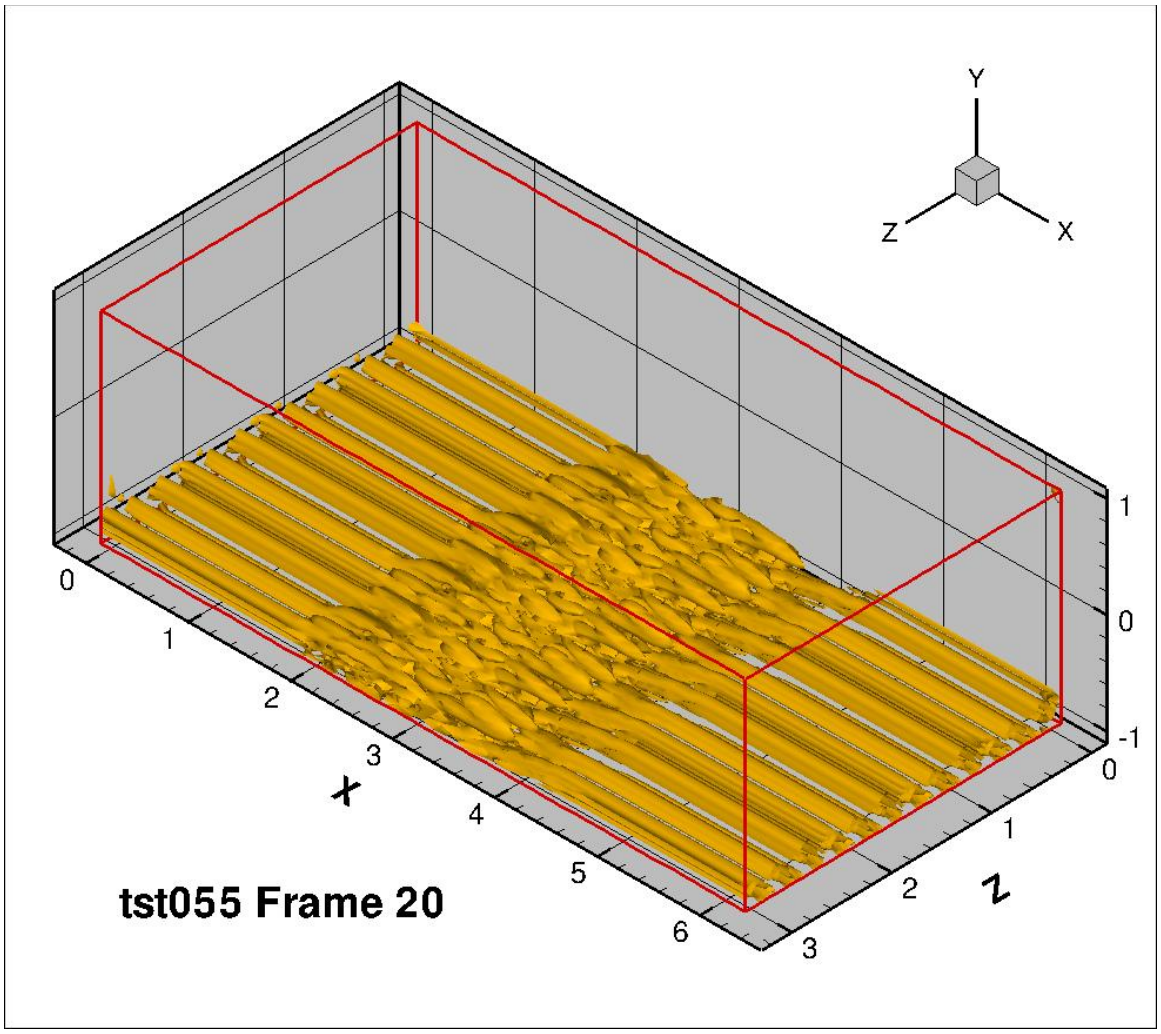

*Figure 45: 12 longitudinal co-rotating vortices with trip bar, frame 20*

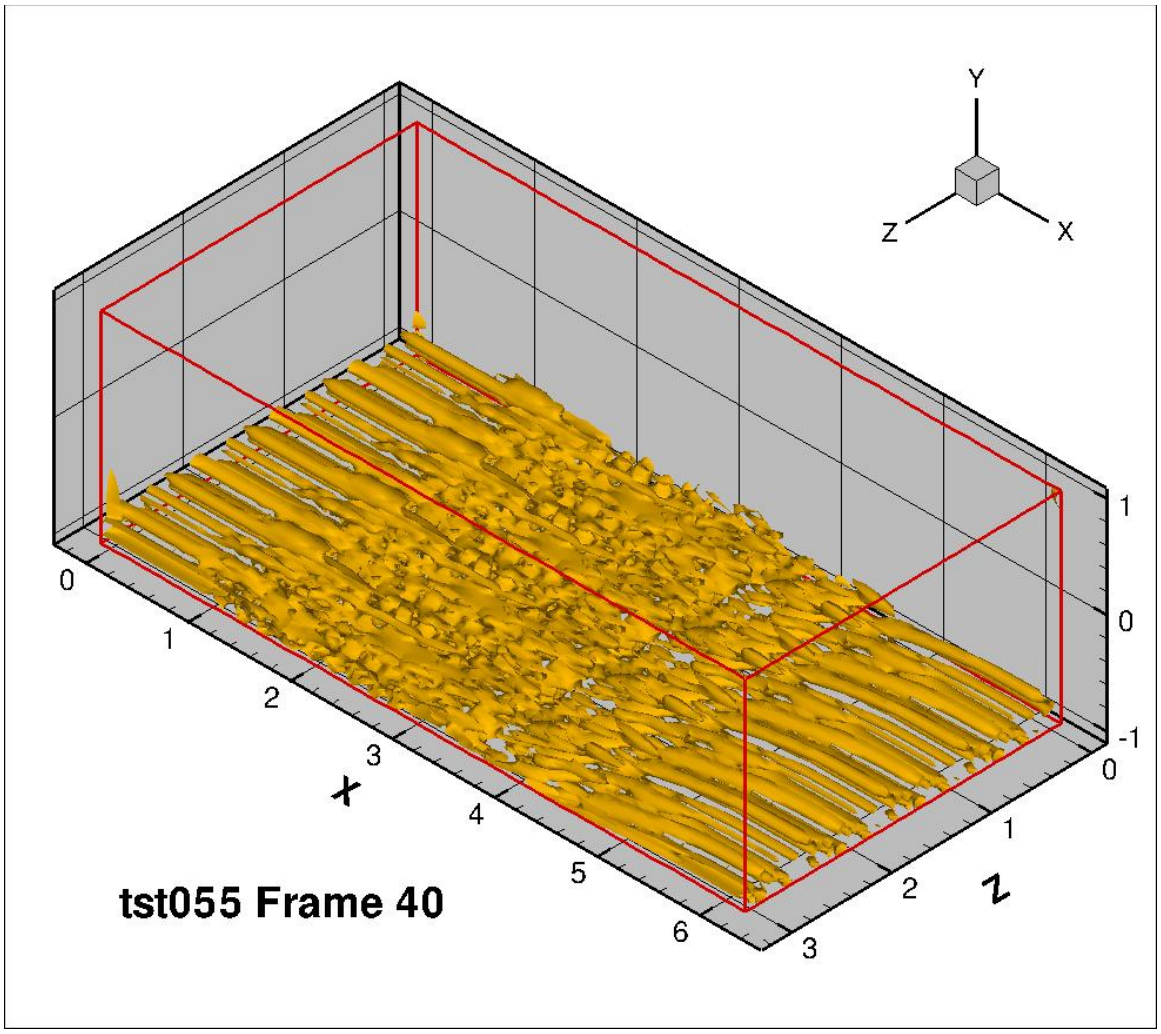

*Figure 46: 12 longitudinal co-rotating vortices with trip bar, frame 40*

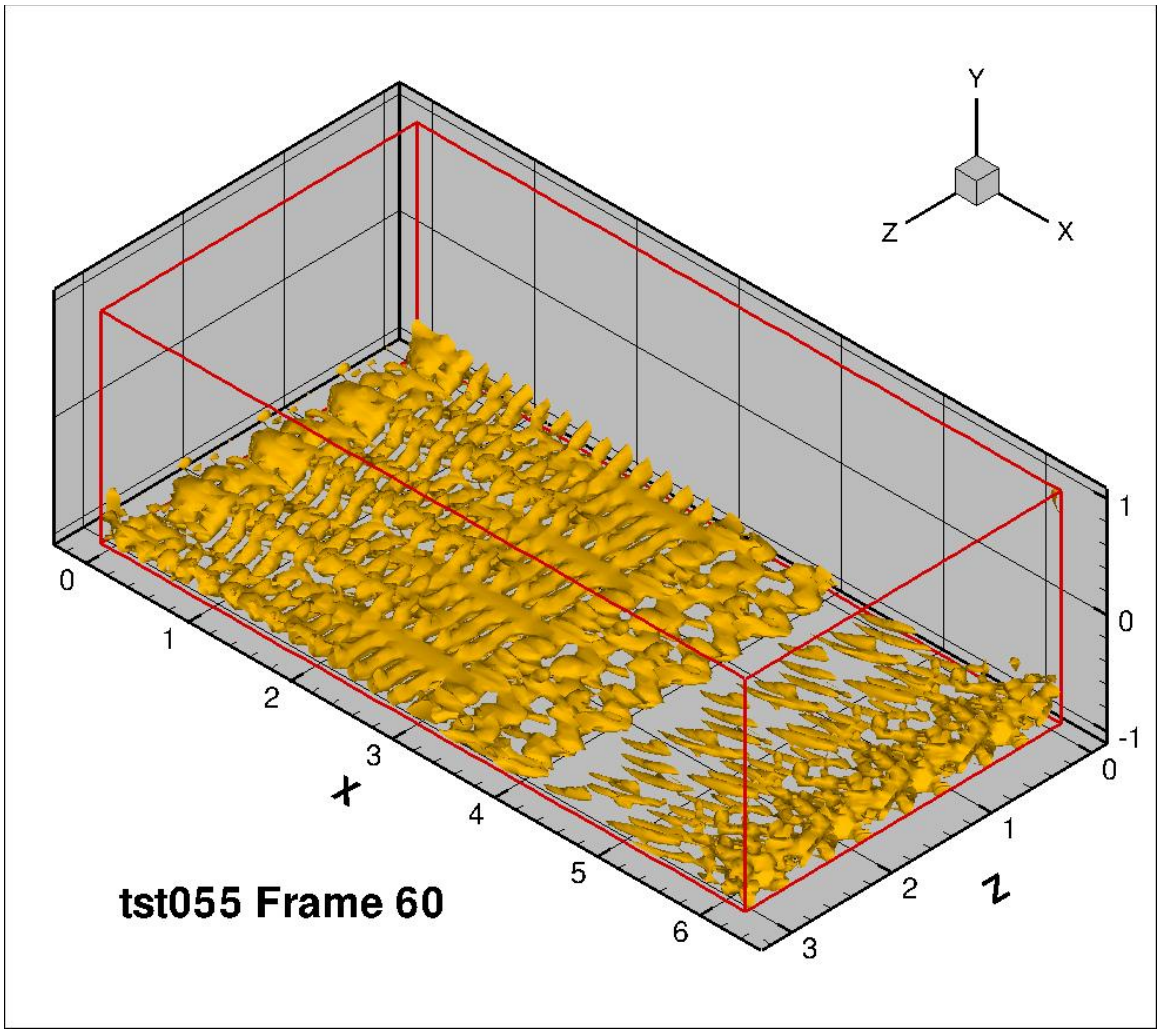

*Figure 47: 12 longitudinal co-rotating vortices with trip bar, frame 60*

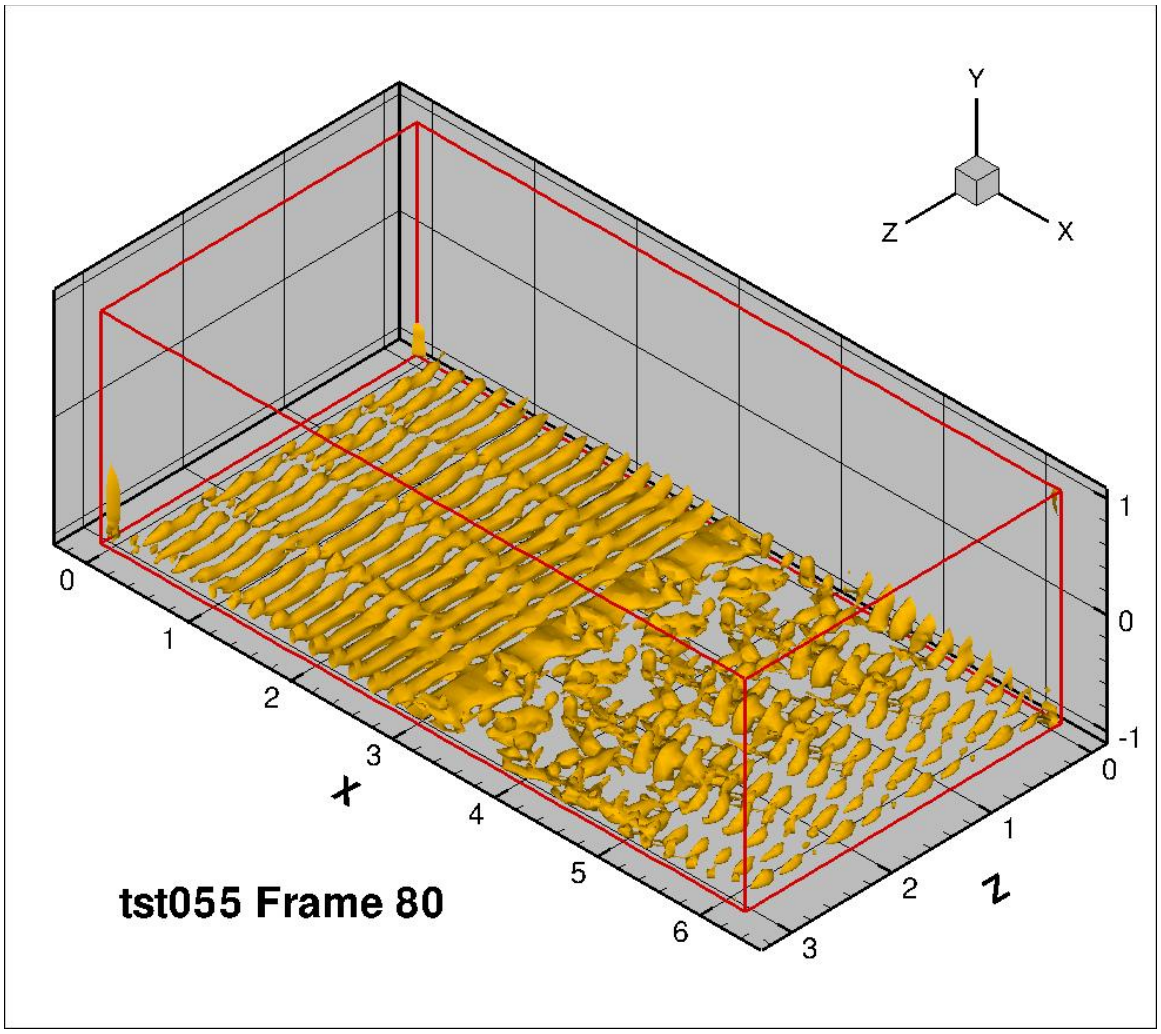

*Figure 48: 12 longitudinal co-rotating vortices with trip bar, frame 80*

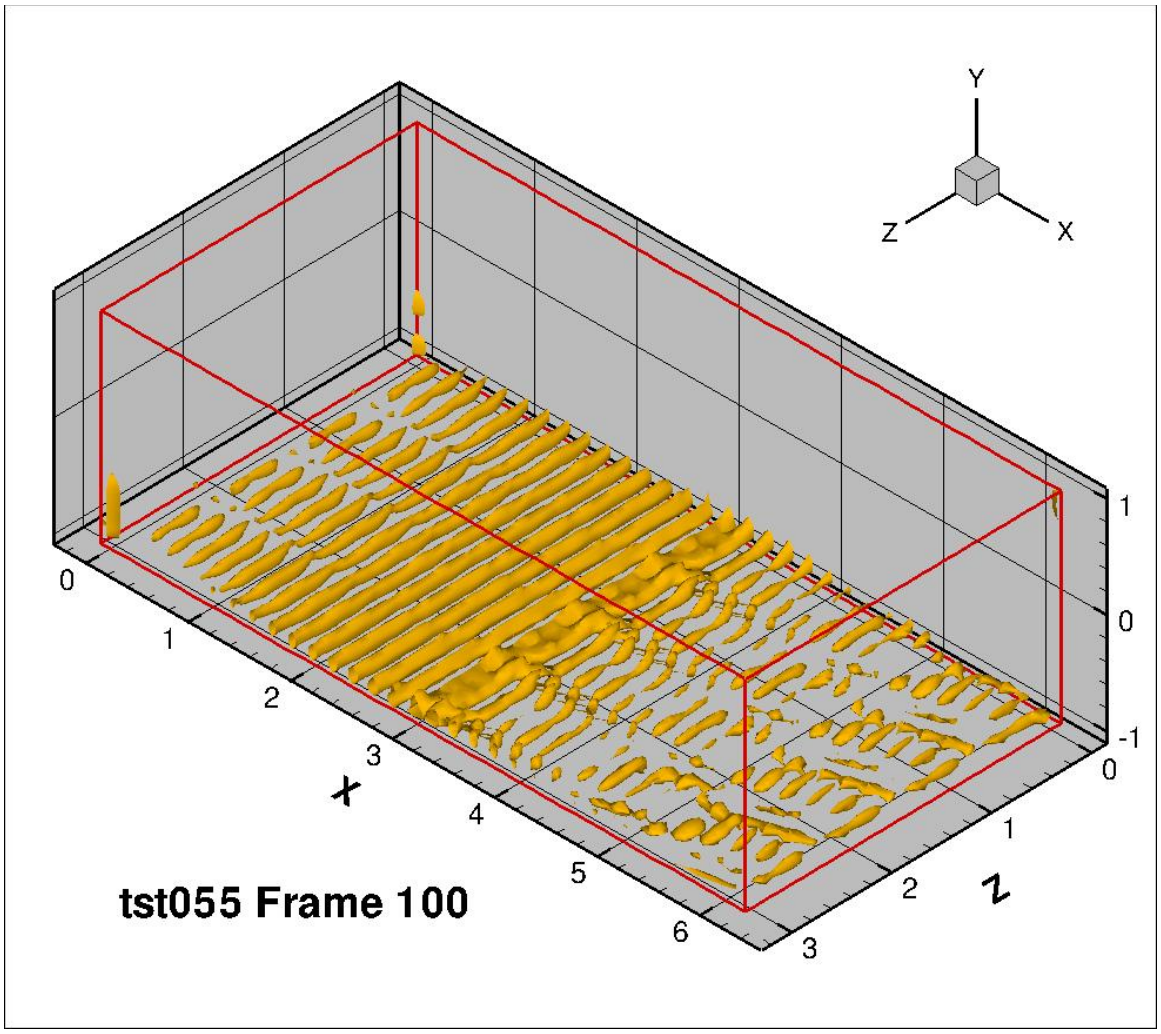

*Figure 49: 12 longitudinal co-rotating vortices with trip bar, frame 100*

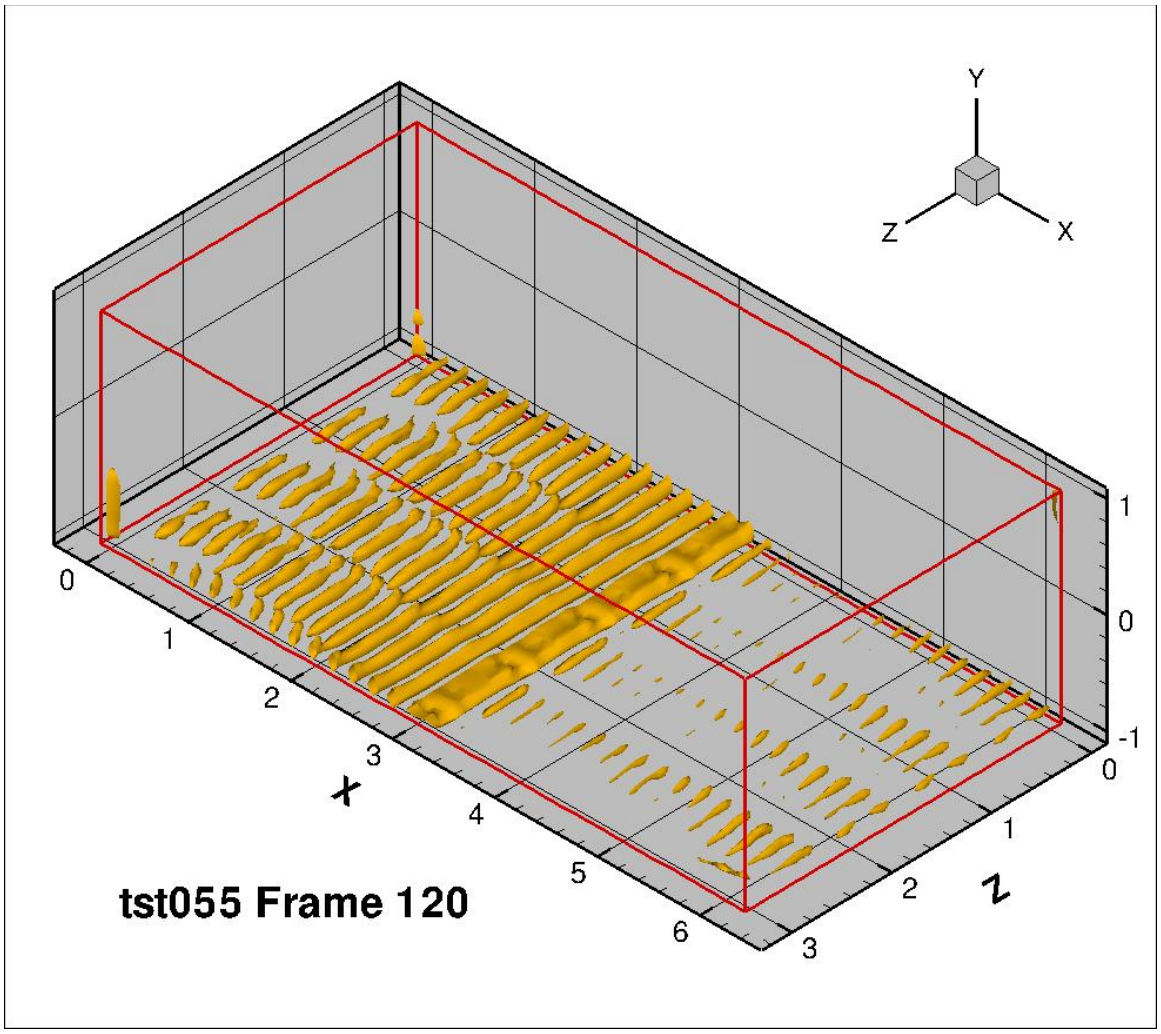


*Figure 50: 12 longitudinal co-rotating vortices with trip bar, frame 120*

### *Twelve Counter-Rotating Vortices with Trip Bar*

This simulation was very similar to Twelve Co-Rotating Vortices with Trip Bar (tst055_iso.avi) however with co-rotating vortices. The simulation immediately showed significant instability in the vicinity of the trip bar. This instability moved both upstream and downstream from the trip bar with the disturbances overtaking one another due to the recurring boundaries. There was no evidence of stretched inclined vortices immediately downstream from the trip rail as with

tst055_iso.avi; however, much larger vortical structures emerged and remained above the standing waves that had formed upstream of the trip bar. These structures passed through the channel several times before dissipating. Several of the upstream longitudinal vortices briefly reorganized, but then were obscured by the formation of upstream waves parallel to the trip bar. The waves that coalesced upstream of the trip bar were more uniform than in the previous simulation of co-rotating vortices, tst055_iso.avi.

Movie: tst056_iso.avi, twelve longitudinally placed counter-rotating vortices at y=-0.9 with trip bar.

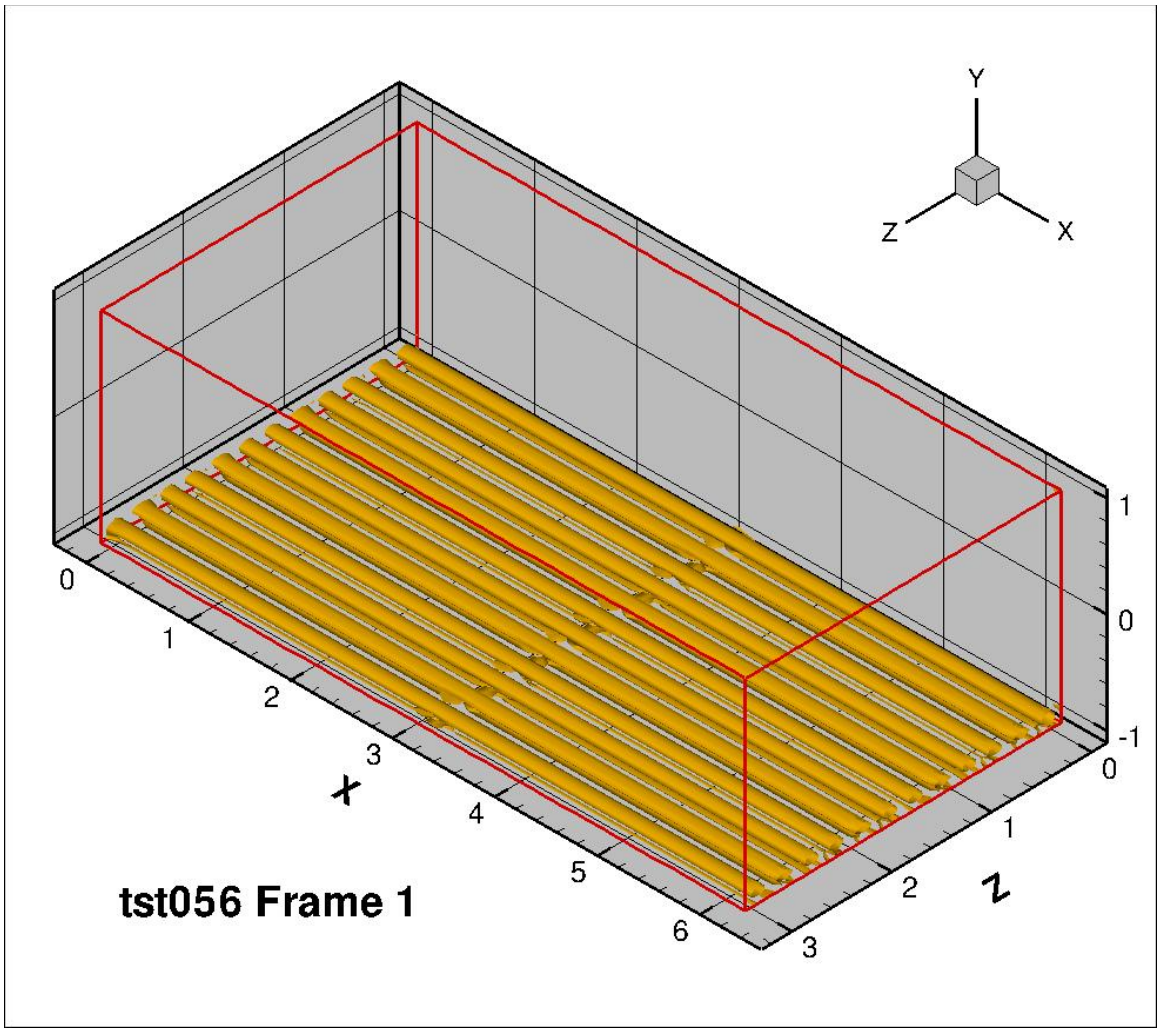


*Figure 51: 12 longitudinal counter rotating vortices with trip bar, frame 1*

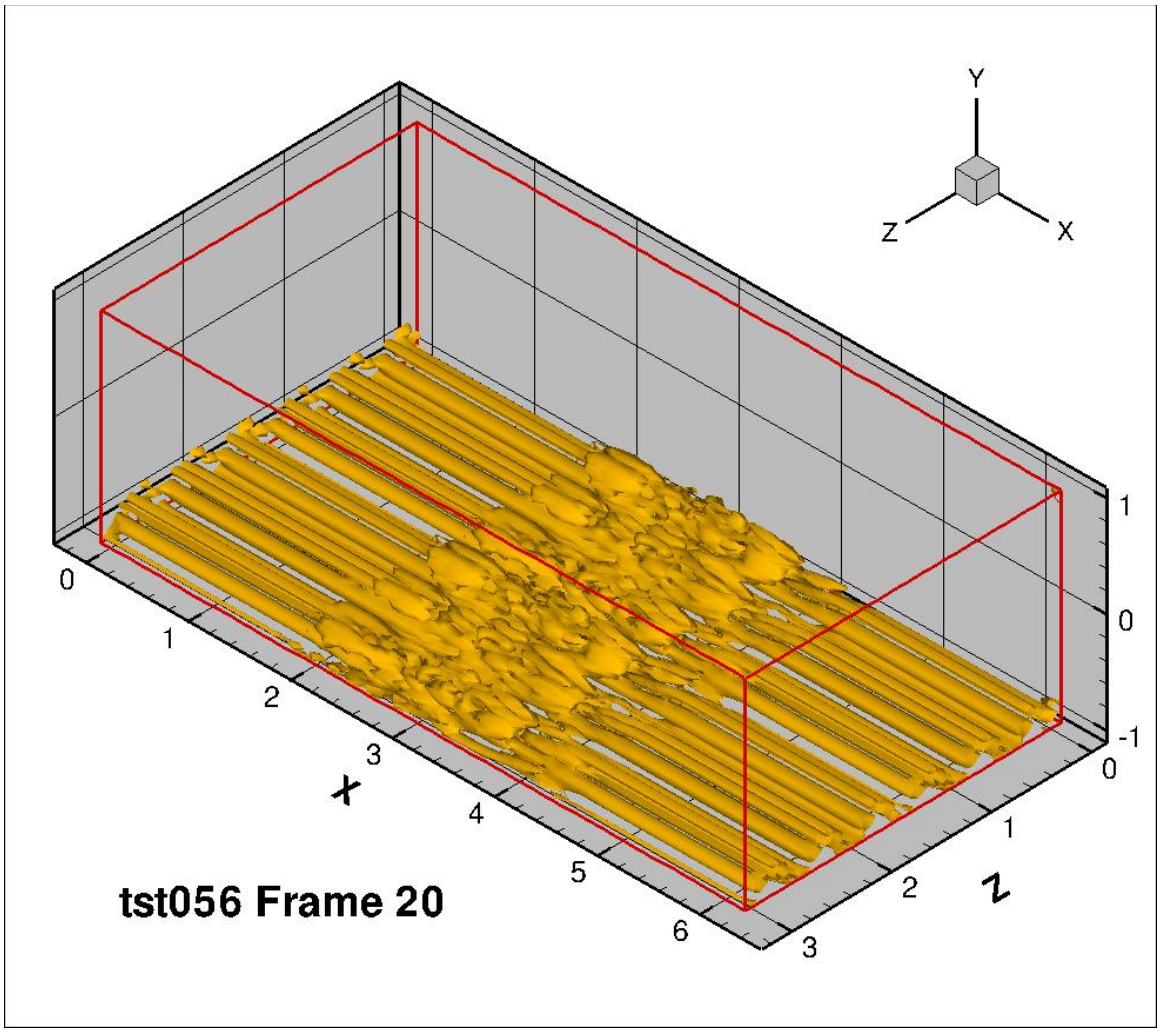

*Figure 52: 12 longitudinal counter rotating vortices with trip bar, frame 20*

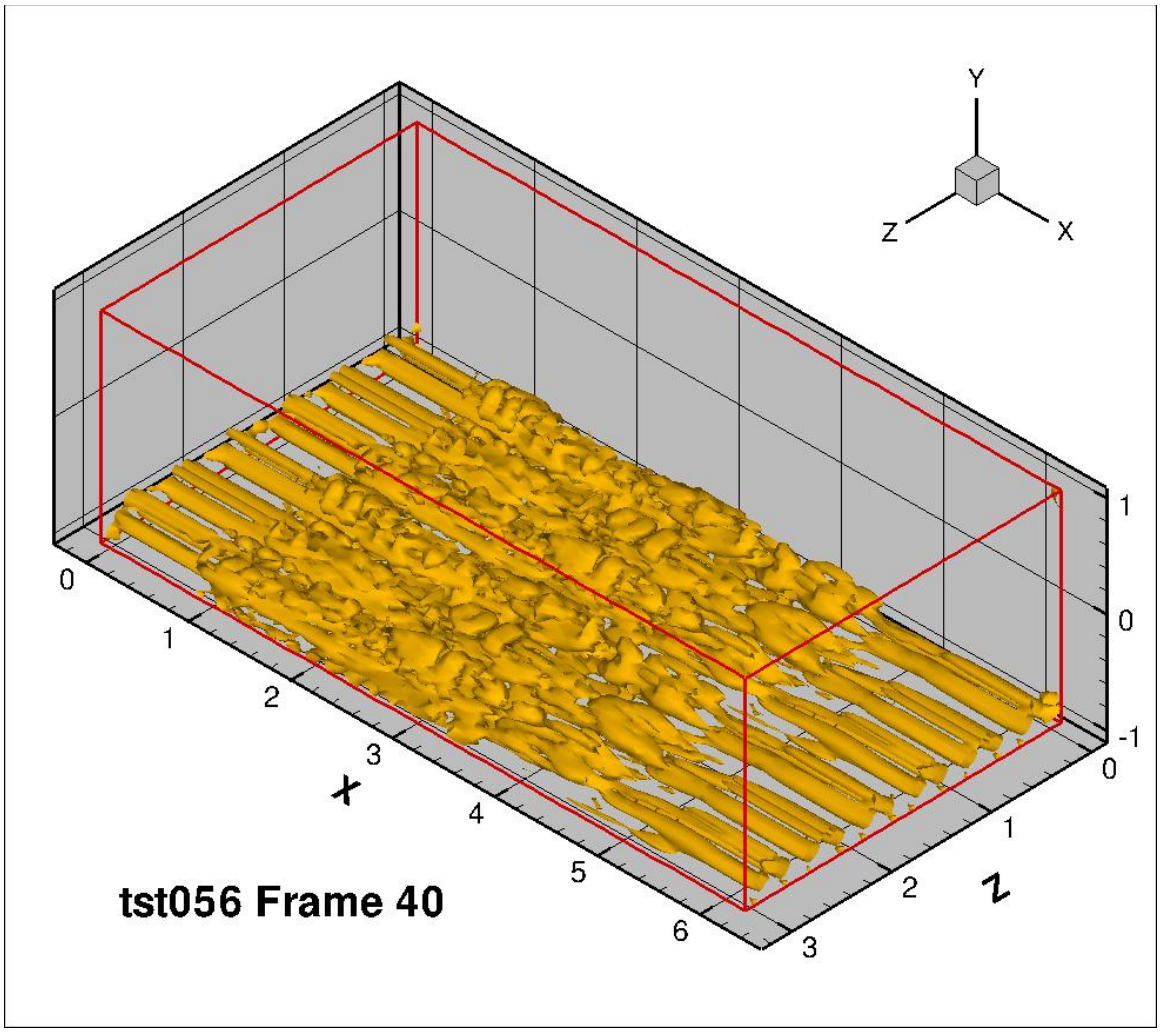

*Figure 53: 12 longitudinal counter rotating vortices with trip bar, frame 40*

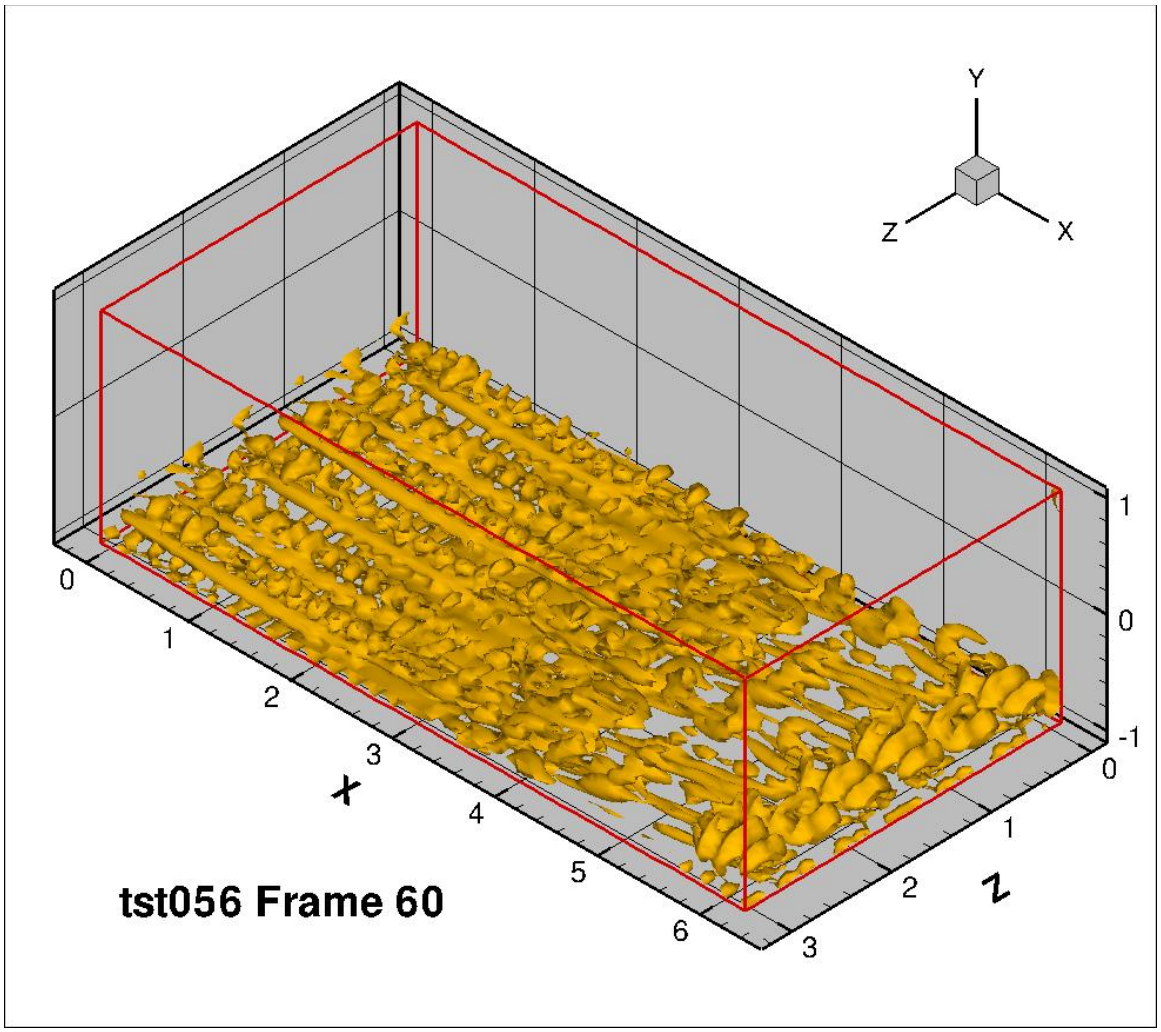


*Figure 54: 12 longitudinal counter rotating vortices with trip bar, frame 60*

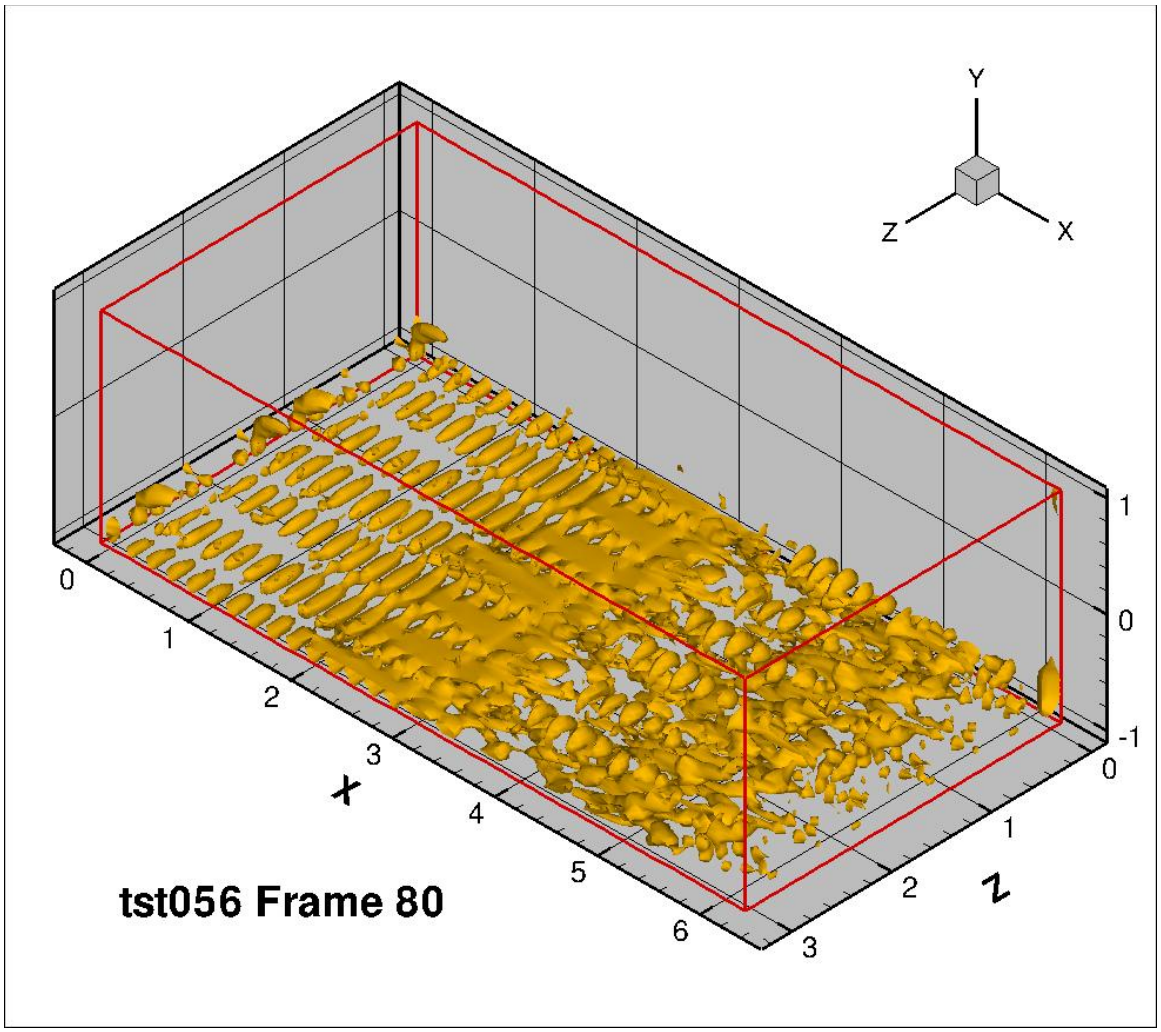

*Figure 55: 12 longitudinal counter rotating vortices with trip bar, frame 80*

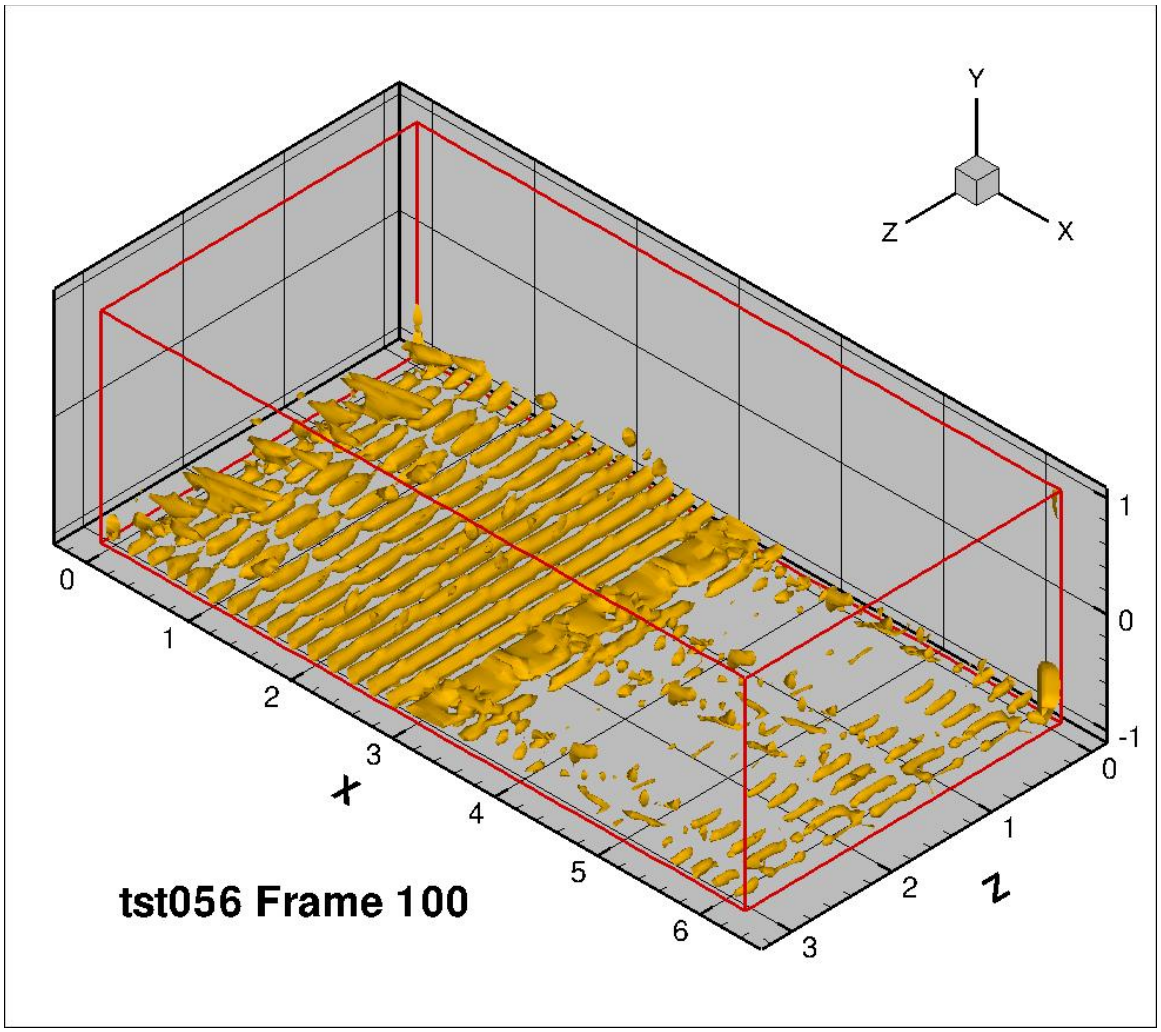

*Figure 56: 12 longitudinal counter rotating vortices with trip bar, frame 100*

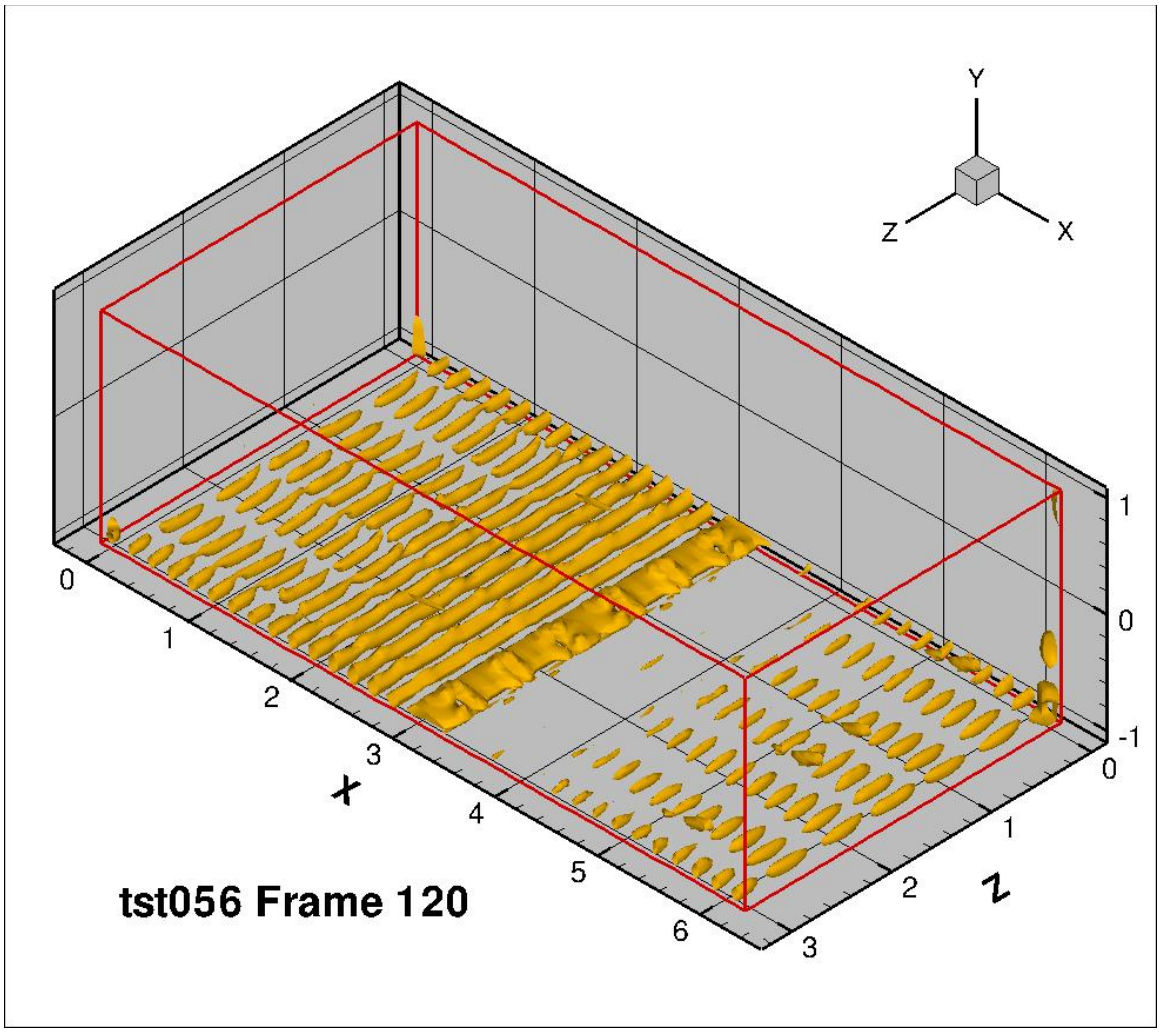

*Figure 57: 12 longitudinal counter rotating vortices with trip bar, frame 120*

## *4.3 Lateral Vortices Extending Wall to Wall*

Vortices were placed laterally across the channel extending from lower solid boundary to upper solid boundary. This arrangement placed the ends of the vortices perpendicular to the wall and in the boundary layer. The initial location of the vortices was approximately 1/6$^{th}$ the length of the channel from the entrance. Vortices were placed in counter-rotating pairs with both upstream and downstream flow between the vortices. These will be referred to as upstream

and downstream vortex pairs. The upstream rotating pairs were located at approximately z=0.78, while the downstream rotating vortex pairs were located at approximately z=2.2.

***Lateral Vortices, H=0.2, tst072_iso.avi***

Immediately after start of the simulation, both sets of vortex pairs induced additional vortices that moved both upstream and downstream. These upstream and downstream moving structures passed through the upstream and downstream recurring channel boundaries and reentered the channel from the opposite ends, then passed through each other.

The sections of vortices that were within the upper and lower boundary layer were swept downstream and stretched. In the case of the upstream vortex pair, the section of vortex between the upper and lower boundary layer was well behaved and vortices remained smooth and distinct. While for the downstream vortex pair, the section of vortices between the upper and lower boundary layers became unstable with considerable linking between the vortices that seemed to join and then break and and then rejoin.

After some dissipation the downstream vortex pair produced two symmetrical pairs of vortices at about mid channel that were longitudinally oriented and appeared to be stretched. The upstream vortex pair evolved to a pair of

stretched vortices in the boundary layer that were connected to a pair of stretched vortices in the boundary layer at the opposite wall by large vortices.

After further dissipation the downstream vortex pair was almost completely gone leaving only the two pair of symmetrical vortices at mid channel oriented longitudinally and a pair of vortices that were oriented perpendicular to the walls also at mid channel.

Further dissipation of the upstream vortex pair resulted in further development of the stretched vortex pairs within the boundary layer. The structure also induced in-line vortices parallel to the legs of the stretched vortices and a series of vortices that bridged across the downstream ends of the two stretched vortices much like the head of the pin of a hairpin vortex but slightly upstream.

At the end of the simulation the downstream vortex pair had completely dissipated. The upstream vortex pair appeared to have only the stretched vortex pairs and induced in line vortices in the boundary layer. The vortices that had connected the vortices from one wall to the opposite wall had dissipated completely.

Movie: tst072_iso.avi,

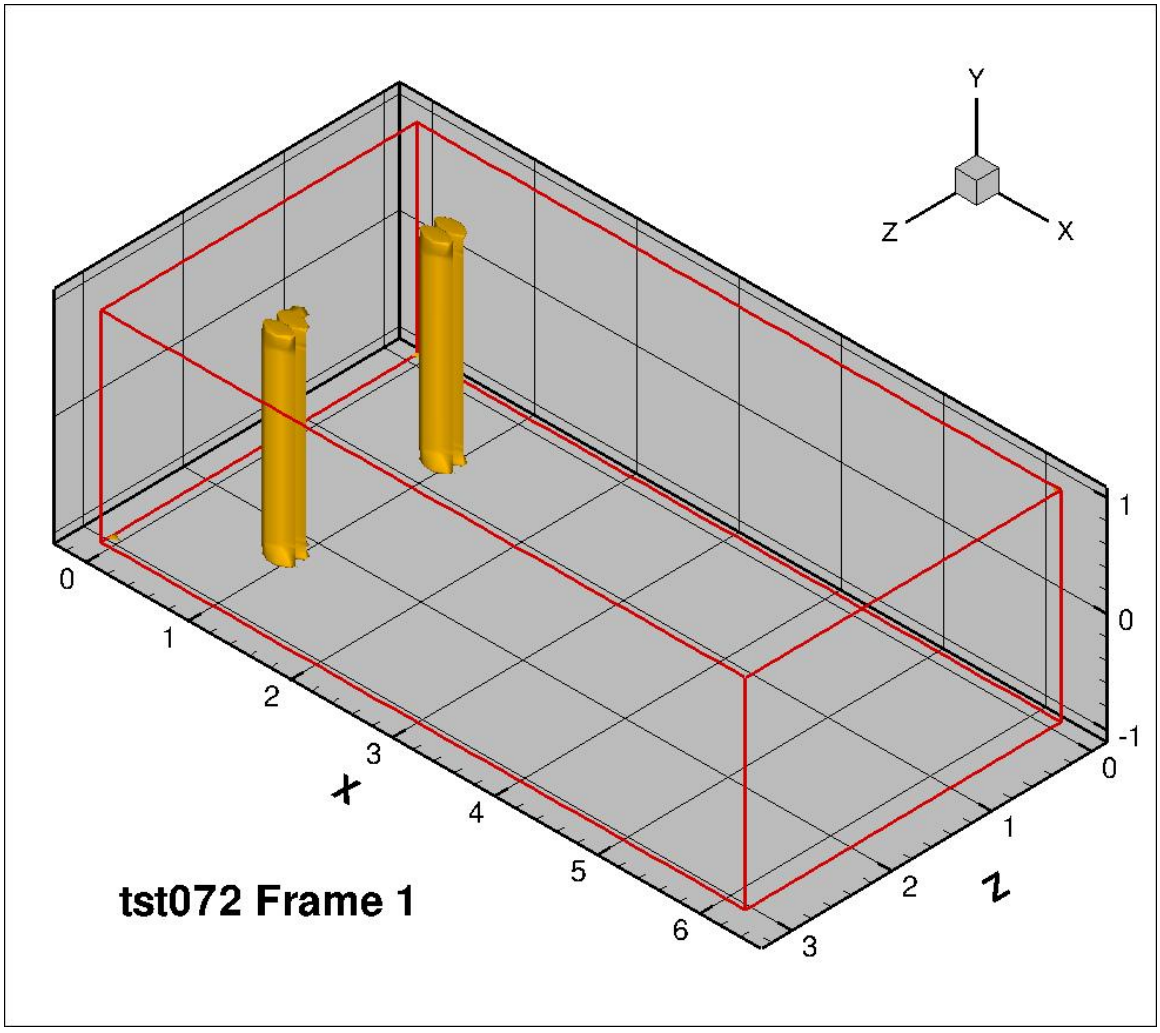

*Figure 58: 2 pair vortices, wall to wall, frame 1*

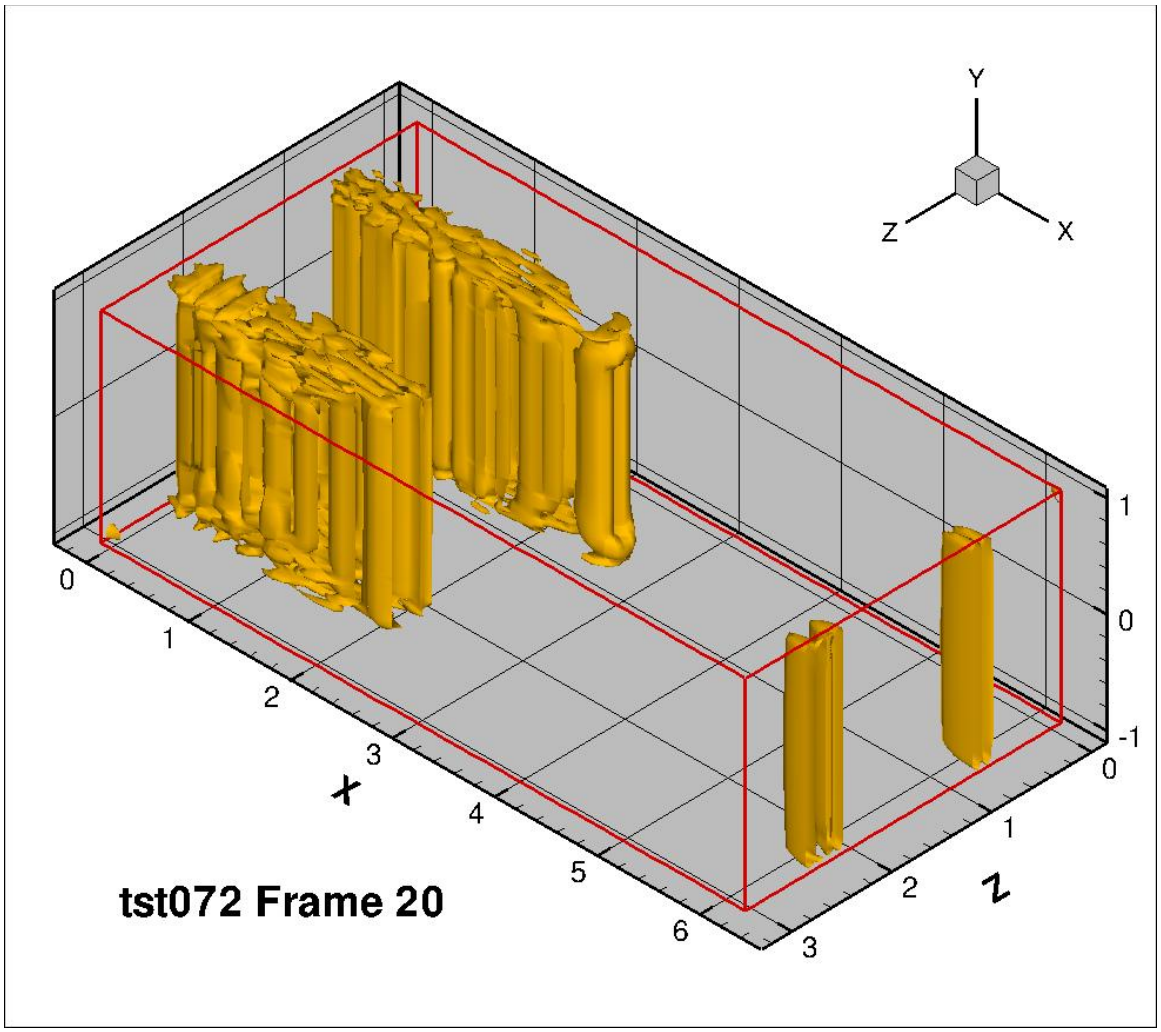

*Figure 59: 2 pair vortices, wall to wall, frame 20*

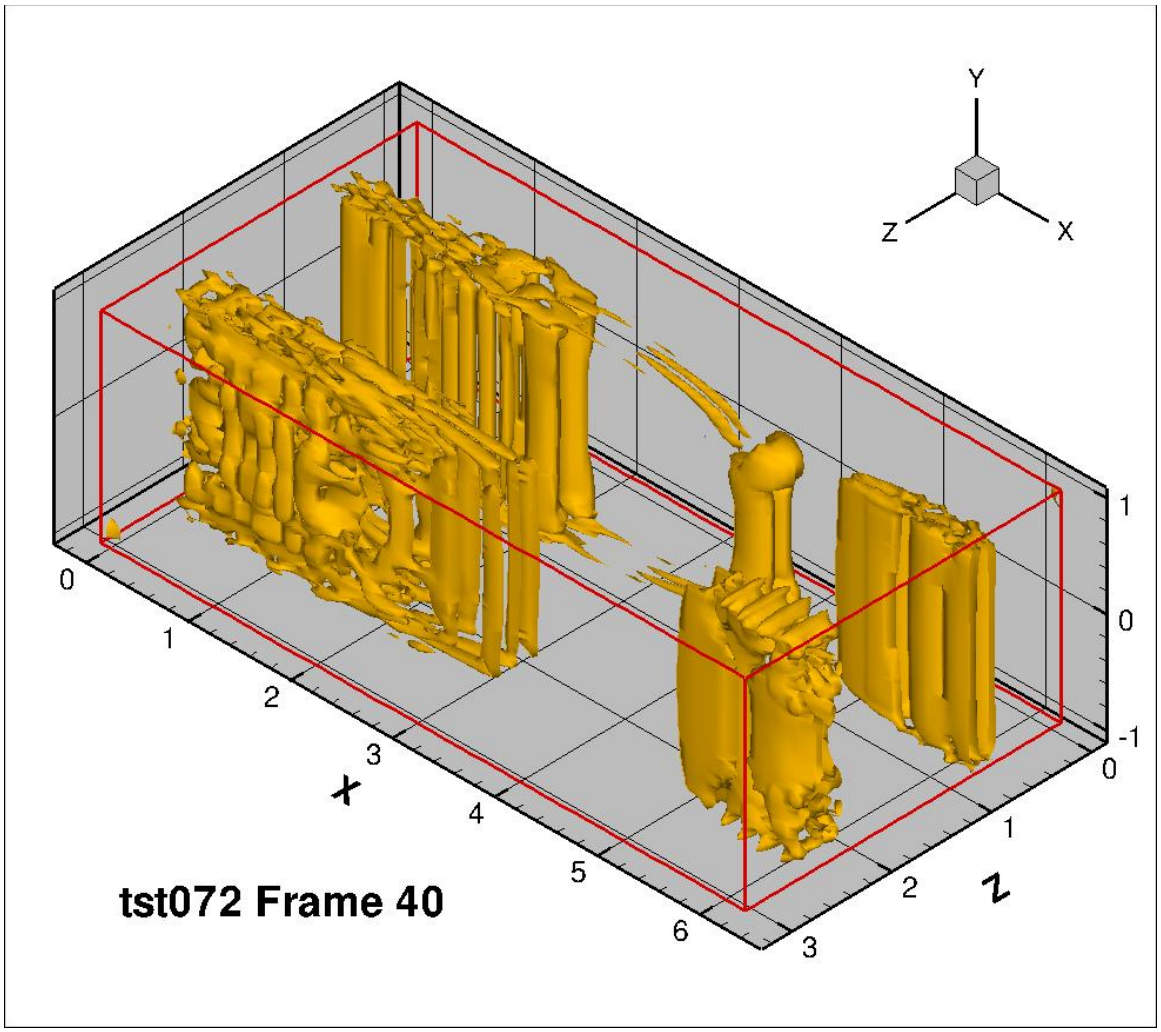

*Figure 60: 2 pair vortices, wall to wall, frame 40*

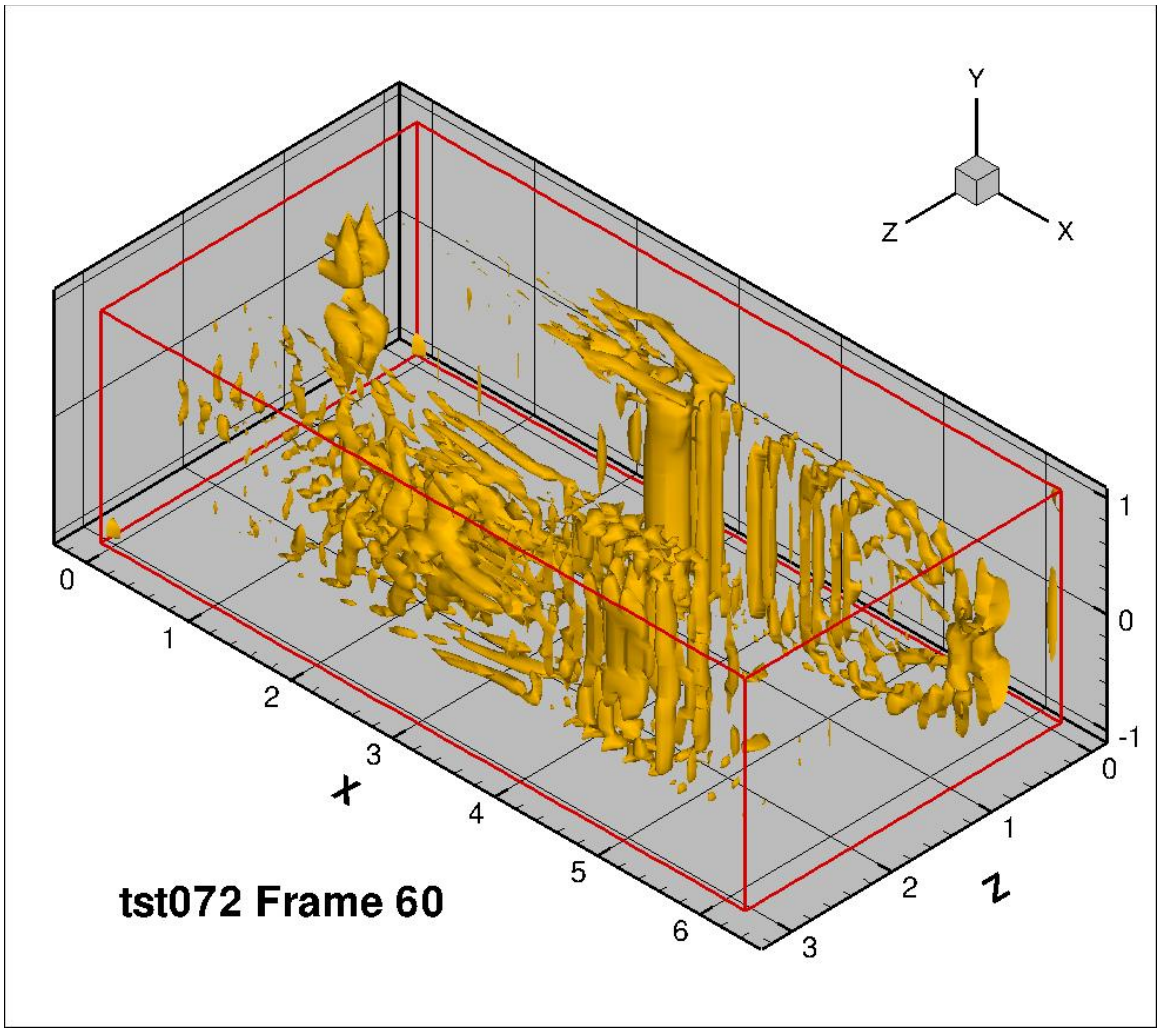

*Figure 61: 2 pair vortices, wall to wall, frame 60*

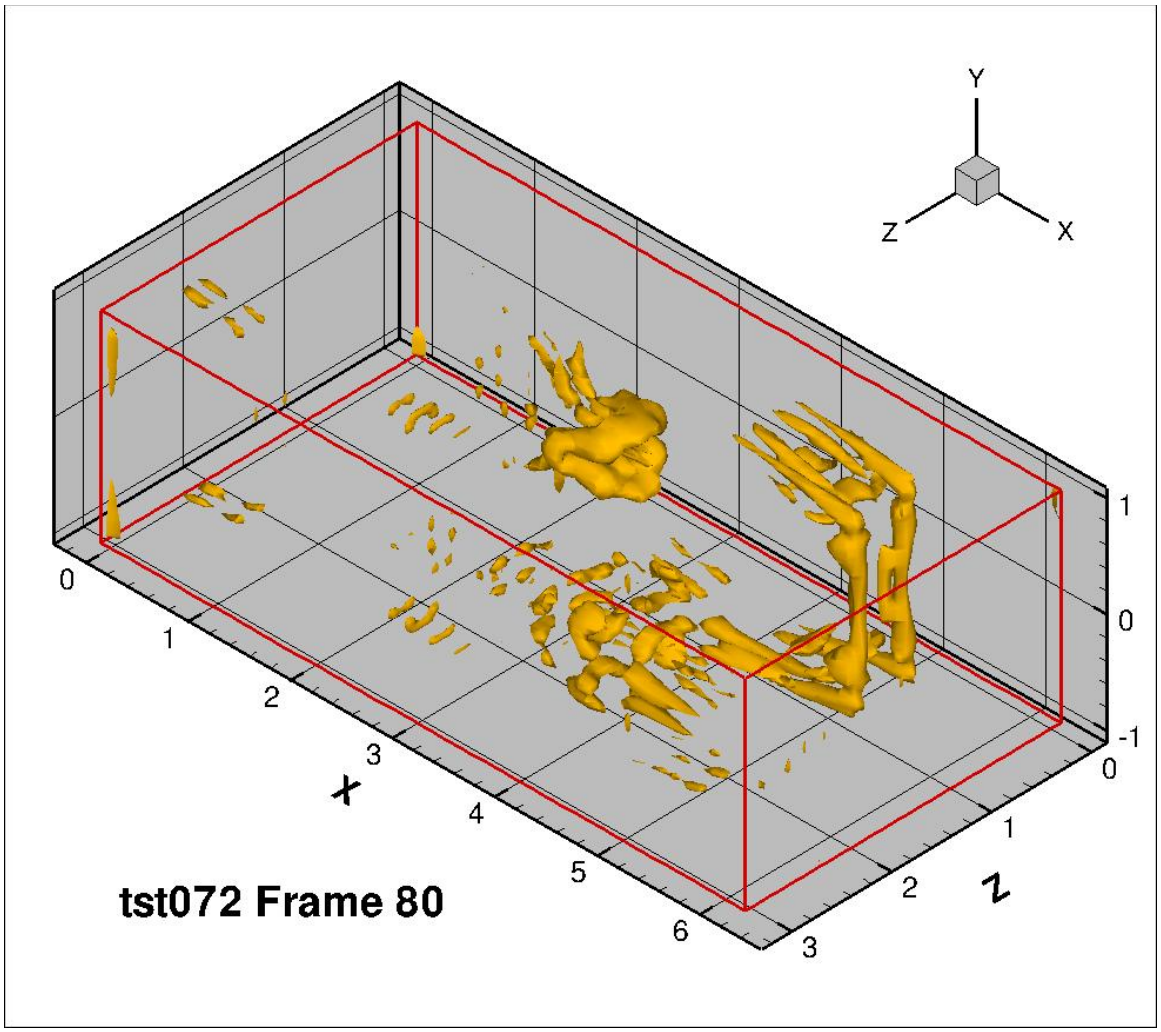

*Figure 62: 2 pair vortices, wall to wall, frame 80*

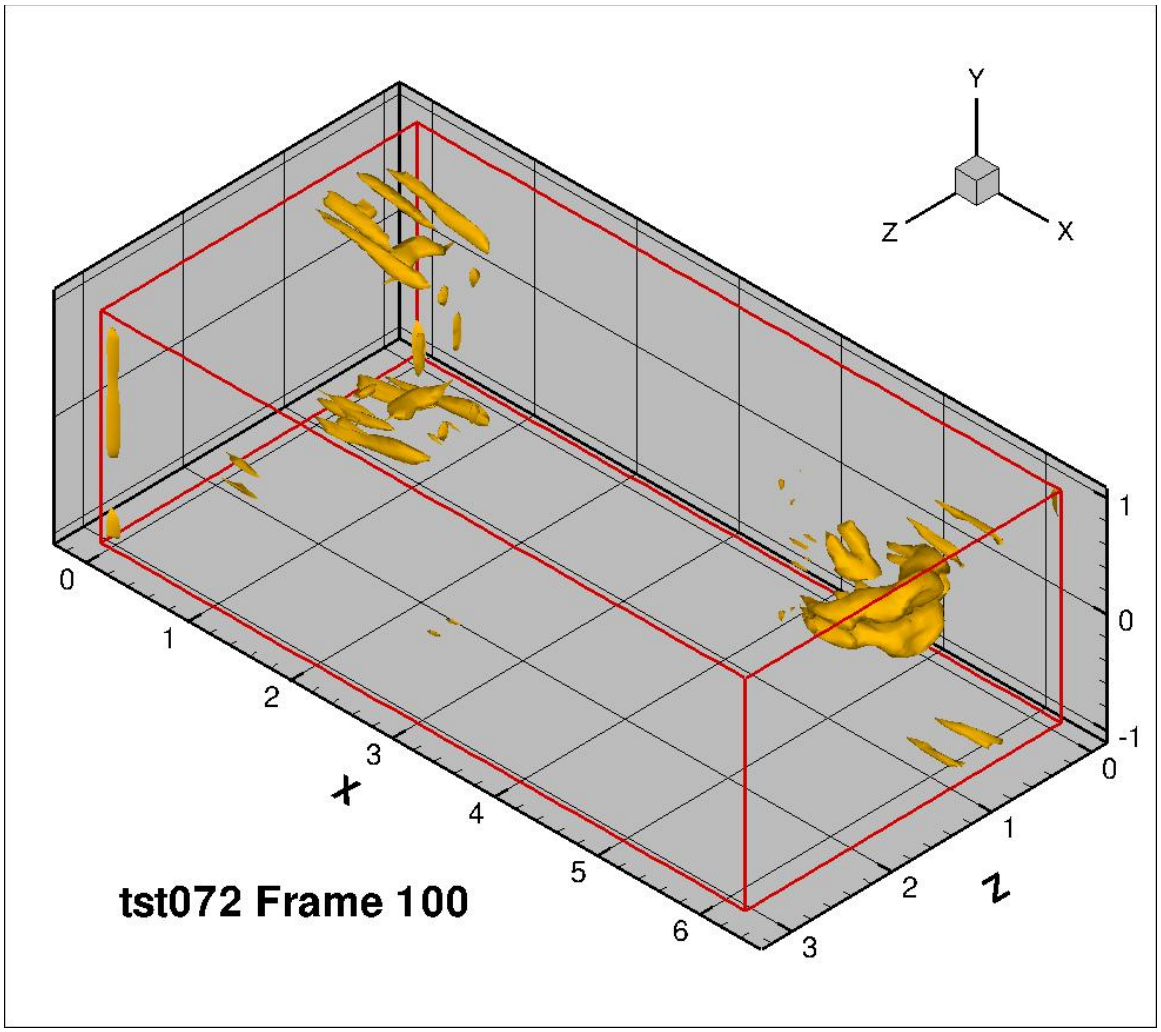

*Figure 63: 2 pair vortices, wall to wall, frame 100*

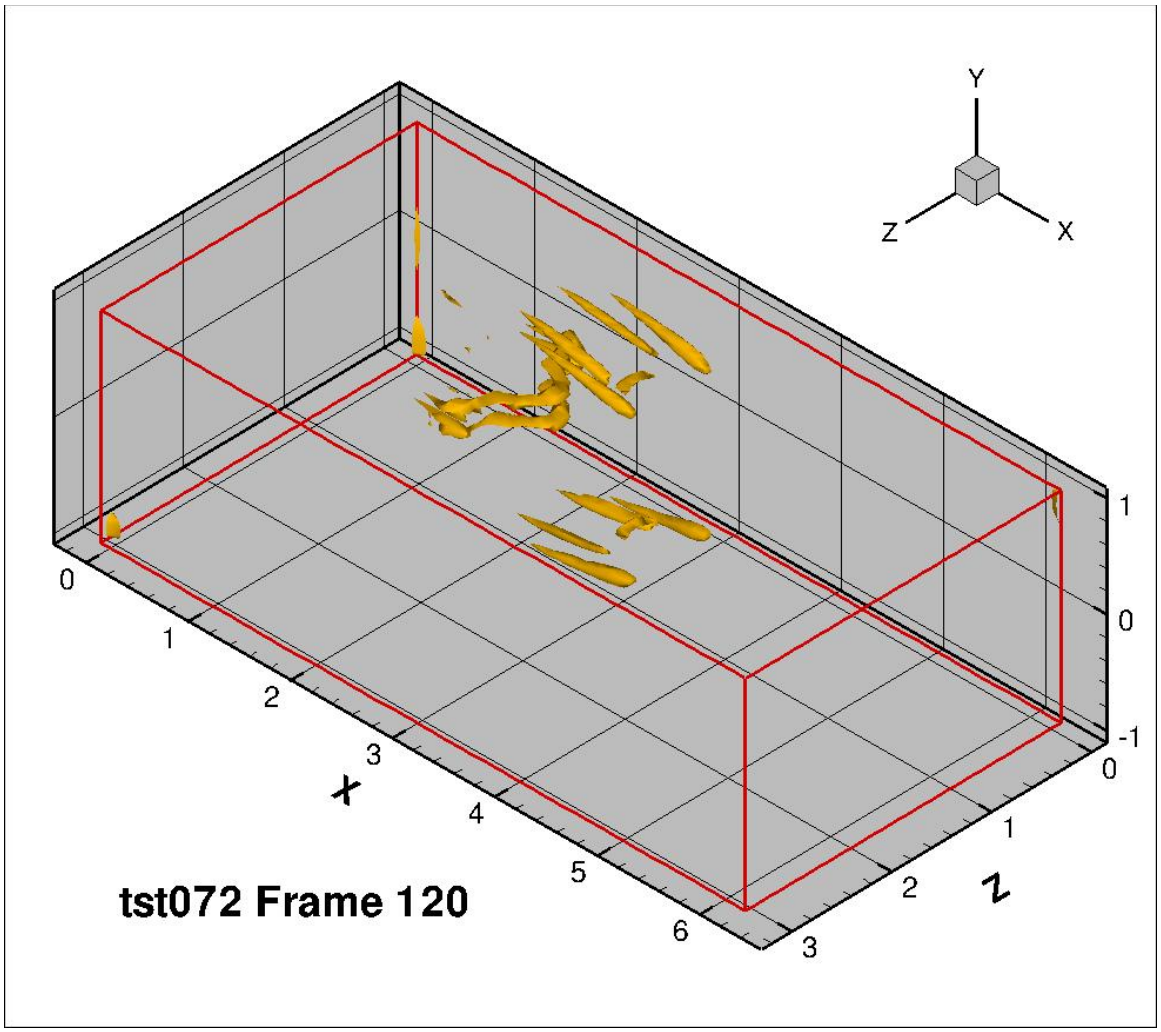

*Figure 64: 2 pair vortices, wall to wall, frame 120*

### *Lateral Vortices, H=0.3, tst073_iso.avi*

This simulation, conducted with a larger starting vortex momentum (H=0.3), was very similar to the preceding simulation where H=0.2. Both upstream and downstream vortex pairs generated vortices that moved upstream and downstream simultaneously passing through the recurring boundaries and then reentered the channel and passed through each other. Both the upstream and

downstream vortex pairs showed instability in the vortices extending wall to wall and connected the stretched vortices at the walls.

The stretched vortices in the boundary layer that were present after the recirculation of the structures through the recurring boundaries were larger than in the previous simulation. However, the stretched structures that were present mid-channel from the downstream vortex pair were not present during this simulation.

Later in the simulation, the downstream vortex pair had almost completely dissipated, while the upstream vortex pair had induced a very complicated set of complimentary vortices in addition to the principal stretched inclined vortices. Of note was that the single pair of vortices that connected the stretched vortex pairs at each wall in the previous simulation were not present.

Movie: tst073_iso.avi

## *0.1 4.4 Vortices Created from Flow about Obstructions*

Simulations were conducted of vortices that were created by inserting obstructions in the flow field. These vortices were intended to resemble the type of structure that would be created by a MEMS device that could be used for active control of turbulence. These simulations also provided examples of the development of canonical hairpin structures.

### 4.4.1 Rail and Blade Obstruction

In order to simulate a lateral vortex parallel to the wall, a trip rail was placed along the bottom wall. In the center of the rail, a small rectangular blade was placed extending above the rail. The blade generated two vertical sections of a vortex joined at the top with a short section of horizontal vortex. The intention of this arrangement was to create a lateral vortex similar to a Tollmein-Schlichting wave with a section of vortex that had been raised extending into the faster moving regions of the boundary layer. This structure was similar to an unstable boundary layer wave and appeared in the boundary layer for only a brief time $(5.00 \le t \le 5.01)$.

Movie: tst062_iso.avi, rail and blade obstruction present $5.00 \le t \le 5.01$

Immediately after the appearance of the rail and blade, a lateral vortex appeared parallel to the lower wall along the rail and on both sides of the blade. Around the blade, a vortex appeared which followed the shape of the blade. The lateral vortex from the rail generated multiple vortices that moved upstream from the rail and stayed close to the lower wall of the channel. The vortex around the blade also generated upstream traveling vortices along with the primary hairpin shaped vortex. The upstream moving and downstream moving lateral vortices from the

rail dissipated quickly leaving the vortex structure formed by the blade to move downstream. The structure resulting from the blade took on a form similar to the canonical hairpin vortex. As the structure moved downstream, the head of the pin decayed and then reestablished several times. The simulation ended before the head of the hairpin vortex decayed completely; however, the behavior was similar to the other simulations that produced a hairpin vortex then dissipated to the form of a pair of stretched vortical structures.

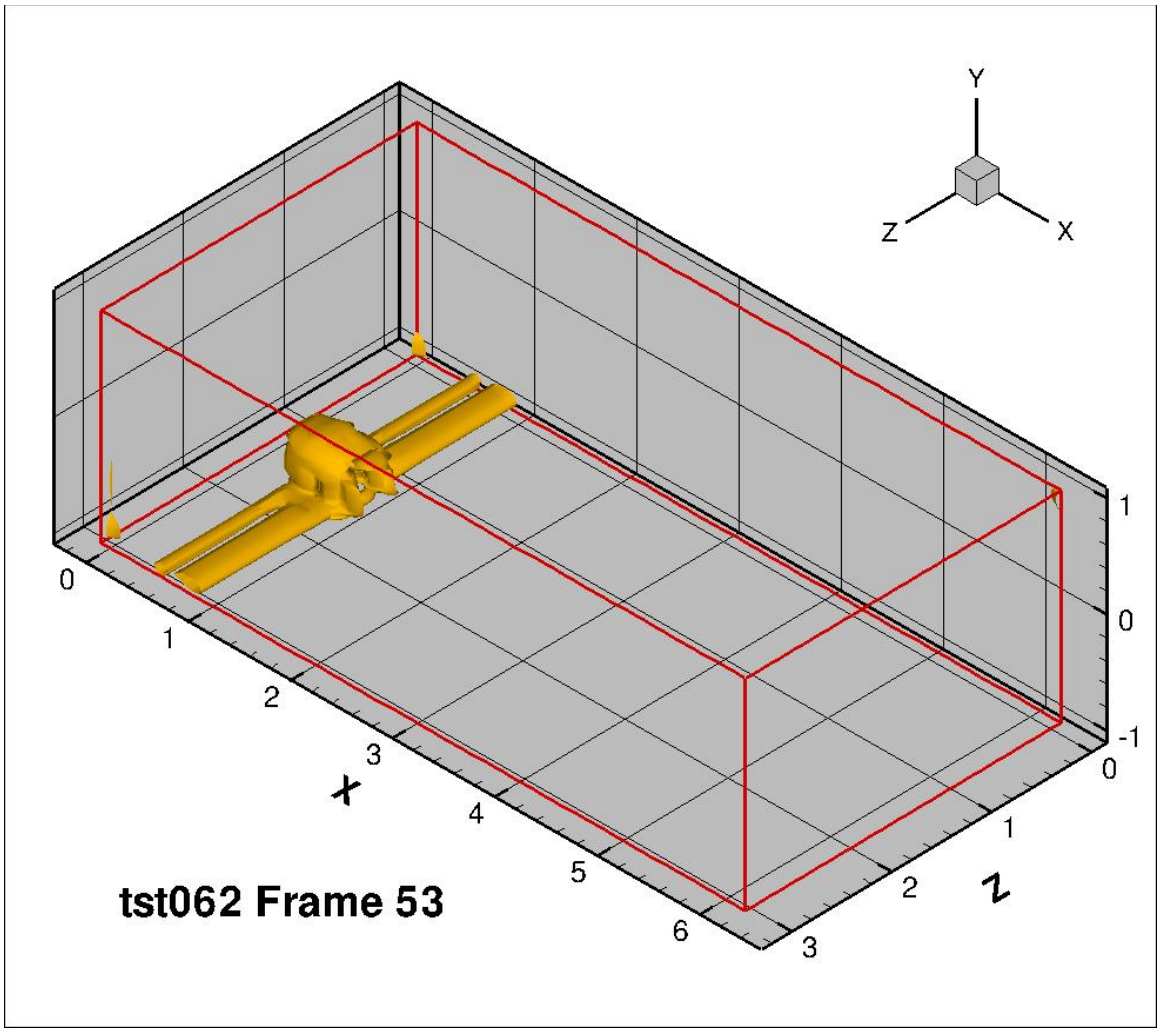


*Figure 65: Rail and blade obstruction on channel wall, frame 53*

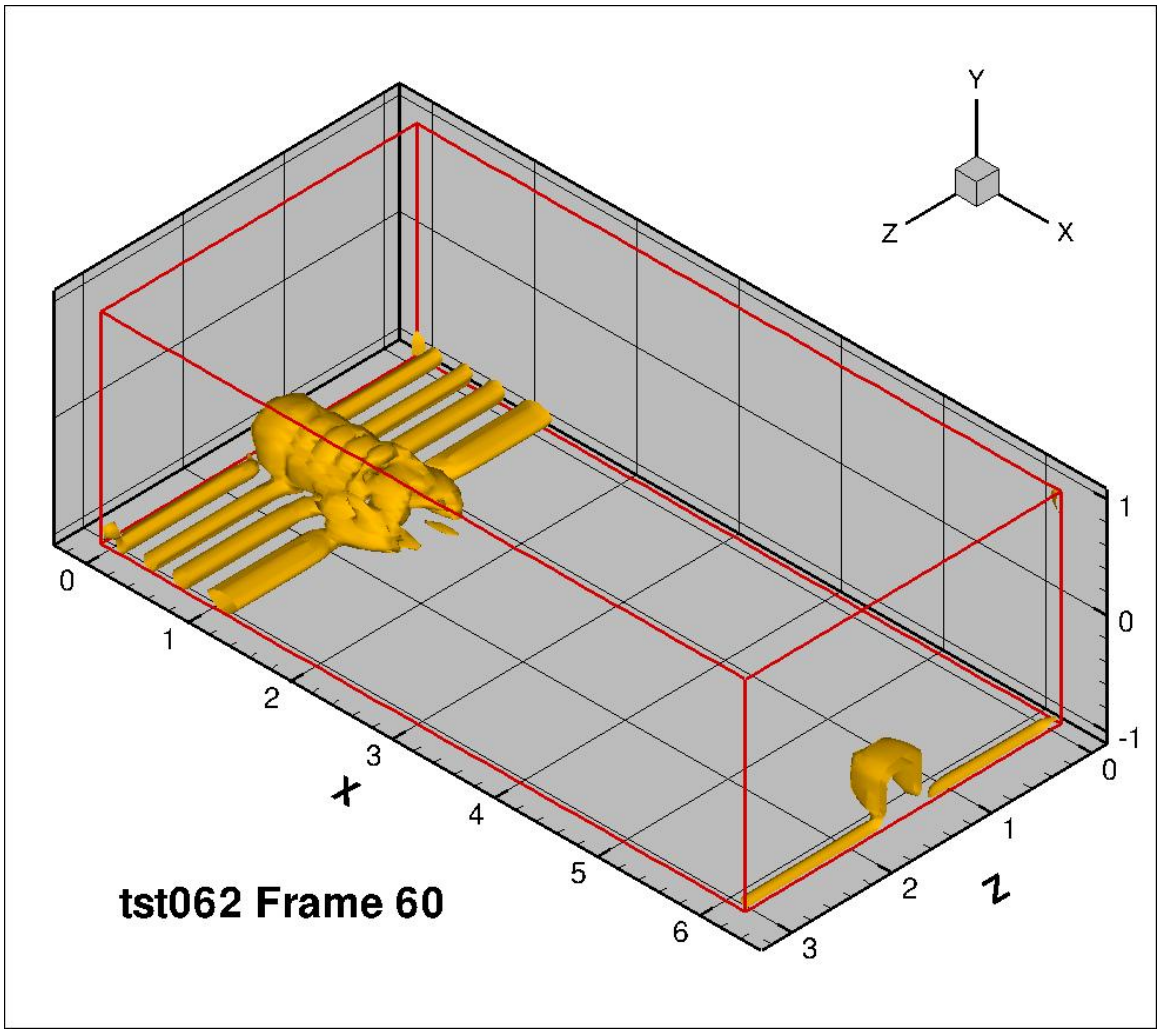


*Figure 66: Rail and blade obstruction on channel wall, frame 60*

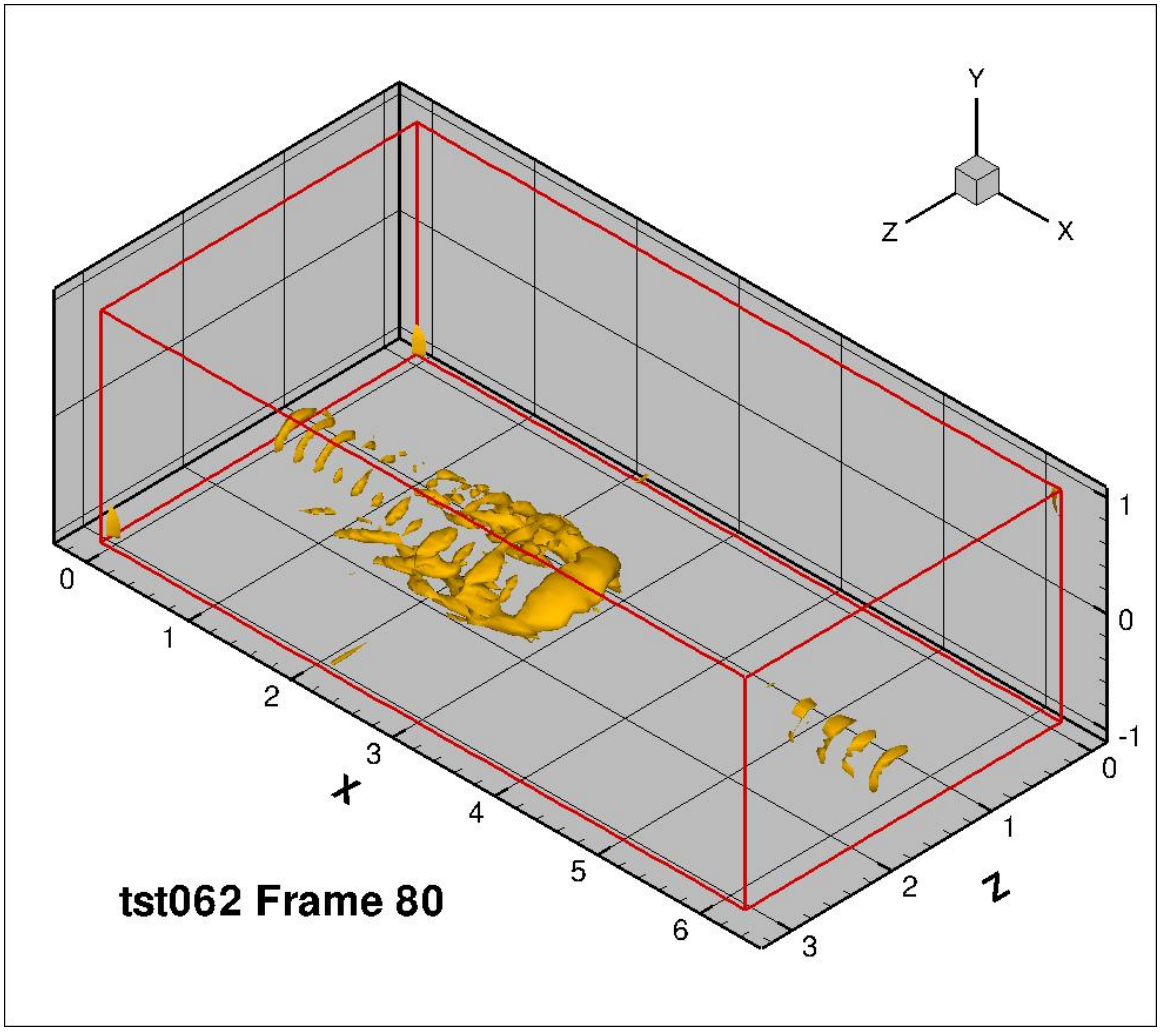


*Figure 67: Rail and blade obstruction on channel wall, frame 80*

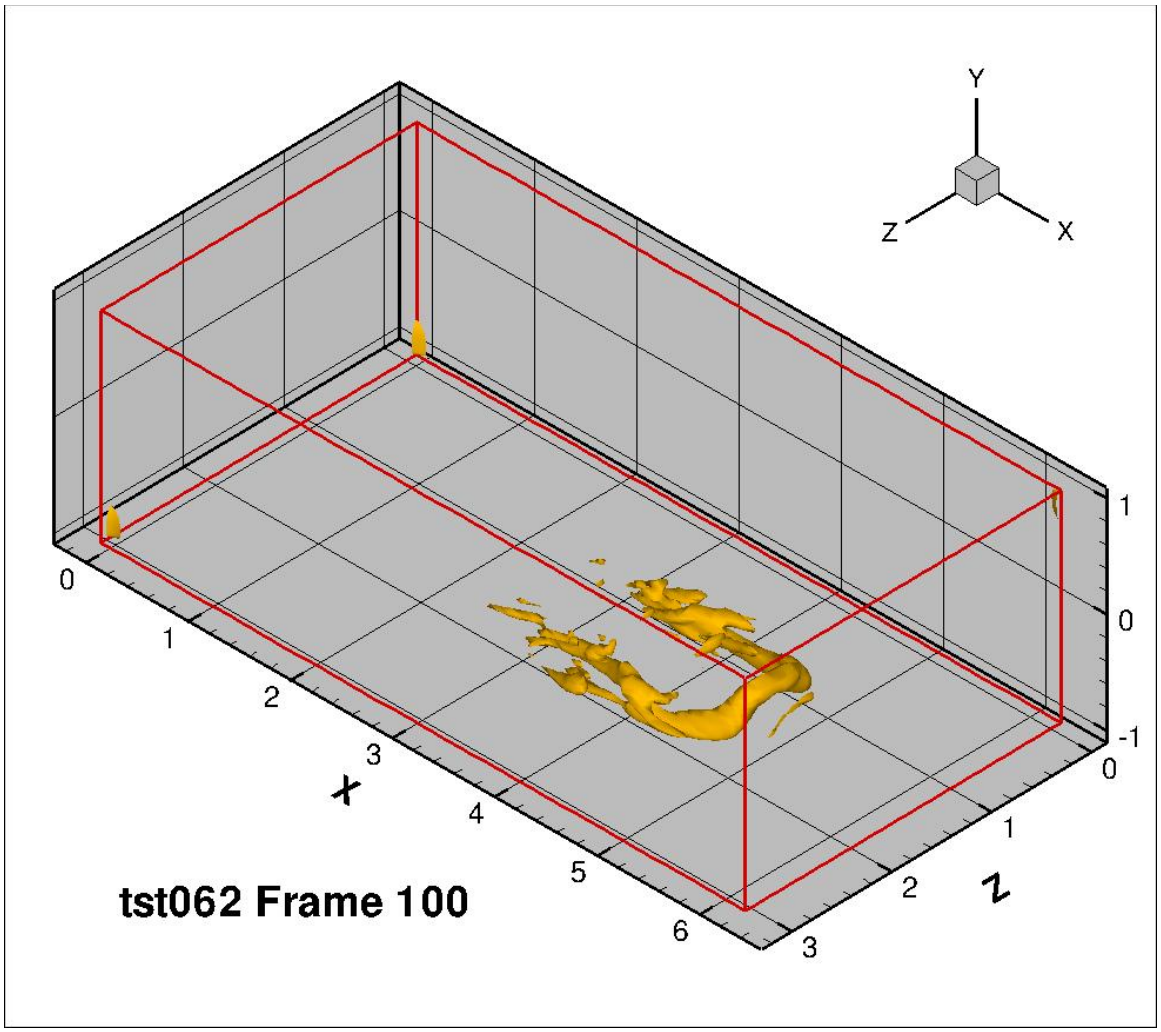

*Figure 68: Rail and blade obstruction on channel wall, frame 100*

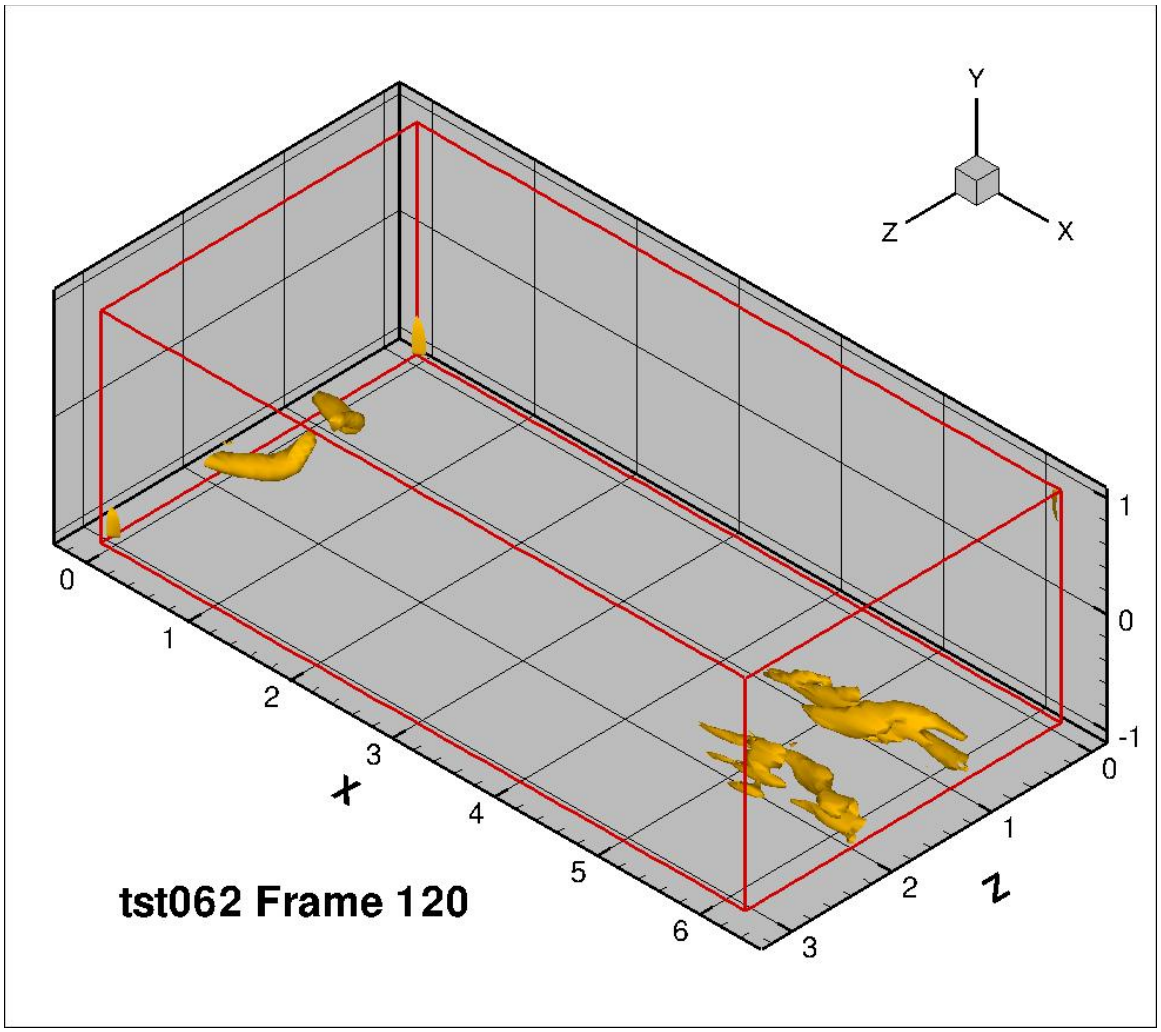

*Figure 69: Rail and blade obstruction on channel wall, frame 120*

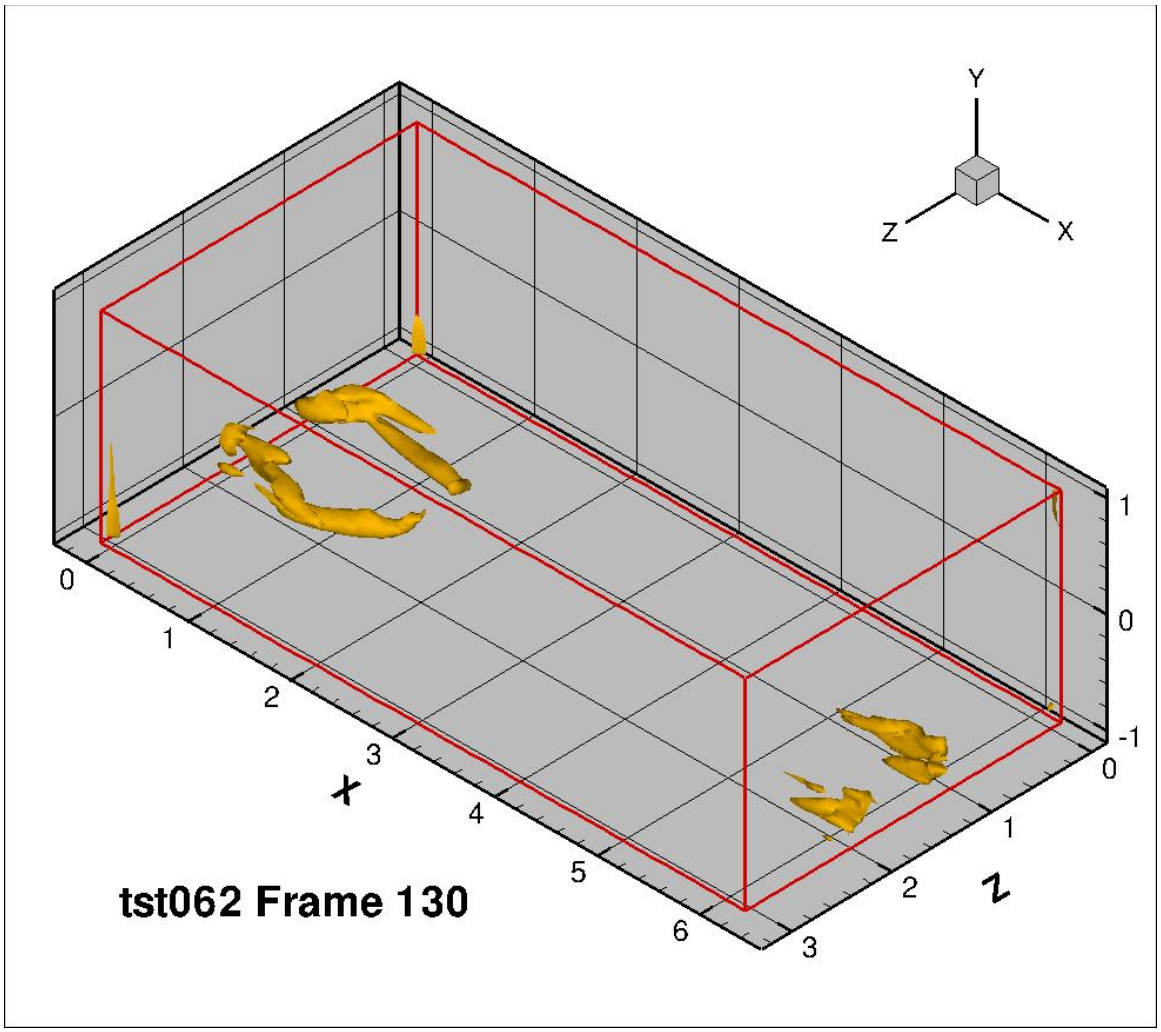

*Figure 70: Rail and blade obstruction on channel wall, frame 130*

## *0.2 4.5 Wall to Wall Obstruction*

In another simulation, a narrow fixed obstruction was placed in the channel extending from the fixed lower wall to the fixed upper wall of the channel. This wall to wall obstruction remained in the flow for a short duration $(0.1 \le t \le 0.2)$. As a result of the obstruction, a series of vortical waves were formed moving upstream along with a strong pair of vortices at the edges of the obstruction. The

upstream traveling vortical waves decayed quickly, while the vortices formed at the edges of the obstruction were advected downstream. As the edge vortices moved downstream, the portions in the boundary layer were inclined downstream and stretched while the sections in mid channel flow between the upper and lower boundary layers dissipated then reestablished several times reconnecting the upper and lower inclined vortices. Finally, the section of vortex connecting the inclined vortices at the upper an lower wall dissipated leaving inclined vortical structures. These vortical structures are very similar to the vortices created by the rail and blade and lateral vortex pair simulations described above.

Movie: tst066_iso.avi, obstruction extending bottom wall to upper wall, $0.1 \le t \le 0.2$ .

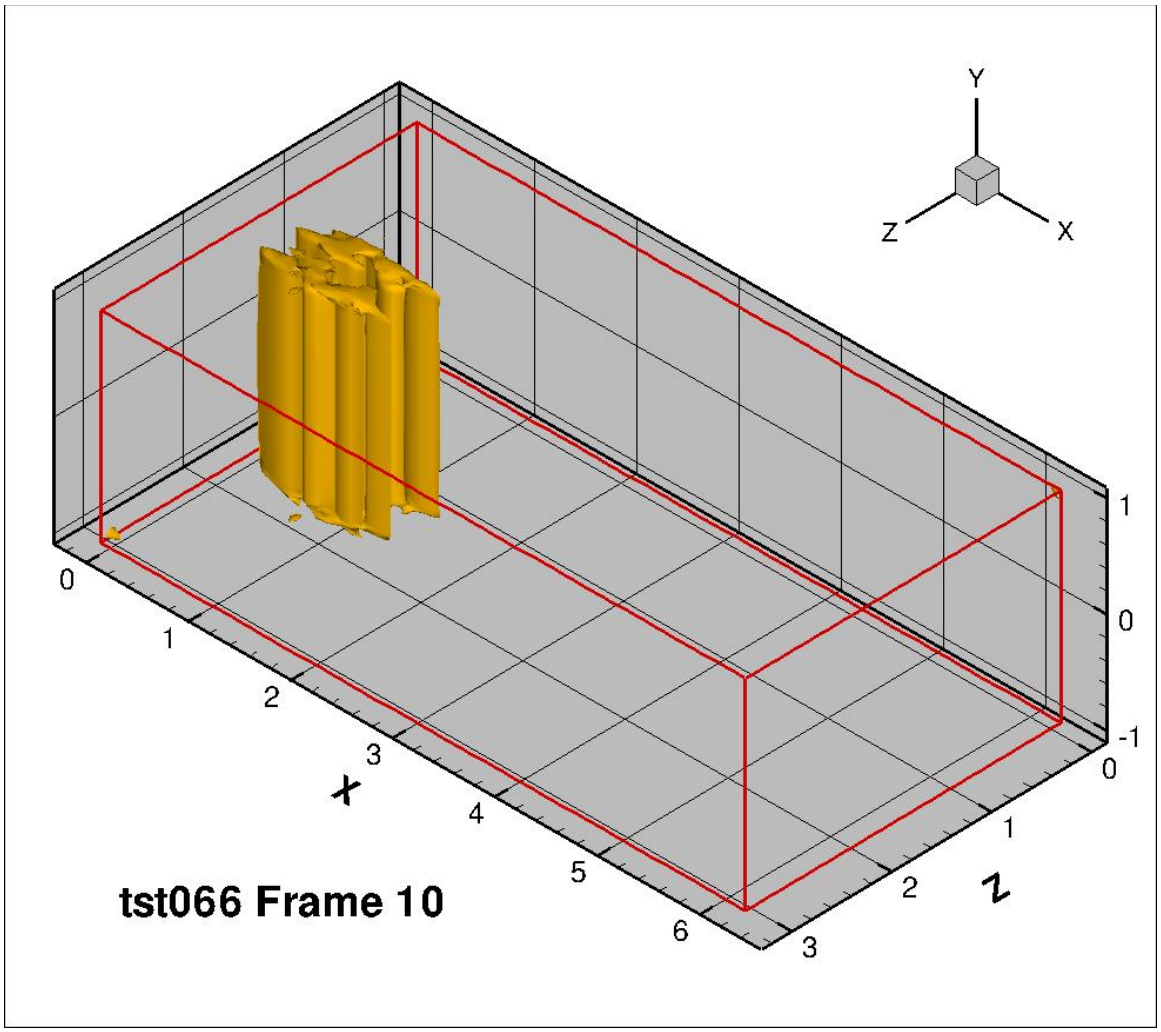

*Figure 71: Narrow obstruction wall to wall, frame 10*

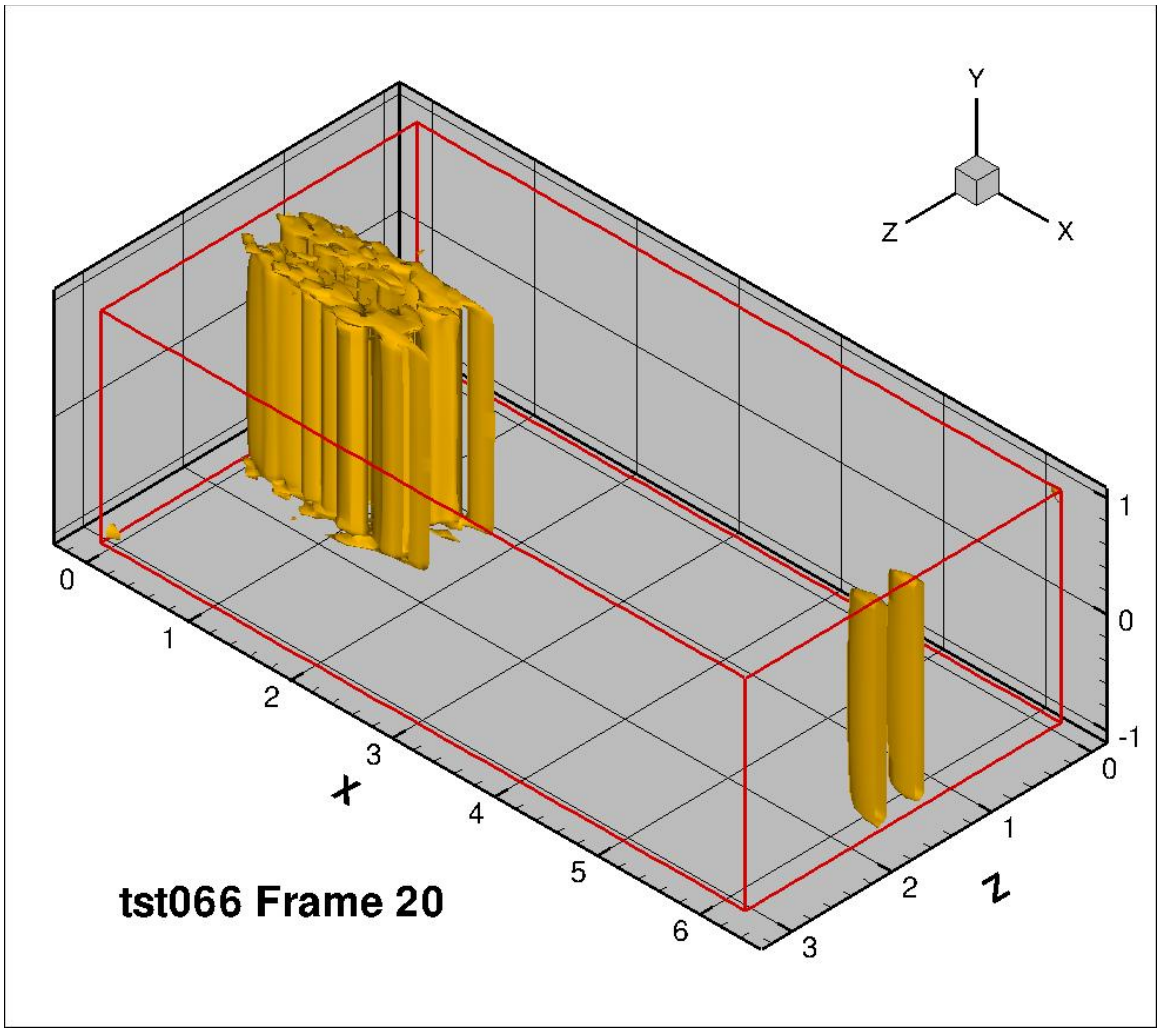

*Figure 72: Narrow obstruction wall to wall, frame 20*

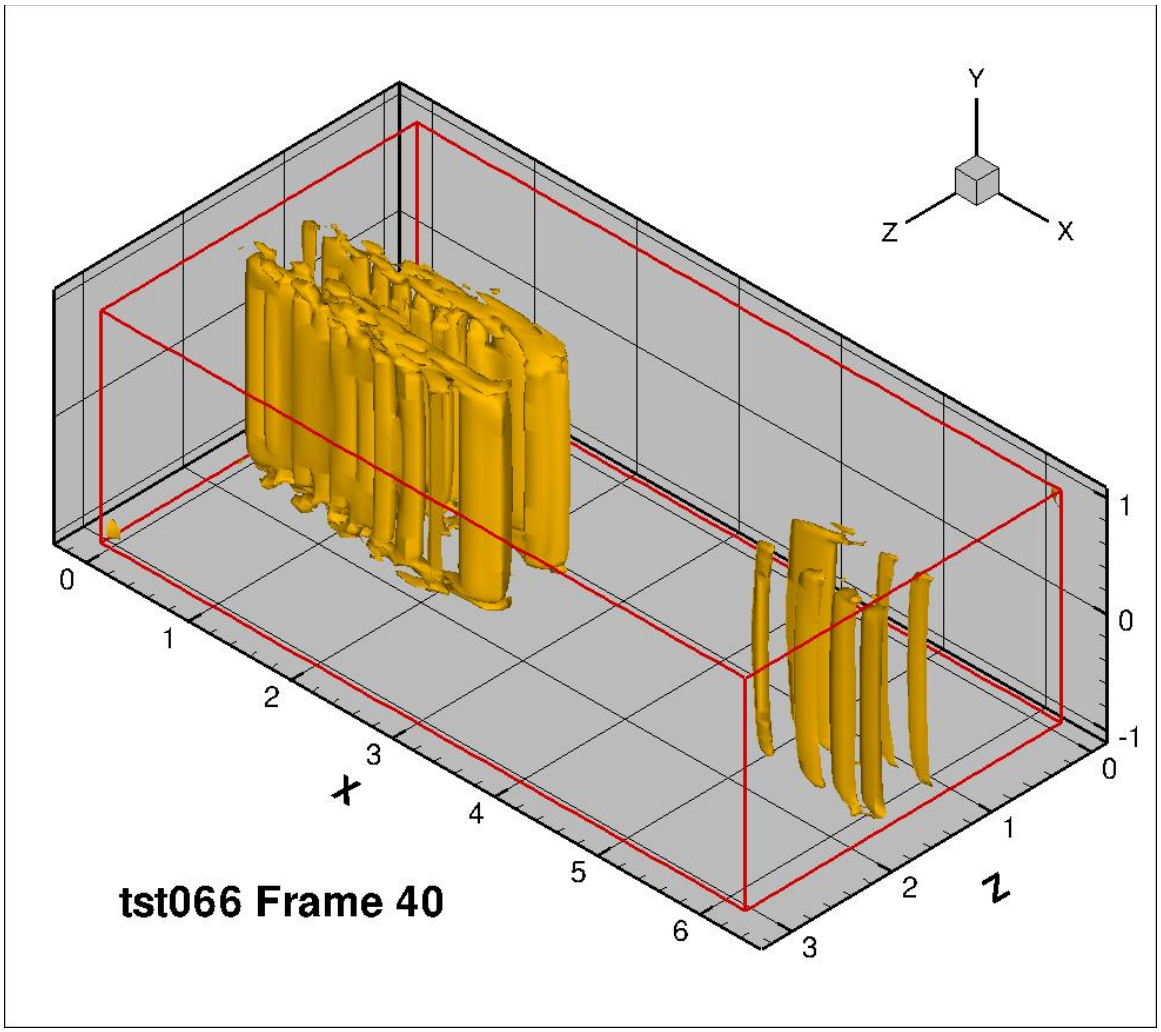


*Figure 73: Narrow obstruction wall to wall, frame 40*

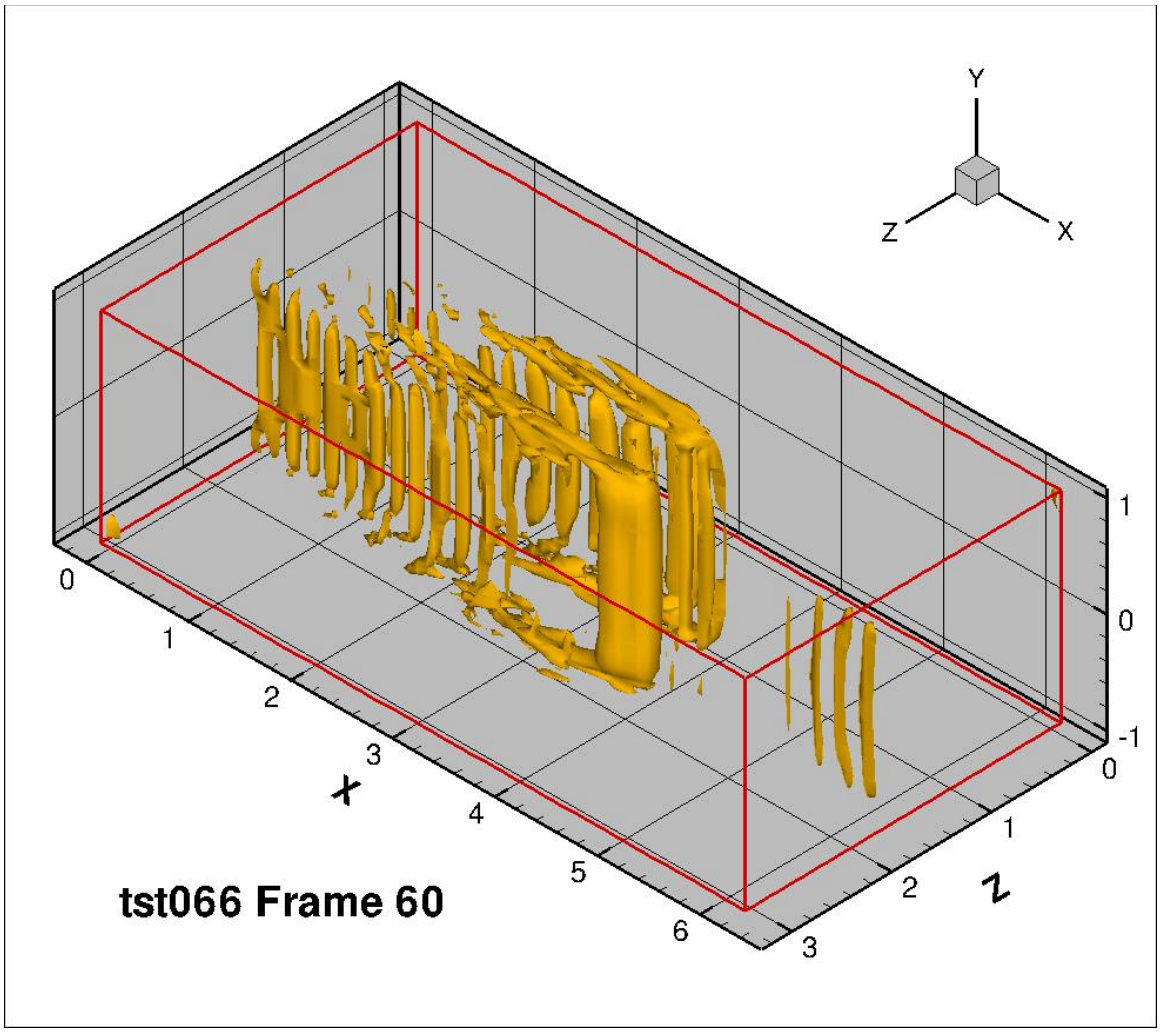

*Figure 74: Narrow obstruction wall to wall, frame 60*

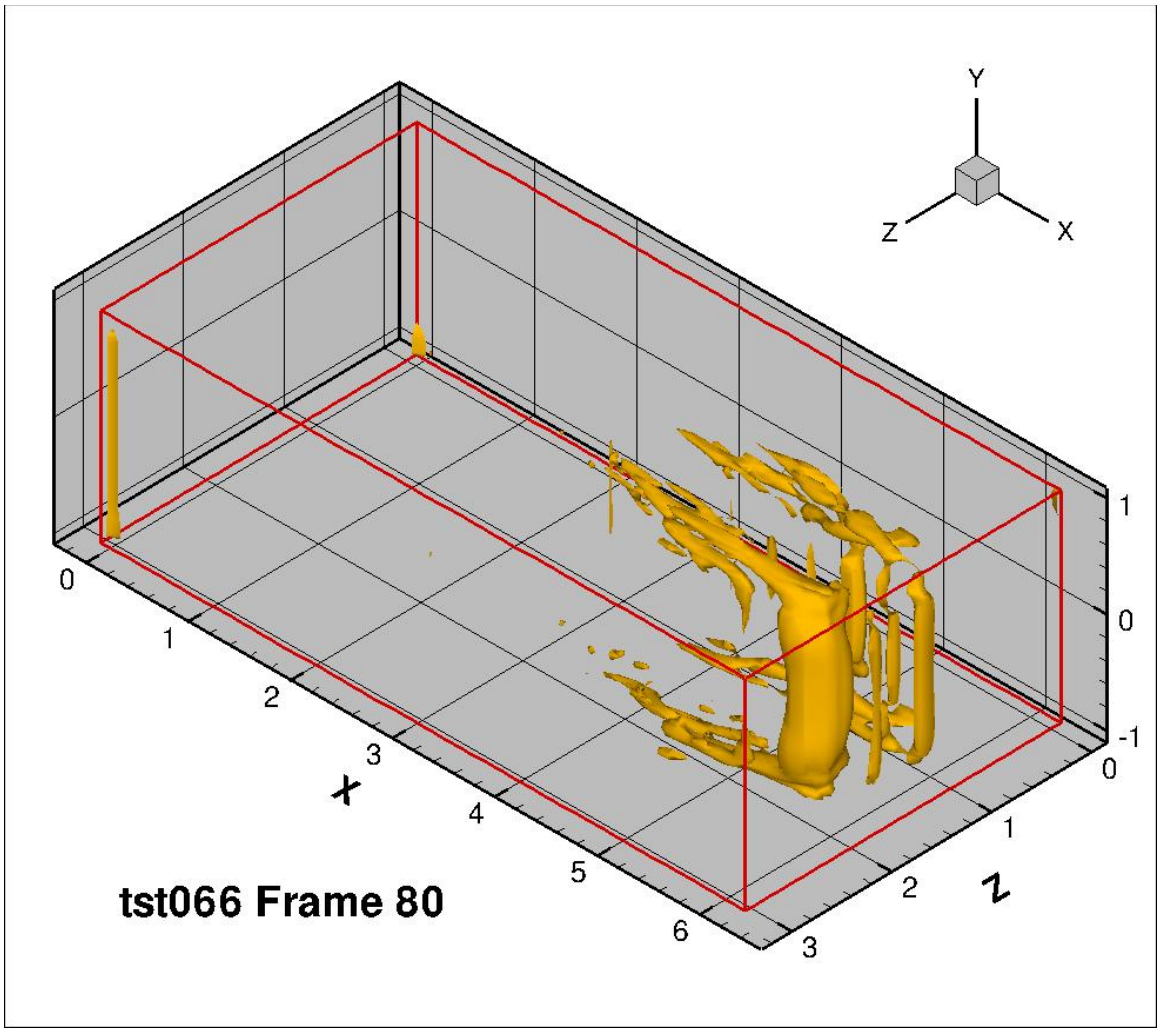

*Figure 75: Narrow obstruction wall to wall, frame 80*

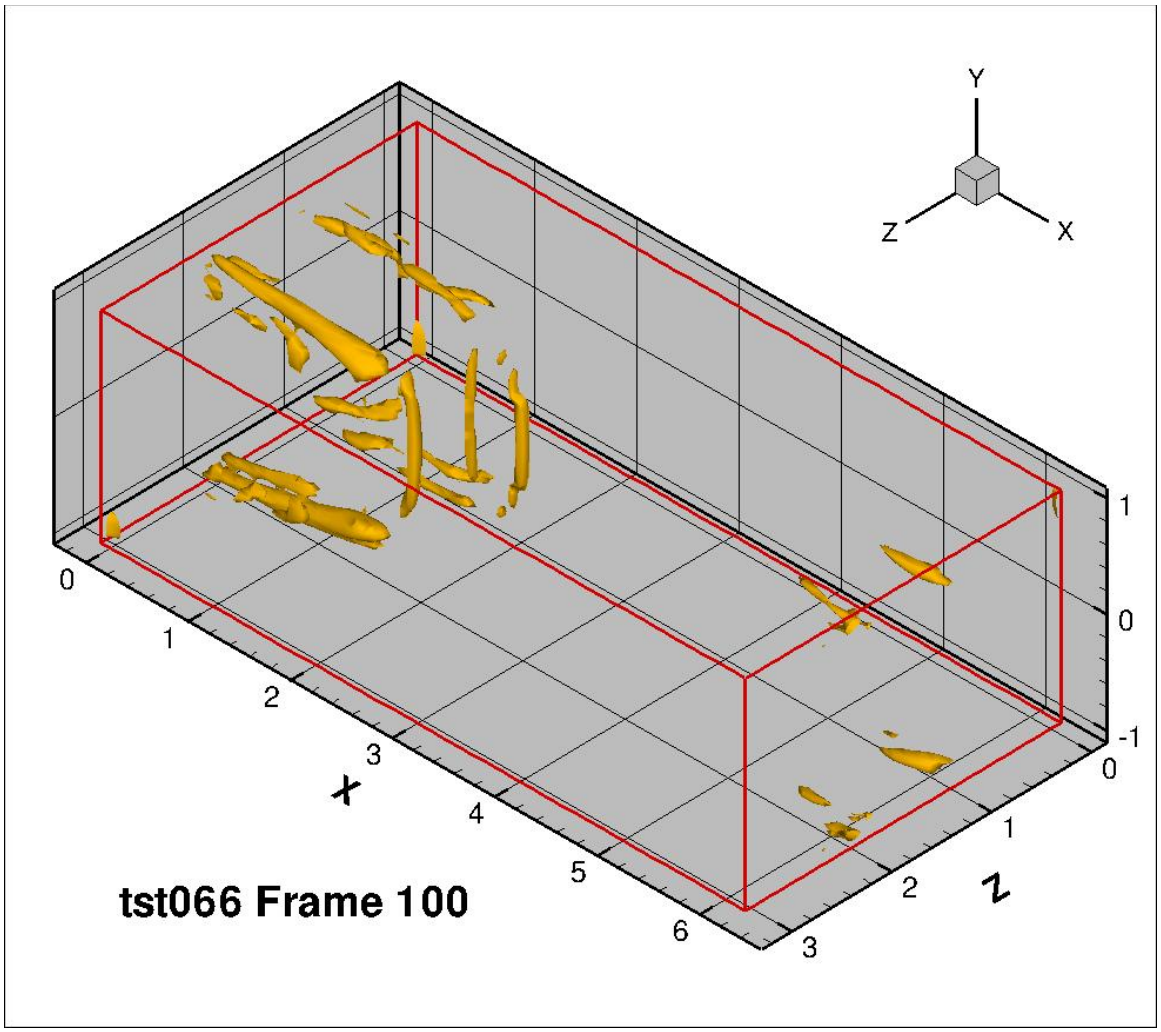

*Figure 76: Narrow obstruction wall to wall, frame 100*

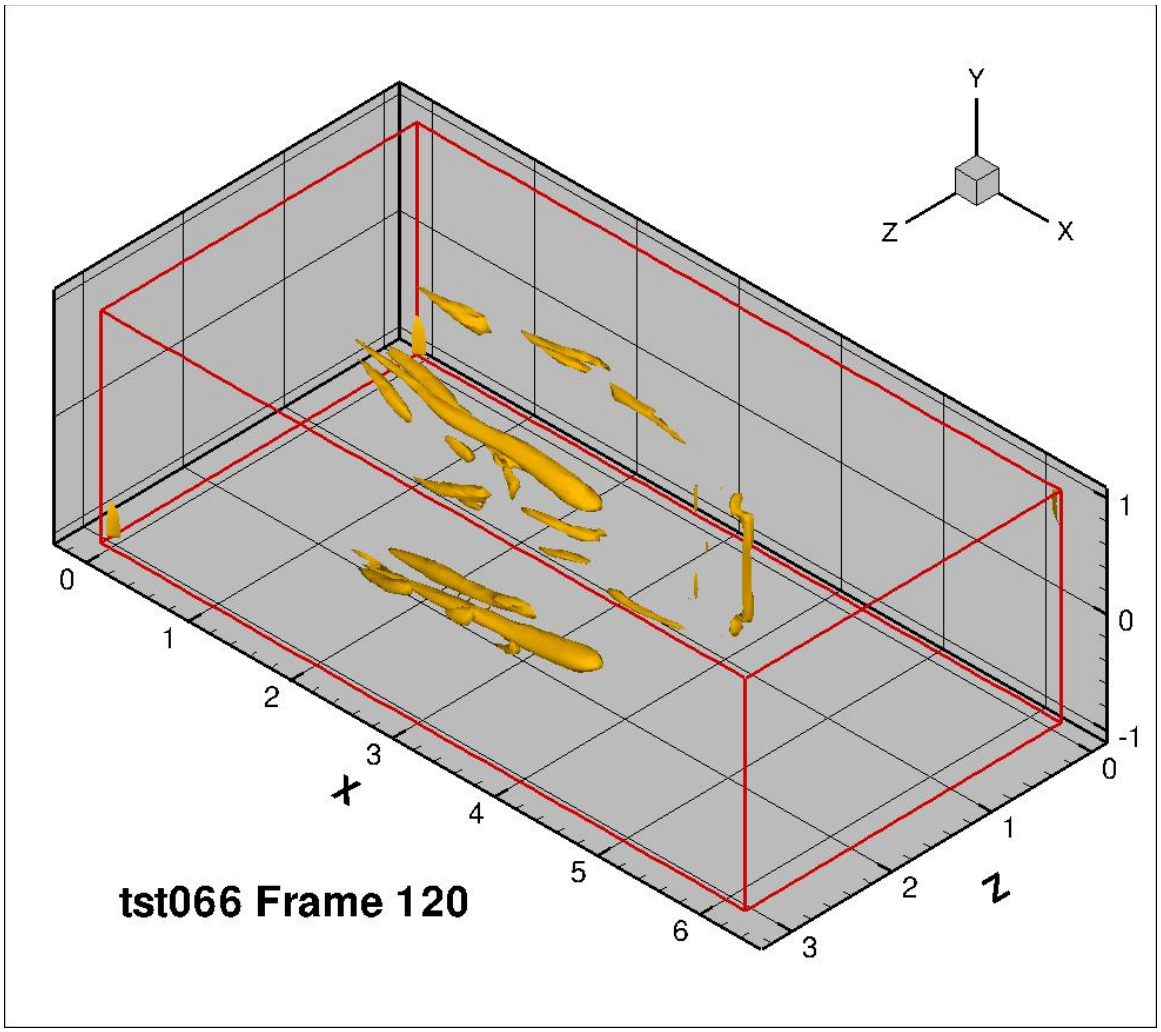

*Figure 77: Narrow obstruction wall to wall, frame 120*

## *0.3 4.6 Vortices Created from Fluid Injection*

To provide a basis for comparison to experimental work by Haidari and Smith (1994) and simulation by Singer and Joslin (1995), a simulation was conducted of hairpin vortex generation method common to these works.

The simulation was conducted using Direct Numerical Simulation of channel flow while injecting fluid through a longitudinally oriented slot in the floor or lower solid

boundary of the channel. This technique required steady injection of fluid at a velocity of approximately .25U through a longitudinally oriented slot of proportions 1x5. Simultaneous withdrawal of an equal volume of fluid was required for continuity reasons. Fluid injected in this manner provided a reduction in momentum at the wall and an inflection in the boundary layer velocity profile. The resulting instability from the velocity inflection initiated the formation of a hairpin vortex. Along with the hairpin vortex, another vortex was generated upstream and complimentary vortices were developed adjacent to the sides of the primary hairpin vortex.

As the hairpin vortex was advected by the flow, the head of the hairpin vortex decayed, moved downward, disappeared momentarily, then reattached and then dissipated again leaving the inclined stretched vortices within the boundary layer. This pair of inclined stretched vortices persisted for several passes through the channel.

Ultimately, the hairpin vortex generated by fluid injection means looked like the vortex pair generated by all of the methods described above.

Movie: tst063_iso.avi

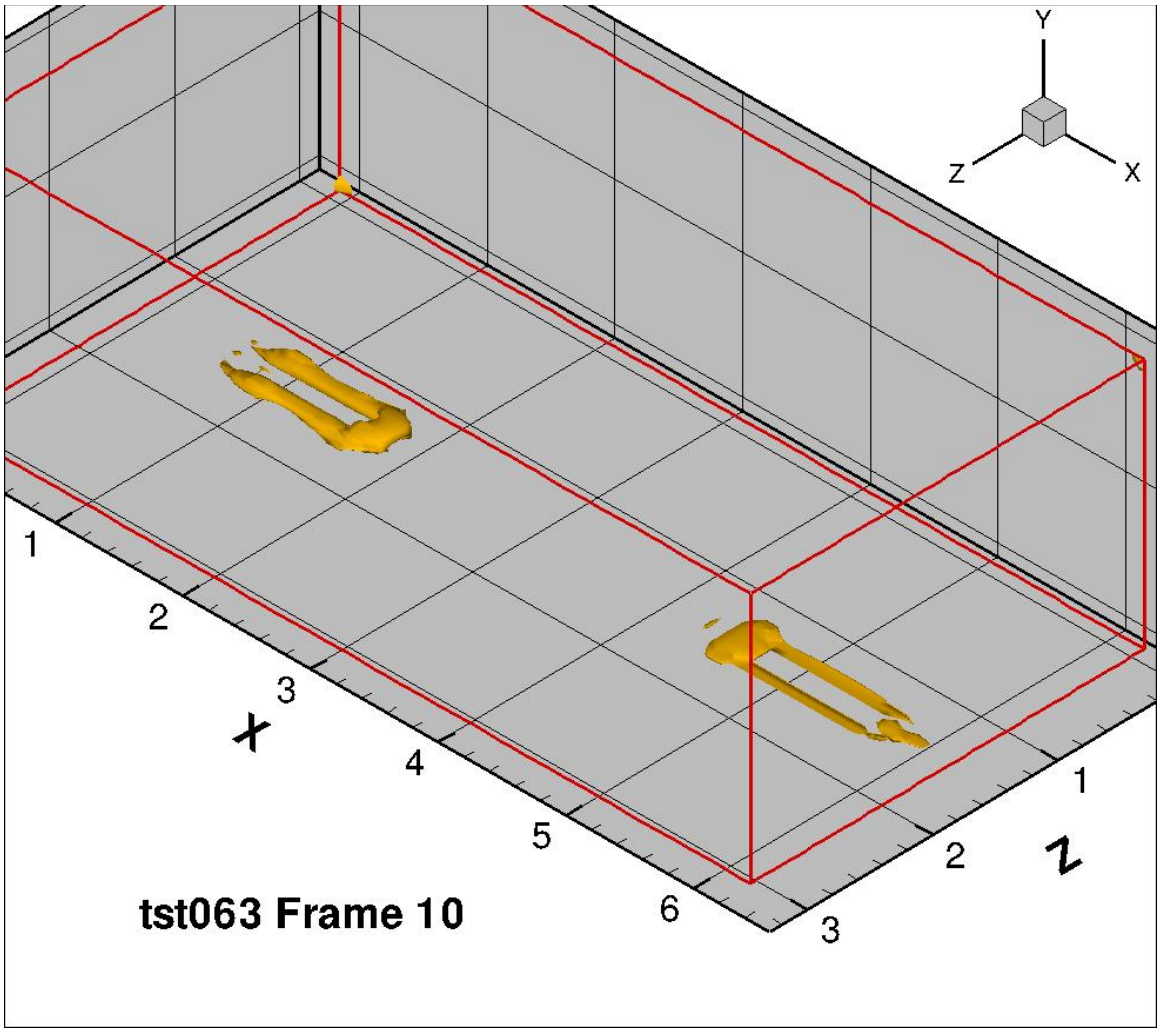

*Figure 78: Vortices from fluid injection, frame 10*

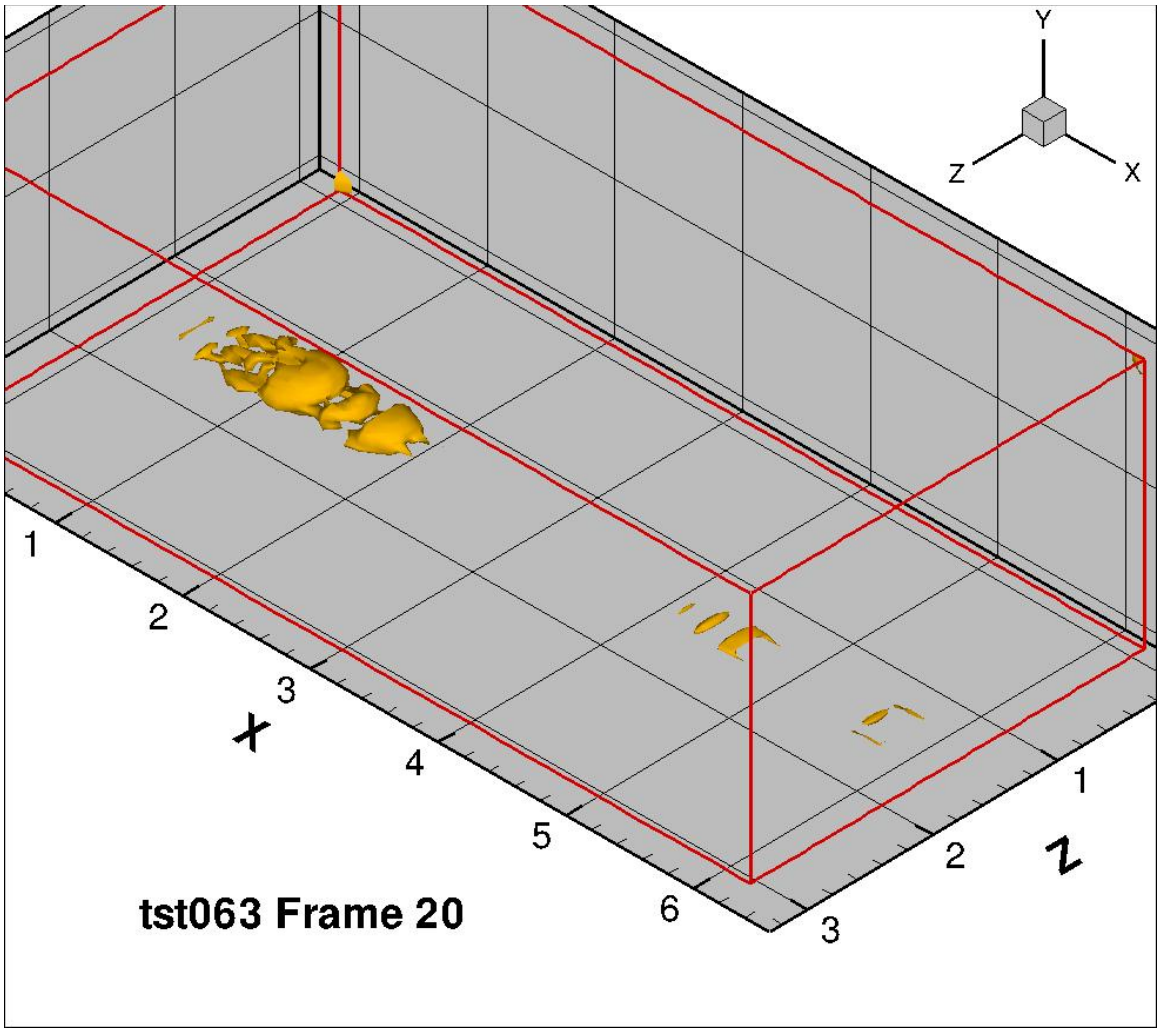

*Figure 79: Vortices from fluid injection, frame 20*

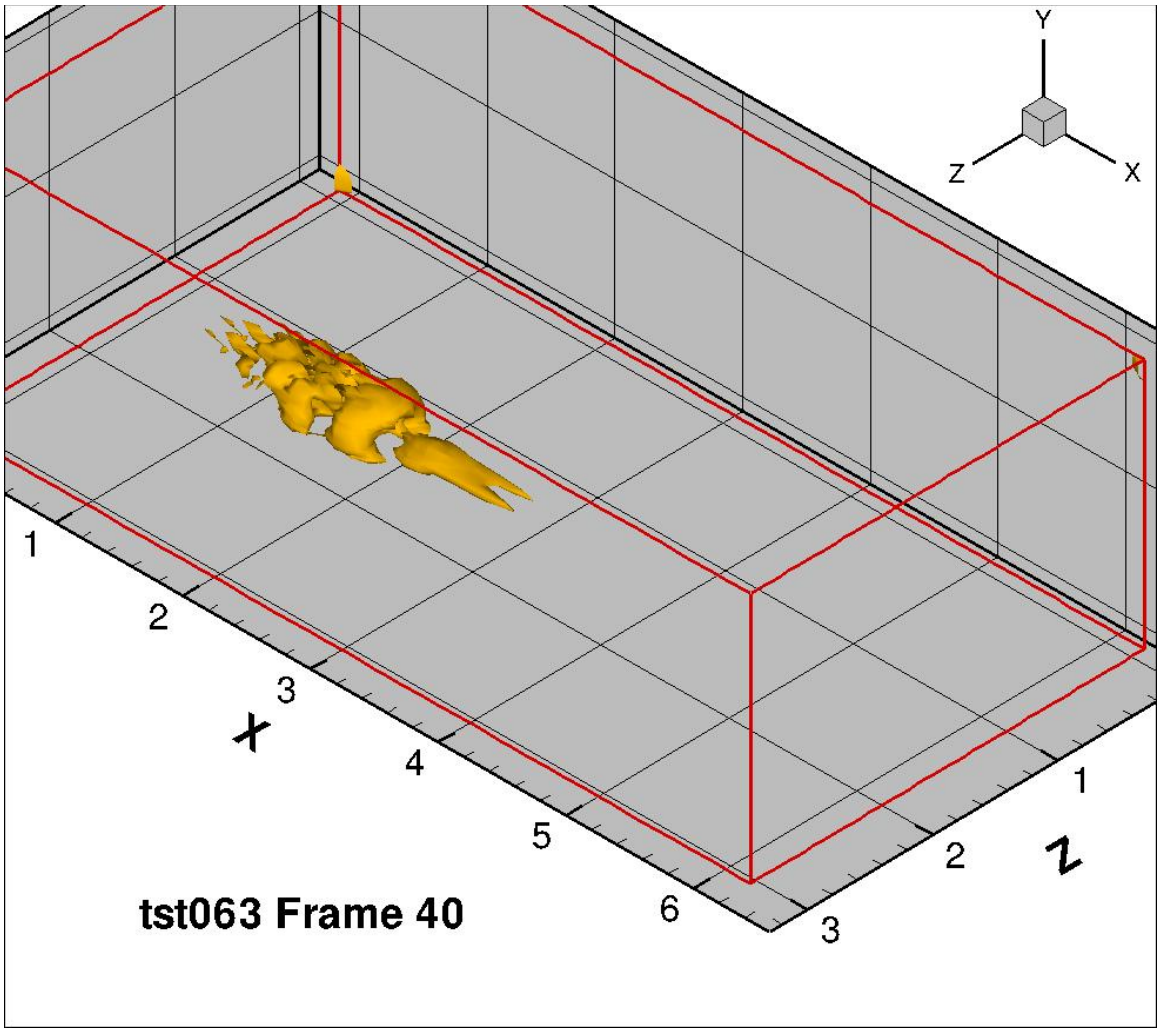

*Figure 80: Vortices from fluid injection, frame 40*

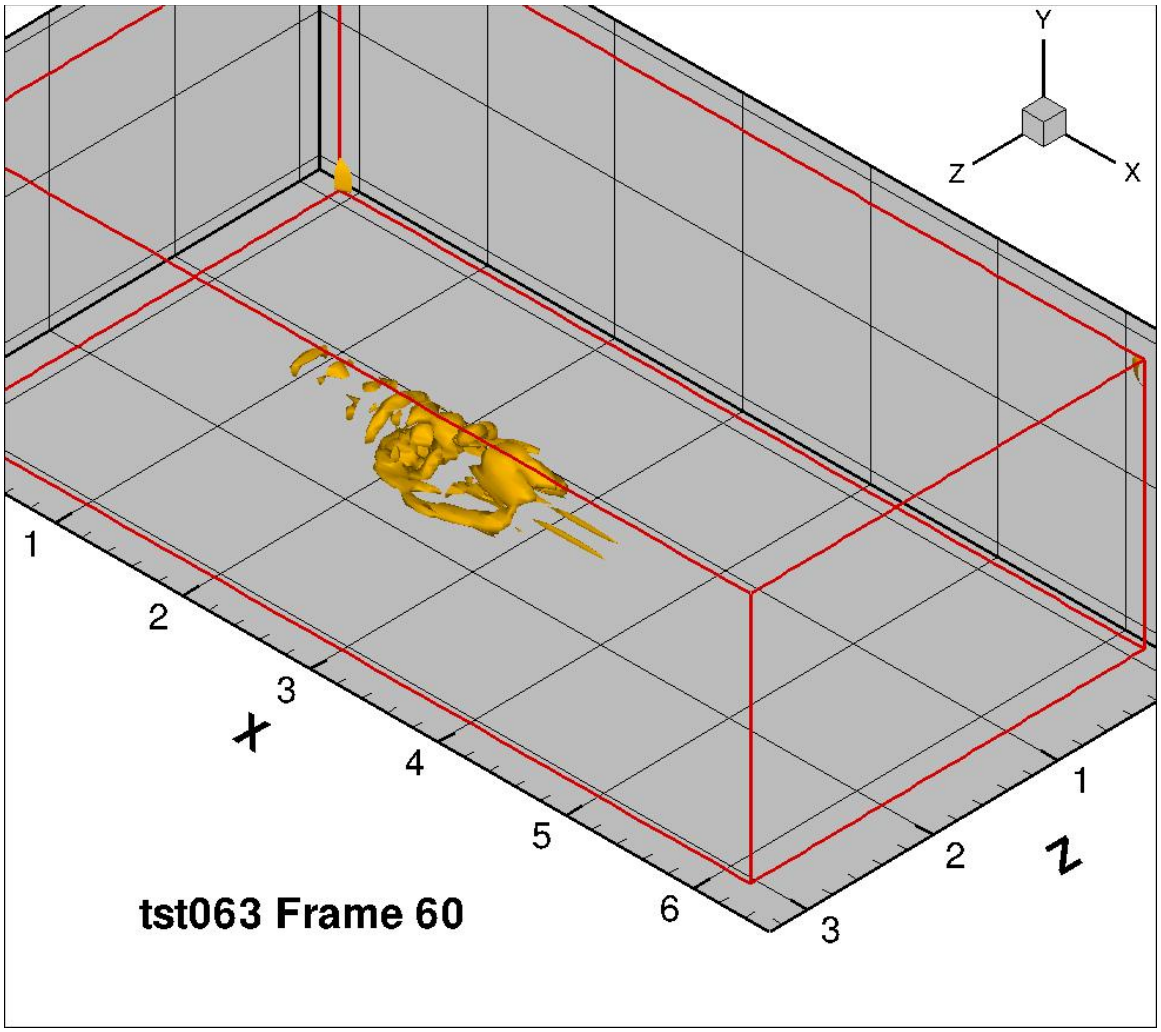

*Figure 81: Vortices from fluid injection, frame 60*

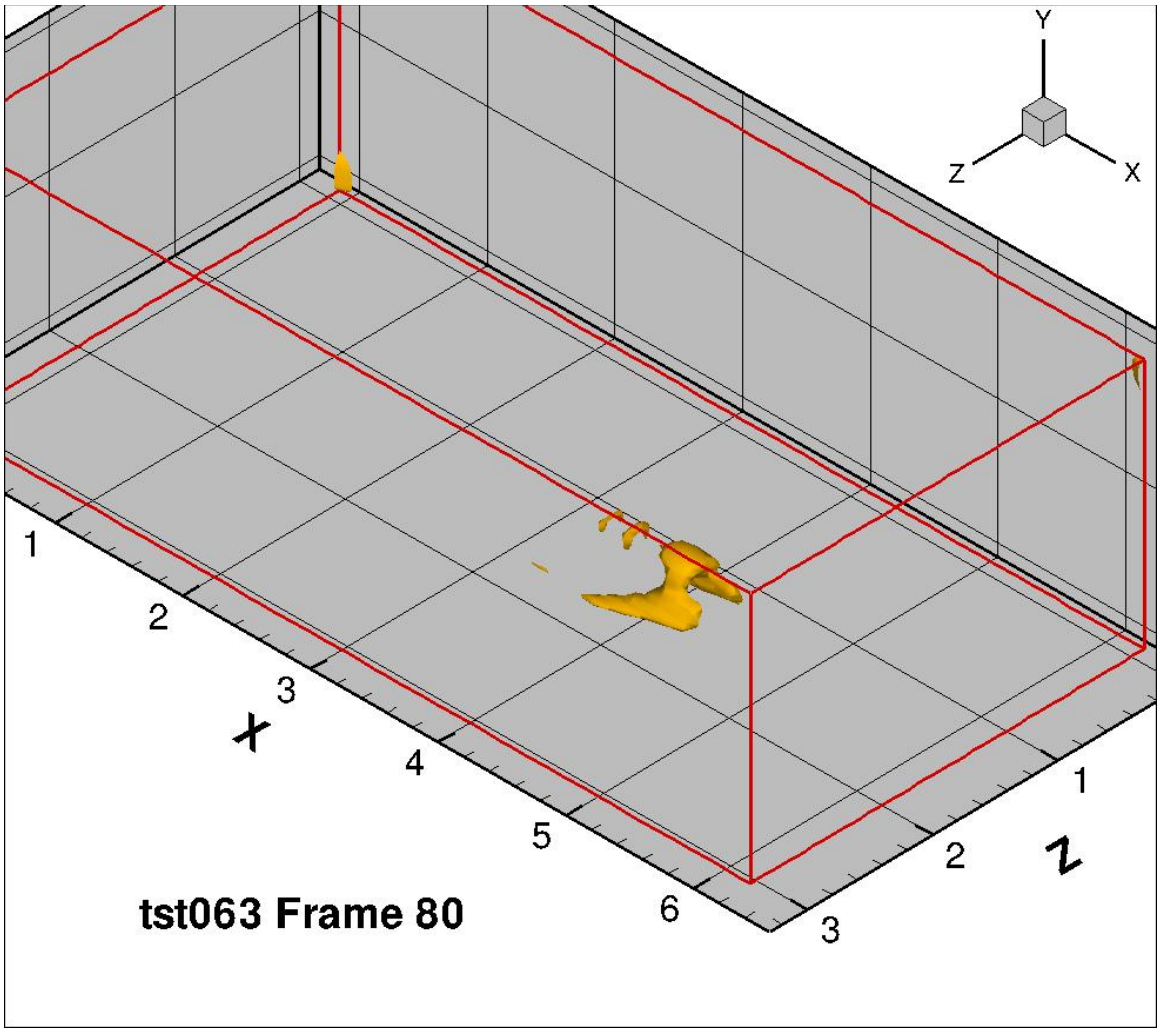

*Figure 82: Vortices from fluid injection, frame 80*

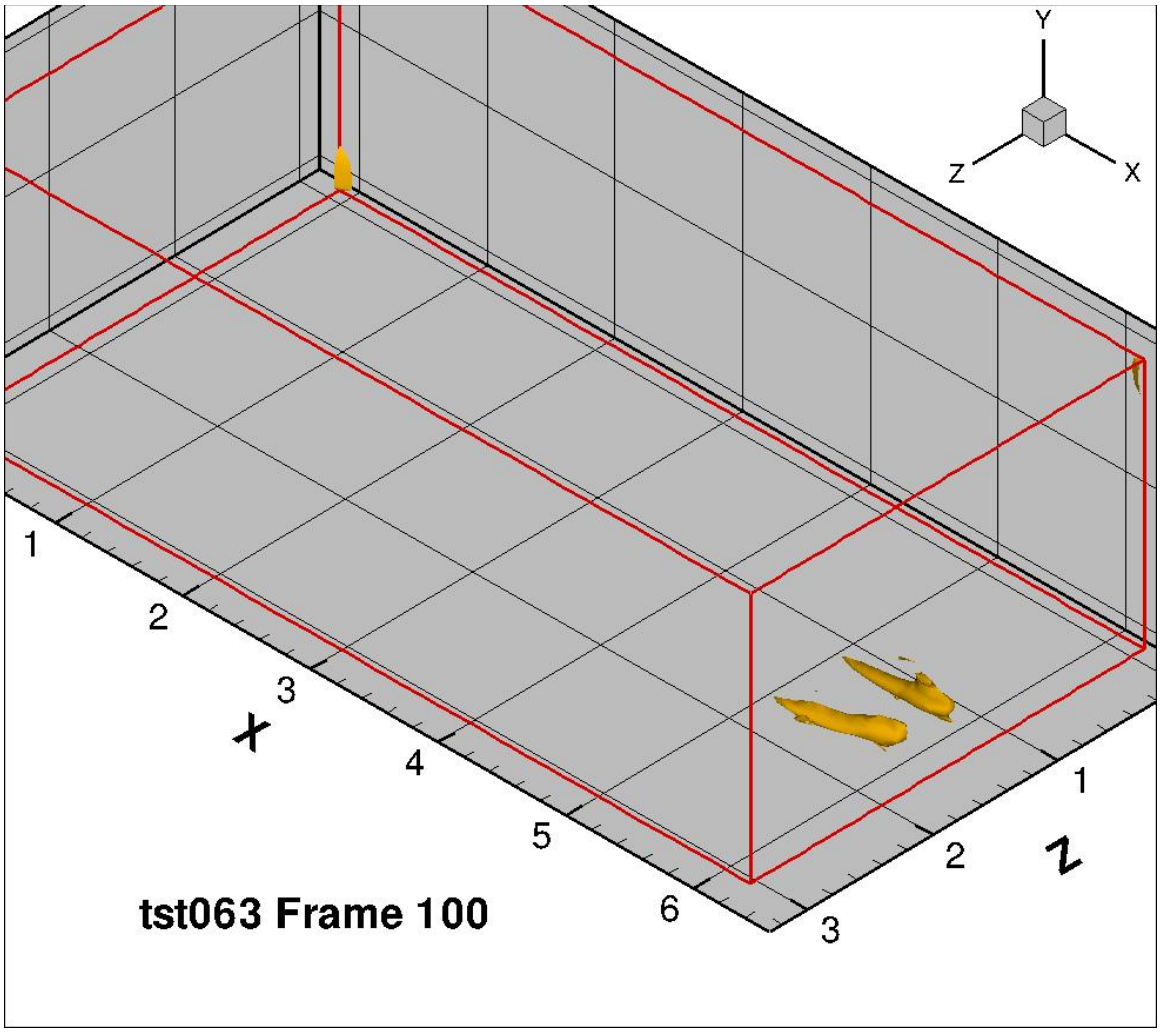

*Figure 83: Vortices from fluid injection, frame 100*

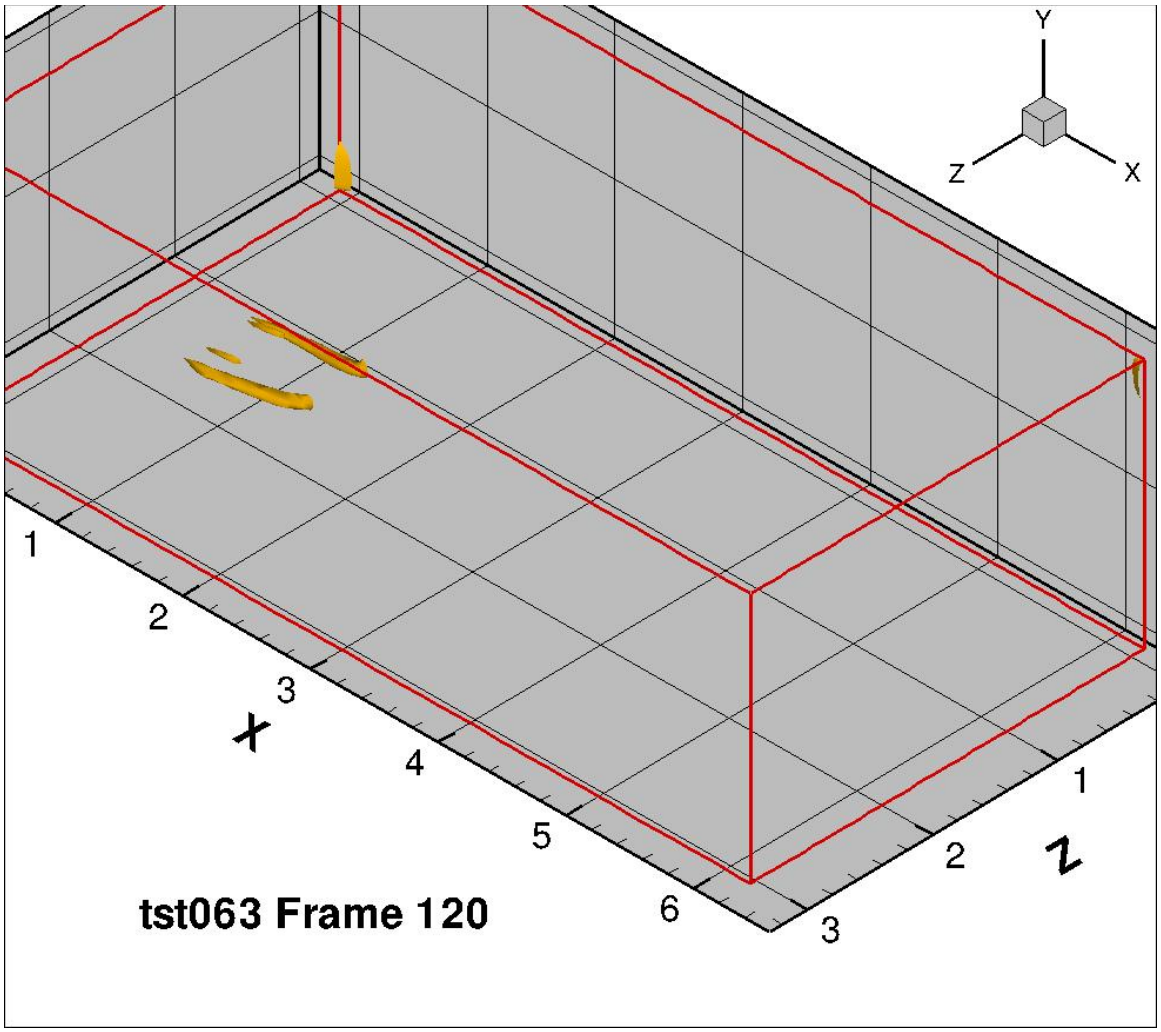

*Figure 84: Vortices from fluid injection, frame 120*

# 5.Discussion

## *5.1 Similarity of vortical structures*

Since the discovery of the turbulent burst, there has been significant effort placed in observing, studying, and simulating this phenomenon. It is believed that the turbulent burst mechanism provides the key to the presence of increased drag in turbulent flow. As part of the study of turbulent bursts, much emphasis has been placed upon the transition to turbulence and the study of instability of the laminar boundary layer. Of note was that the all methods used to simulate hairpin vortices used in this work were capable of creating a hairpin vortex or vortex with significant similarity to the canonical hairpin vortex along with accompanying induced vortical structures.

## *5.2 Contribution of turbulent Bursts*

Throughout the literature, there was mention of fast spots or streaks that have been shown to accompany turbulent bursts. The assumption has been made that these streaks are a result of turbulent bursts, which result in increased shear stress and drag. The mechanism of the turbulent burst did show that the sweeping action bringing high velocity fluid close to the wall will result in the observed fast spots and streaking. At issue with the turbulent burst as the primary mechanism for increased boundary layer shear and drag was that simulations of the fully turbulent boundary layer show little evidence of the

canonical hairpin vortex or generation of the hairpin vortex. What was present are single ended or half hairpin vortices similar to the structures created through the efforts related to this paper.

The goal of this work was to further an understanding of the mechanism that contributes to wall shear stress and resulting drag so that more effective devices can be developed for drag reduction. In the furtherance of this goal, the study of the turbulent burst was not likely to be of significant use. The turbulent burst, though likely the mechanism to initiate the onset of turbulence, was not significantly present after turbulent flow is established.

## *5.3 Requirements for a Stable Vortex*

From the literature, it was clear that the stable vortex in a viscous fluid must undergo continuous strain or it will dissipate. A vortex will have a tendency to align with the direction of strain. A vortex will also entrain fluid through the sides and up through the core and out the end or ends. This was demonstrated both mathematically and in physical experiments discussed above.

The simulations conducted in this work showed little tendency to instability of vortices that were parallel to the wall or that had no exposure to strain from the shear present in the boundary layer. From the simulations conducted in this

work, it is likely that vortical structures introduced into the boundary layer with any vertical development, one end higher than the other, will become aligned with the flow due to strain produced by the effects of boundary layer shear and will persist in the flow as a result of stretching from the action of boundary layer shear.

From the literature, it was also clear that fluid surrounding the vortical structure will be dragged around the vortex due to viscous effects much like a stirring rod spun in a bucket of paint. This action surrounding an inclined vortex will cause a mixing of fluid between the upper and lower regions of the boundary layer and a resulting exchange of momentum.

# 6.Conclusions

## *6.1 Boundary Layer Momentum Transfer*

The single end vortical structures or half hair pins are the mechanism for momentum transfer within the boundary layer, forming a vortical structure momentum transfer mechanism (VSMTM). These micro vortical structures behave like tiny tornados, both dragging fluid around the perimeter like a tornado or a rotating stirring rod, but also drawing fluid into the vortex core and transporting the fluid out the top into the upper regions of the boundary layer where shear is insufficient to provide enough axial strain to sustain a vortex. The vortical structures are inclined as they are continuously strained by the shear of the boundary layer. Due to the inclination of the vortical structure, fluid dragged around the perimeter is moved vertically within the boundary layer exchanging high speed fluid with low speed fluid.

Blowing and suction can affect the vortical structures, especially when arranged such that they can act in pairs countering the vortical structure rotation, resulting in the reduction of angular momentum of the structure sufficient to eliminate the vortex. Notable however is that blowing is a means of creating turbulent bursts and that indiscriminate blowing will only add turbulent structures to the boundary layer.

## *6.2 Drag Reduction Devices*

The VSMTM explains the actions of a number of successful devices for drag reduction. These devices act upon the mechanisms that sustain the momentum transfer mechanism.

### 6.2.1 Blowing and suction

Where wall blowing jets and suction have been used either in physical experiments or in simulations, the effect is to arrest the rotation of the vortical structures. Vortical structures are in a critical balance between viscous dissipation and strain. The actions of jets or suction adjacent to the vortical structure or on both sides can counter the angular momentum of the structure causing it to dissipate.

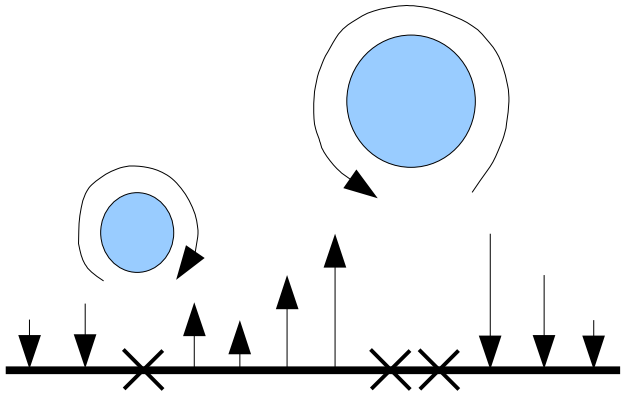

*Figure 85: Concept of suction and blowing to reduce angular momentum about vortical structures*

Jets, however, are a mechanism for introducing turbulent bursts and excessive jet strength may introduce more vorticity than it removes. Here the sensing of

the location of the vortical structure is critical to provide the greatest effectiveness and to avoid introducing more vorticity or unstable boundary layer conditions.

### 6.2.2 Riblets

Adhesive backed sheet with riblets is commercially available. The effect of this device on the vortical structure is two-fold. The ribs themselves act to block the viscous mixing action of the vortical structure by acting as barrier, or baffle, which blocks fluid from being dragged around the vortex.

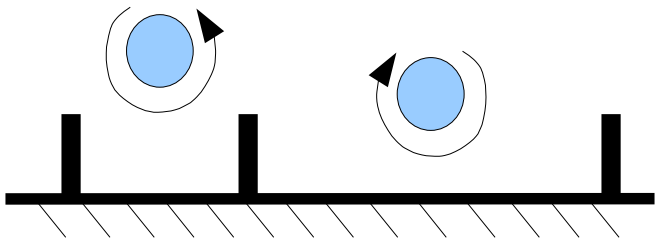

*Figure 86: Riblets, drag reduction concept*

Second, the riblets function as standoffs keeping the vortical structure from getting close to the wall and limit the shear stress that can be placed upon the vortical structure thus limiting the axial strain.

## *6.3 Similarity with Prandtl's Mixing Length Theory*

Prandtl's mixing length theory (PMLT) was an early attempt to provide a model of turbulence. PMLT was based upon some very crude assumptions such as two-

dimensional turbulence and the concept of a rotating chunk of fluid exchanging momentum between upper and lower regions of the boundary layer. Despite being a crude model, PMLT was quite useful. Interestingly, the mixing length suggested by the vortical structures as mixing devices is of the same order as Prandtl's mixing length. The significant difference is that the axis of rotation of the vortical structures is orthogonal to that of the model proposed by Prandtl.

## *6.4 Kolmogorov length scale*

Kolmogorov had predicted an energy cascade consisting of smaller and smaller eddy structures that dissipate energy. Subsequent to the development of his model experimental evidence showed that the energy scale does not progress entirely in one direction but that there is considerable production of turbulence of increasing scale as well as decreasing scale. This was consistent with the observations of turbulent vortical structures in this work and others that showed simultaneous dissipation and generation of vortical structures.

The balance of production versus dissipation is quite sensitive to boundary layer conditions. This sensitivity provides an opportunity for development of mechanisms and resulting devices that can affect the quantity of vortical structures present in the boundary layer by affecting production of new structures and dissipation of existing structures.

# 7. Future Work

The next task is to closely examine the vortical structure to gain a clearer understanding of how the vortical structure exchanges fluid between the upper and lower layers of the boundary layer and to determine the energy balance necessary to keep the vortical structure intact.

The internal flow of the vortical structure needs to be examined along with the pressure field from the wall to the upper end of the vortical structure and into the center of the channel. This will help determine the degree of strain applied by the boundary layer shear as well as the rate of flow through the vortex core.

Before selecting particular types of devices for drag reduction, studies should be conducted using DNS to inject fluid to counteract the rotation of vortical structures to determine the degree of interference required to kill the structure and thus stop the momentum transfer mechanism.

# 8 Appendix

## *8.1 List of Movies*

### 8.1.1 Longitudinal Vortices

| | |
|---|---|
| WorkE_iso.avi | pair of counter-rotating vortices y=-0.5 |
| tst050_iso.avi | 8 longitudinal counter-rotating vortices, y=-0.9 |
| tst055_iso.avi | 12 longitudinal co-rotating vortices, with trip bar, y=-0.9 |
| tst056_iso.avi | 12 longitudinal counter-rotating vortices, with trip bar, y=-0.9 |

### 8.1.2 Lateral Vortices, vortices parallel to wall

| | |
|---|---|
| tst020_iso.avi | 8 lateral co-rotating vortices, y=-0.9 |
| tst036_iso.avi | 8 lateral counter-rotating vortices, y=-0.9 |

### 8.1.3 Lateral Vortices, vortices extending wall to wall

| | |
|---|---|
| tst072_iso.avi | 2 pair vortices, H=0.2, y=-0.9 |
| tst073_iso.avi | 2 pair vortices, H=0.3, y=-0.9 |

### 8.1.4 Vortical Structures resulting from obstructions

| | |
|---|---|
| tst062_iso.avi | rail and blade obstruction on channel wall |
| tst066_iso.avi | narrow obstruction extending wall to wall |

### 8.1.5 Vortical Structures resulting from fluid injection

| | |
|---|---|
| tst063_iso.avi | fluid injection through slot in channel wall |

# 9 References

1 Dahm, W. J. A., Diez-Garias, F. J., "Microactuator Arrays for Sublayer Control in Turbulent Boundary Layers Using Electrokinetic Principle", AIAA Paper No. 2000-0548.
2 Bewley, T. R., Moin, P., Temam, R.,"DNS based predictive control of turbulence: an optimal benchmark for feedback algorithms", , *Journal of Fluid Mechanics, (2001), vol 447, pp* 179-225.
3 Panton, R.L., Incompressible Flow, , Wiley Interscience, 1996, pp586
4 Bernard, P.S., Wallace, J. M., Turbulent Flow, Analysis, Measurement and Prediction, John Wiley and Sons,2002. pp111
5 O. Reynolds, "An Experimental Investigation of the Circumstances Which Determine whether the motion of Water Shall Be Direct or Sinuous, and the Laws of Resistance in Parallel Channels", *Trans. Roy. Soc. London*, vol.174, 1883
6 Schlichting, H., Boundary Layer Theory, McGraw-Hill, Seventh Edition, 1979, pp579.
7 Schlichting, H.,"Boundary Layer Theory, McGraw-Hill, Seventh Edition, 1979, pp578.
8 Libby, Paul, A., Introduction to Turbulence, Taylor and Francis, 1996, pp103
9 Schubauer, G.B., and Klebanoff, P.S. "Contributions on the mechanics of boundary layer transition." NACA TN 3489 (1955) and NACA Rep. 1289 (1956)
10 Schlichting, H., Boundary Layer Theory, McGraw-Hill, Seventh Edition, 1979, pp456.
11 Dahm, W. J. A., Diez-Garias, F. J. "Microactuator Arrays for Sublayer Control in Turbulent Boundary Layers Using Electrokinetic Principle", AIAA Paper No. 2000-0548.
12 Dahm, W. J. A., Diez-Garias, F. J., "Microactuator Arrays for Sublayer Control in Turbulent Boundary Layers Using Electrokinetic Principle", AIAA Paper No. 2000-0548.
13 Hussain, J. J., Schoppa, W., Kim, J., "Coherent Structures near the wall in turbulent channel flow", *Journal of Fluid Mechanics (1997), vol 332, pp* 185-214
14 Bewley, T. R., Moin, P., Temam, R., "DNS based predictive control of turbulence: an optimal benchmark for feedback algorithms", *Journal of Fluid Mechanics, (2001), vol 447, pp* 179-225.
15 Cowley, S. J., van Dommelen, Lam, S. T., "On the use of Lagrangian variables in descriptions of boundary layer separation," *Phil. trans. Royal Society London A* 333, 343 (1990)
16 Acarlar, M. S., Smith, C. R., "A Study of Hairpin Vortices in a Laminar Boundary Layer. Part 1. Hairpin Vortices Generated by a Hemisphere Protuberance," *Journal of Fluid Mechanics* **175**, 1 (1987)
17 Acarlar, M. S., Smith, C. R., "A Study of Hairpin Vortices in a Laminar Boundary Layer. Part 1. Hairpin Vortices Generated by Fluid Injection," *Journal of Fluid Mechanics* **175**, 42 (1987)
18 Amini, J., Lespinard, G., "Experimental Study of an 'Incipient Spot' in a Transitional Boundary Layer," Physics of Fluids, **25**, 1743 (1982)
19 Singer, B., Joslin, R., "Metamorphosis of a Hairpin Vortex into a Young Turbulent Spot," (1995)
20 Tufo, H., Fischer, P., Papka, M., Szymanski, M., "Hairpin Vortex Formation, a Case Study for Unsteady Visualization," Mathematics and Computer Science Division, Argonne National Laboratory,(1999)
21 Durbin, P., Wu, X., "Transition Beneath Vortical Structures," *Annual Review of Fluid Mechanics*, 2007.39:107-128
22 Panton, R.L., Incompressible Flow, Wiley Interscience, 1996, pp721
23 Schlichting, H., Boundary Layer Theory, McGraw-Hill, Seventh Edition, 1979, pp660.
24 Moffatt, H.K., Kida, S., Ohkitani, K., "Stretched Vortices-the sinews of turbulence; large-Reynolds-number asymptotics," *Journal of Fluid Mechanics* (1994), vol 259, pp. 241-264
25 Petitjeans, P., "Stretching of a vortical structure: filaments of vorticity," *French Physical Society*, 132, pp.4 December 2001.
26 Libby, Paul, A., Introduction to Turbulence, Taylor & Francis, 1996, pp103
27 Singer, B., Joslin, R.,"Metamorphosis of a Hairpin Vortex into a Young Turbulent Spot," American Institute of Physics, (1995)
28 Jeong, J., Hussain F., "On the Identification of a Vortex", Journal of Fluid Mechanics (1995), vol 285, pp 69-94
29 H.M. Tufo, P.F. Fischer, M.E. Papka, M. Szymanski, "Hairpin Vortex Formation,a Case Study for Unsteady Visualization", Mathematics and Computer Science Division, Argonne National Laboratory, 1999

30 Tecplot 9.0, AMTEC Engineering Inc., Bellevue, Washington, USA